Understanding QCD jet substructure and its simulation

Yasuhito Sakaki

Doctor of Philosophy

Department of Particle and Nuclear Physics
School of High Energy Accelerator Science
SOKENDAI (The Graduate University for Advanced Studies)

Understanding QCD jet substructure and its simulation

Yasuhito Sakaki

The Graduate University for Advanced Studies School of High Energy Accelerator Science Department of Particle and Nuclear Physics

Doctoral Thesis

For the degree of Doctor of Philosophy in physics

Abstract

Studies on jet substructure have evolved significantly in recent years. We show that in studies of light quark- and gluon-initiated jet discrimination, it is important to include the information on softer reconstructed jets (associated jets) around a primary hard jet. This is particularly relevant while adopting a small radius parameter for reconstructing hadronic jets. The probability of having an associated jet as a function of the primary jet transverse momentum (p_T) and radius, the minimum associated jet p_T and the association radius is computed up to next-to-double logarithmic accuracy (NDLA), and the predictions are compared with results from `Herwig++`, `Pythia6` and `Pythia8` Monte Carlo event generators. We demonstrate the improvement in quark-gluon discrimination on using the associated jet rate variable with the help of a multivariate analysis. The associated jet rates are found to be insensitive to the effects of initial state radiation and underlying event. In addition, the number of k_t subjets of an anti-k_t jet can be an observable that leads to a rather uniform prediction across different Monte Carlo generators, broadly being in agreement with predictions in NDLA, as compared to the often used number of charged tracks observable.

Predictions of jet substructure are usually different among Monte Carlo event generators, and are mainly governed by the parton shower algorithm implemented. For leading logarithmic parton shower, even though one of the core variables is the evolution variable, its choice is not unique. We examine evolution variable dependence of the jet substructure by developing a parton shower generator that interpolates between different evolution variables using a parameter α. Jet shape variables and associated jet rates for quark and gluon jets are studied to demonstrate the α-dependence of the jet substructure. We find angular ordered shower predicts wider jets, while relative transverse momentum ($p_\perp$) ordered shower predicts narrower jets. This is qualitatively in agreement with the fact that there is the missing phase space in $p_\perp$ ordered showers. Such difference can be reduced by tuning other parameters of the showering algorithm, e.g., strong coupling constant, and starting/hadronization scale, especially in the low energy region, while the difference tends to increase for high energy jets.

Contents

1 Introduction

Particle physics is a study to reveal what are elementally objects and how they interact. Building blocks of the current standard model (SM) of particle phyiscs are obtained in the sequence of the high energy physics interactions, and finally the last particle of the SM, higgs boson is discovered at the Large Hadron collider (LHC) at CERN. Now, we have great hopes that LHC Run II will bring a lots of fantastic information to the particle physics yet to be obtained. LHC is a circular type accelerator, and proton or heavy ion (lead) is used as beam. The beam was operated at 7 and 8 TeV with integrated luminosity about 5 and 20 fb^{-1} in the period between 2009 and 2013. The next operation Run II has been planed at 13-14 TeV from 2015 to 2018 with integrated luminosity 150 fb^{-1}. As a long-range plan, the integrated luminosity will reach 3000 fb^{-1} throughout Run III and High Luminosity LHC.

One of main purpose at LHC is search for the higgs boson and the understanding the origin of electro-weak symmetry breaking. ATLAS and CMS reported that they found a new particle around 125 GeV in 2012 [1]. Properties of the particle, e.g., spin, CP charge and the strength of the interaction, agree with those of Higgs boson in the Standard Model (SM) within the range of experimental error.

Another target of the LHC is to find out physics beyond the Standard Model (BSM). Although experimental results at LHC seem to be consistent with predictions in SM, we have many question for the nature and theoretical frame work in SM. The mass parameter of the Higgs potential receives the radiative correction propotinal to the square of the cut off scale. Given the precision study of EW processes, it is natural to consider the scale is much higher than 10TeV. This cause the fine tuning problem in the Higgs sector. Moreover the four point interaction of Higgs potential turns out to be negative around 10^{10}GeV. While the current vacuum is metastable, this cast the question how the current Universe is made after the inflation and subsequent reheating. Moreover, we do not know how the Baryon asymmetry of the Universe is formed, and how the dark matter is understood in the manner consistent with the SM.

To explain the questions above, many models, such as dynamical symmetry breaking models, supersymmetric models, and extra dimension models, are proposed. These models predict new particles and new phenomena, which are the target of the future run of the LHC. To achieve the target, we need precise prediction for both SM and BSM processes.

One of the difficulties in the calculation of high-energy hadron collision stem from the fact that initial state proton is composite particle rather than elementary

particle. Hadrons are composed by valence quarks which carry the quantum number of its hadron, and those quarks are confined by strong interactions mediated by gluons. At the high energy collision of protons, only the fraction of energy can be used, and probability that quark and gluon participate in the hadron collision, which is called parton distribution function (PDF) must be determined from the experimental data. Interaction between quark and gluon is described by Quantum chromodynamics (QCD). The hard quark and gluon branch into quark and gluon, leading many soft quarks and gluons in the final state, which is beyond the fixed order calculation because of the infrared singularity of the QCD processes. Finally, because quark and gluon must be confined in the hadrons, which cannot be calculated perturbatively. Hence we need good model for the calculation, which respects quantum field theory and predict various observables well.

The calculation model for the hadron-hadron collider sketchily divided by following steps.

step 1: Quarks, anti-quarks or gluons in proton beams called as initial *parton* interact in small spacetime, and exchange large momentum, then final partons and/or other SM and BSM particles are produced. This interaction is called as *hard process*, which occur in short distance. The hard process has an energy scale (hard scale), which is typically given by the order of invariant mass square of initial partons or square of exchanged momentum.

step 2: The initial and final partons emit additional particles. These radiations are described by mainly QCD. The radiations from initial and final particles are called as *initial state radiation* (ISR) and *final state radiation* (FSR). Energy scale for the initial partons increases with each ISR, and the scale may reach up to the order of hard scale. Then energy scale for final parton decreases with each FSR. The radiation continues until the scale reach an given scale called as hadronization scale. The calculation model for the radiations is called as *parton shower*.

step 3: When the emitted coloured partons and proton-beam remnants [1] take $\mathcal{O}$(fm) away for each other, QCD potential increase and quark pairs from QCD vacuum and gluon form non-coloured hadrons. This part is called as *hadronization*.

[1] When initial parton is up quark (u), proton-beam remnant formed ud diquark system which have an anti-triplet colour charge. When initial parton is gluon, proton-beam remnant formed uud system which can conveniently be subdivided into a colour triplet quark and a colour anti-triplet diquark [38].

In step 1, flavors of initial parton are decided in the probability of PDF. Factorization theorem [2] justifies the division of the hard process part and the PDF part. Step 1 and 2 are carried by perturbation theory, especially perturbative QCD. QCD is SU(3) non-abelian gauge theory, which describes an interaction between quarks and gluons. Quarks and gluons are the fundamental and adjoint representation of SU(3). Asymptotic freedom which is an property of QCD says the strength of QCD interaction becomes smaller as energy scale of QCD interactions Q increases, and vice versa. Experimentally, valid range of the perturbative QCD is $Q \gtrsim 1\text{GeV}$. Hence an minimal hard scale in step 1 and an hadronization scale in step 2 should set around 1GeV. In step 3, we need models describe physics in the non-perturbative region. Sprays of hadrons calculated by above steps are called as *jet*. Four momenta of hadrons and other particles are measured in detectors, and those are combined to four momenta of jets. The jet momentum is one of the basic observables at LHC.

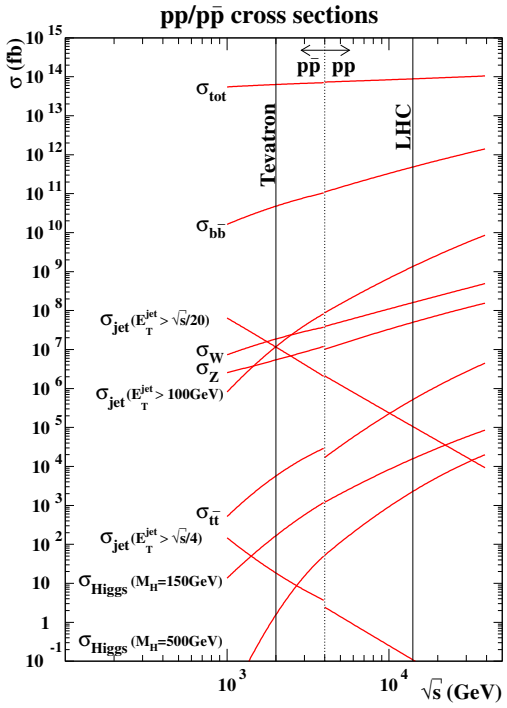

Figure 1: Production cross sections for several representative processes at hadron colliders. The discontinuity is due to the Tevatron being a proton-antiproton collider while the LHC is a proton-proton collider. From Ref. [3].

Hadronic jets are the most abundant objects at LHC, therefore the hadronic decay of new particle maybe easily missed. Production cross sections for several representative processes at hadron colliders are shown in Fig. 1. The finding signature which only gives hadronic jets is very difficult to cope with large QCD back-

grounds. For example, significances of the hadronic Higgs decays like $H \to b\bar{b}$ are considered as low due to the large QCD background like $pp \to b\bar{b}X$. However, the situation might be improved for boosted particles [4]. The authors use the information of internal structure of jets, so-called *jet substructure*, namely the distribution of four momenta of hadrons in jets. Quarks from the boosted Higgs boson and top quark decay create the multiple centers in a jet, called as subjets. The momentum balance of the subjets and the ratio of the jet mass and subjet masses are different between Higgs jets and QCD jets. By using the differences, it is demonstrated that significance of $H \to b\bar{b}$ improves. After that, study of jet substructure has also evolved significantly in recent times [5, 6, 7, 8]. Jet substructure techniques are particularly useful in identifying the origin of jet(s) in the hard process [4, 9, 10, 11, 12, 13, 14, 15, 16, 17, 18, 19], and also in removing contamination from pile-up or underlying event [4, 20, 21, 22, 23, 24, 25].

Recently, there appear several studies concerning the identification of the origin of QCD jets, namely, if they are originated from a quark or a gluon at the point where they appear from the hard process. Although both quark and gluon subsequently emit gluons in the parton shower, initial colour information is conserved in the parton shower process because the splitting functions are different. Discrimination of quark-initiated jets from gluon-initiated ones is also an important subject of jet substructure, and has a lot of potential in improving the search for new physics.

Searching new particles predicted in supersymmetric (SUSY) models is one of the main issue at LHC. One of the signals in the model is pair gluino production ($pp \to \tilde{g}\tilde{g}$). In the three body decay, $\tilde{g} \to q\bar{q}\chi_1^0$, the initiated flavour of jets is dominantly quark. On the other hands, the main background for the process is $Z + jets$ in which the gluon jet is dominant. The detection of two body decay, $\tilde{g} \to g\chi_1^0$, gives a detailed information related to scenarios in which the scalar SUSY particles are heavy [26]. The Higgs mass around 125 GeV implies a possibility of a large size of the two body decay of the gluino. A hard gluon jet is produced via the decay, on the other hands, the hardest jet in background $Z + jets$ is basically the quark jet. Being away from SUSY, jets in the background process for di-quark production related with new particles are dominantly gluon jets. Therefore, better way to distinguish the quark jet and the gluon jet can help the discovery of new particles and the examination of properties of that, and different methods for quark-gluon discrimination have been devised [27, 28, 29, 30, 31, 32, 33, 34], with corresponding performance studies [35, 36, 37] for LHC.

In **Sec. 2**, I review the parton shower, definitions of jet, and the jet substructure technique, especially the discrimination of quark-initiated jets from gluon-initiated. In **Sec. 4**, a new variable concerned with *associated jet* to improve the performance

of quark-gluon discrimination will be introduced. Associated jets are softer jets which are nearby a harder jet. Previous researches for quark-gluon discrimination have focused on the structure of harder jet only. We focus on not only the harder one but also softer jets.

Theoretical estimates for the performance of such tagging algorithms are primarily carried out with the help of Monte Carlo (MC) simulation tools, such as, `Pythia` [38, 39], `Herwig` [40, 41] and `Sherpa` [42]. Even though qualitative features are in agreement, differences in the predictions of the different MC generators have been noted as far as quantitative estimates of the quark-gluon tagger performance is concerned. The primary reason for this can be traced back to the fact that the distribution of observables related to gluon jets varies significantly across the MC generators, while those for the quark jet are largely similar. One possible cause of such a feature might be that while tuning the parameters of the MC generators, the precise jet data from the Large Electron-Positron Collider (LEP) have been crucial, and at leading order in electron-positron collision, the jet data is dominantly from quark-initiated processes. As far as the LEP data is concerned, the properly tuned versions of the MC generators have been successful in achieving very good agreement with the jet data and are also consistent among each other, even in the soft-collinear and the non-perturbative regions.

Recent studies carried out by the ATLAS and CMS collaborations indicate that the data on certain observables related to quark-gluon discrimination lies in between the predictions of the two MC generators `Pythia` and `Herwig` [36, 43, 44]. Although it might be difficult to pinpoint the reason for such differences in the jet substructure observables predicted by different generators, understanding the difference between the central components of the MC generators can be useful in developing more precise simulation tools. To this end, at a first order, if we postpone the consideration of the non-perturbative and underlying event effects for simplicity, the substructure of a quark or a gluon jet is governed by the pattern of QCD radiation, which is controlled by the parton shower algorithm. One of the core variables of a parton shower is the evolution variable, different choices for which are made in different MC generators.

In **Sec. 5**, our aim is to understand the effect of modifying the evolution variable and access its impact on jet substructure observables. We also ask the question whether certain choice of evolution variables can better reproduce the data on quark-gluon discrimination observables, as discussed above.

2 Parton shower

2.1 Parton shower algorithm

Parton shower algorithm is method to calculate high multiplicity final states in QCD processes. The main concept of parton shower is to factorize soft-collinear radiations from a hard process. When the quarks and gluons are soft and/or collinear, the amplitudes for QCD process diverge. We need to regularize the singularity appropriately.

First of all, I introduce Sudakov form factor, which plays an important role in parton shower, and contain a dominant contribution of an all-order amplitude in the soft-collinear phase space. The parton shower algorithm is based on the DGLAP equation [45, 46], which describe an energy scale dependence of states, e.g., a parton distribution function:

$$t\frac{\partial}{\partial t}f(x,t) = \int_0^1 \frac{dz}{z}\frac{\alpha_S(t)}{2\pi}P(z)f(\frac{x}{z},t), \tag{2.1}$$

where $P(z)$ is a *regularized* splitting function and $f(x,t)$ is a parton distribution function which describe the probability that a flavour have a longitudinal momentum fraction z and energy scale t. The energy scale is typically off-shellness (virtuality) of intermediated partons. We will consider the scale in detail later. This $P(z)$ is related with (unpolarized) *unregularized* splitting function $\hat{P}(z)$ as

$$P(z) = \hat{P}(z)_+, \tag{2.2}$$

where the symbol " $+$ " means plus scription written by,

$$\int_0^1 dz\hat{P}(z)_+F(z) = \int_0^1 dz\hat{P}(z)[F(z) - F(1)]. \tag{2.3}$$

Eq. (2.1) can be written with unregularized splitting function by

$$t\frac{\partial}{\partial t}f(x,t) = \int_0^1 dz\frac{\alpha_S(t)}{2\pi}\hat{P}(z)\left[\frac{1}{z}f(\frac{x}{z},t) - f(x,t)\right]. \tag{2.4}$$

Here I introduce the Sudakov form factor,

$$\Delta(t,t_0) = \exp\left[-\int_{t_0}^t \frac{dt'}{t'}\int_\epsilon^{1-\epsilon} dz\frac{\alpha_S}{2\pi}\hat{P}(z)\right], \tag{2.5}$$

where t_0 is minimal scale in parton shower. A scale below t_0 is dealed as non-perturbative region. The splitting functions are proportional to branching probabilities for each target process in soft-collinear region, which are summarized at the

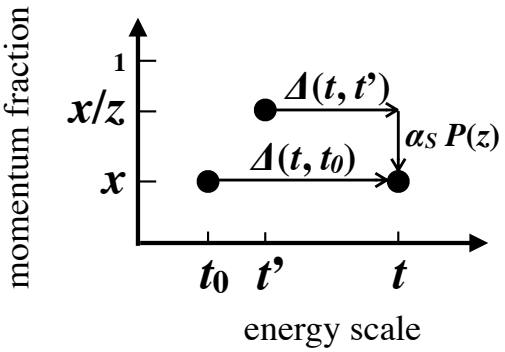

Figure 2: A schematic illustration of Sudakov weighting. A probability state $f(x,t)$, which have energy fraction x at scale t, is formed from $f(x,t_0)$ by a factor $\Delta(t,t_0)$, and also $f(x,t')$ by a factor $\Delta(t,t')$ and the emission probability $(\alpha_S/2\pi)\hat{P}(z)$.

lowest order:

$$\hat{P}(z) = \begin{cases} C_F \frac{1+z^2}{1-z} & (q \to qg), \\ 2C_A[\frac{z}{1-z} + \frac{1-z}{z} + z(1-z)] & (g \to gg), \\ T_R[z^2 + (1-z)^2] & (g \to q\bar{q}), \end{cases} \tag{2.6}$$

where QCD colour factors are $C_F = 4/3$ and $C_A = 3$ for $T_R = 1/2$. Eq. (2.4) becomes

$$t\frac{\partial}{\partial t}\frac{f(x,t)}{\Delta(t,t_0)} = \frac{1}{\Delta(t,t_0)}\int \frac{dz}{z}\frac{\alpha_S}{2\pi}\hat{P}(z)f(\frac{x}{z},t). \tag{2.7}$$

We can solve this equation in integrating form as,

$$f(x,t) = \Delta(t,t_0)f(x,t_0) + \int_{t_0}^{t}\frac{dt'}{t}\int \frac{dz}{z}\frac{\alpha_S(t')}{2\pi}\hat{P}(z)\Delta(t,t')f(\frac{x}{z},t'). \tag{2.8}$$

This equation gives a physical interpretation on the Sudakov form factor. A probability state $f(x,t)$, which have energy fraction x at scale t, is formed from $f(x,t_0)$ by a factor $\Delta(t,t_0)$, and also $f(x,t')$ by a factor $\Delta(t,t')$ and the emission probability $(\alpha_S/2\pi)\hat{P}(z)$. Fig. 2 gives a pictorial representation of the fact. The phyaiscal interpretation of the sudakov form factor will be explained below.

The Sudakov form factor can be written as

$$\begin{aligned} \Delta(t_2,t_1) &= \exp\left[-\int_{t_1}^{t_2}\frac{dt}{t}\int_{z_{min}(t)}^{1-z_{min}(t)} dz\frac{\alpha_S(t)}{2\pi}\hat{P}(z)\right], \\ &= \exp\left[-\int_{t_1}^{t_2}\mathcal{P}(t)dt\right], \\ &= \lim_{N\to\infty}\prod_{i=0}^{N-1}\left[1-\mathcal{P}\left(t_1+id\bar{t}\right)d\bar{t}\right], \qquad d\bar{t} = \frac{t_2-t_1}{N}. \end{aligned} \tag{2.9}$$

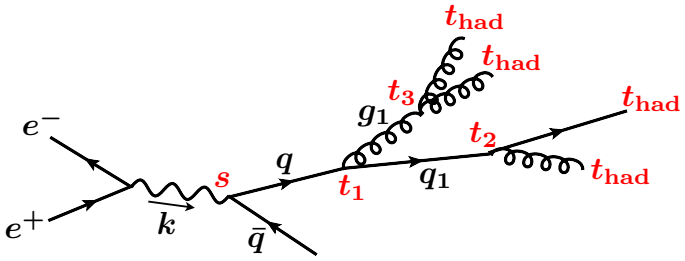

Figure 3: A schematic illustration of sequential decays by the parton shower algorithm.

$\mathcal{P}(t)dt$ show a probability that an emission happen at $t \in [t, t+dt]$, and the last line in Eq. (2.9) is the product of differential non-emission probability in $[t_1, t_2]$. Hence $\Delta(t_2, t_1)$ is non-emission probability from t_1 to t_2. We now notice that states at a given scale t depend only on the present state, not on its past ($t' < t$) states. In other words, the emission process is the Markov process[2]. We assume the energy scale t as an ordering variable (*evolution variable*) in the Markov process of QCD radiation.

We are now ready to construct parton shower algorithm. Let's consider a $e^+e^- \to q\bar{q}$ configuration in Fig. 3, and assume that the energy scale (evolution variable) is virtuality of partons. Scale of the quark starts from $t_0 = s$, where $s = k^2$ is a virtuality of γ/Z. A probability that the quark doesn't emit gluons until a minimal scale $t_{\rm had}$ is $\Delta(t_0, t_{\rm had})$. This minimal scale is called as a hadronization scale, which is a parameter in parton shower model. We often take the value to about 1GeV. A decay may happen at t_1, and the probability is given by

$$Q(t_1) = \frac{d}{dt}[1 - \Delta(t, t_{\rm had})]|_{t=t_1}. \tag{2.11}$$

The starting scales of new partons q_1 and g_1 are t_1.[3] A probability that the partons both don't emit more is $\Delta(t_1, t_{\rm had})^2$. Decays may happen at $t_2(t_3)$ from $q_1(g_1)$ with probability $Q(t_2)(Q(t_3))$. This sequential decay continue until all partons stop to decay. Energy fractions z for each branching at the scale t_i are determined with a probability $\alpha_S(t_i)\hat{P}(z)$. The anti-quark also decay in the same manner.

[2] One of the simplest ordering variables in nature is time, T. A well-known Markov process is nuclei decays. The decay probability at T ($\mathcal{P}(T)$) doesn't depend on its past behaviour . A probability that a nuclei produced at T_1 doesn't decay until T_2 is written as

$$\Delta_N(T_2, T_1) = \exp\left[-\int_{T_1}^{T_2} \mathcal{P}(T)dT\right], \tag{2.10}$$

which is the same form with Eq. (2.9).

[3] The choice of starting scales will be modified in Sec. 5.1.2.

The virtuality is used as evolution variable above, which is a traditional choice of evolution variable. However, even if we use a variable $t_f = f(z)q^2$ as the evolution variable, all equations in this subsection do not change. We can check that by a relation,

$$\frac{dt_f}{t_f}dz = \frac{dq^2}{q^2}dz. \tag{2.12}$$

Therefore we can use the same parton shower formalism with t_f. In this mean, the choice of evolution variable is not unique. For example, a often-used parton shower generator `Herwig++` use $f(z) = 1/z(1-z)$ to realize angular-ordered parton shower, which will be explained next subsection. More detail of the choice of evolution is discussed in Sec. 5.

I should give a comment for the minimal value of momentum fraction $z_{\min}(t)$ in Eq. (2.9). We can see that the QCD radiating probability have IR singularity in Eq. (2.6). The IR singularity should be cancelled at higher order [47, 48]. We often introduce a finite gluon mass or cutoff of relative transverse momentum of emissions, whose values are around $t_{\rm had}$, to remove the singularity.

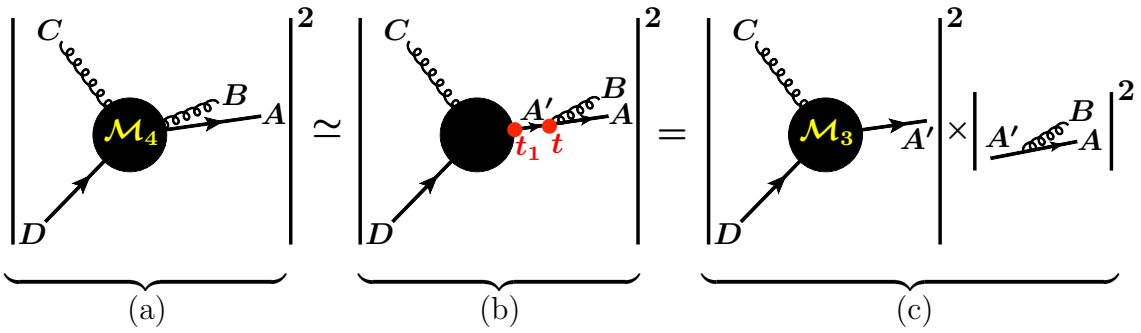

Figure 4: A schematic illustration of collinear factorization of an amplitude.

Next I want to explain that the parton shower algorithm using Sudakov form factor gives a good prediction in collinear regions. Let's consider an four body amplitude as $e^+e^- \to ABCD$ in Fig. 4-(a). Though there are some tree diagrams to contribute to this configuration, only a diagram Fig. 4-(b) is significant when an angle between A and B are small. Because the virtuality of intermediate parton A' becomes small as A and B become collinear, therefore, the propagator term of A' enhance. The amplitude square (b) can be divided by $A'CD$ and $A'AB$ as Fig. 4-(c),

which is written by,

$$\int_{z(B)} |\mathcal{M}_4|^2 d\Phi_4 \simeq |\mathcal{M}_3|^2 d\Phi_3 \times \frac{dt}{t} \int dz \frac{\alpha_S(t)}{2\pi} \hat{P}_{gq}(z), \tag{2.13}$$

$$= |\mathcal{M}_3|^2 d\Phi_3 \times dt\mathcal{P}(t), \tag{2.14}$$

$$= d\sigma_3 \times dt\mathcal{P}(t). \tag{2.15}$$

We can neglect interference terms in the collinear region. In the parton shower algorithm, the first branching $A' \to AB$ at scale t is generated by the probability of

$$d\sigma_3 \times dt \frac{d}{dt}[1 - \Delta(t_1, t)] = d\sigma_3 \times \Delta(t_1, t) dt\mathcal{P}(t). \tag{2.16}$$

We can get a following relation by the Taylor expansion of Sudakov form factor,

$$\Delta(t_1, t) = \frac{d\sigma_3}{d\sigma_3 + d\sigma_3 \int_t^{t_1} dt'\mathcal{P}(t') + d\sigma_3 \int_t^{t_1} dt_2\mathcal{P}(t_2) \int_t^{t_2} dt'\mathcal{P}(t') + ...}. \tag{2.17}$$

The numerator in Eq. (2.17) is the 3-body cross section. The second and third terms of denominator are the cross section for $(3+1)$-body and $(3+2)$-body cross section in the collinear limit. This summation continues up to infinite term. So, the Sudakov form factor is given by the ratio of non-emission event to whole event at all-order and tree level. We can again interpret the Sudakov form factor $\Delta(t_1, t)$ as non-emission between scale t_1 and t at all-order. This interpretation is valid in collinear limit. In Fig. 4, Gluon C show the gluon which is separating widely from other partons. It is inappropriate to generate such wide/hard radiations by the parton shower algorithm. Therefore we generate such wide/hard radiations by fixed order calculations and simulate soft/collinear radiations by the parton shower algorithm. There are several schemes or generators to merge fixed order calculations and parton shower algorithms. Well known methods to merge several leading order matrix elements (ME) and showers are CKKW [49], CKKW-L [50, 51] and MLM [52, 53]. Generators and methods to merge next-to leading order ME for basic processes and showers are `MC@NLO` [54, 55, 56] and `POWHEG` [57].

2.2 Angular ordering

Here I introduce *angular ordering* [58, 59, 60, 61, 62] which is a property in partons shower branching.

A state of n-body final state from colour singlet source like e^+e^- pair annihilation is written by $|1, ..., n\rangle$ and colour-spin specified amplitude is given by

$$\mathcal{M}_n^{c_1,...,c_n;s_1,...,s_n}(p_1, ..., p_n) = \langle c_1, ..., c_n | \langle s_1, ..., s_n || 1, ..., n \rangle, \tag{2.18}$$

where the bra-vectors show a basis in colour and spin subspace, c_i and s_i are indices for colour and spin of parton i, and p_i is momentum of i. For a convenience, we introduce a colour charge $\mathbf{T}_i^c$ which acts a parton i as:

$$\mathbf{T}_i^c|c_1,...,c_i,...,c_n\rangle = T^c_{c_i c_i'}|c_1,...,c_i',...,c_n,c\rangle, \tag{2.19}$$

$$T^c_{c_i' c_i} = \begin{cases} if^{c_i' c c_i} & (i = \text{gluon}), \\ t^c_{c_i' c_i} & (i = \text{quark}), \\ -t^c_{c_i c_i'} & (i = \text{antiquark}), \end{cases} \tag{2.20}$$

The colour charge $\mathbf{T}_i^c$ is associated with the creation of a new colour state whose index is labeled by c, and the colour is connecting to the colour of parton i. A square $(\mathbf{T}_i^c)^2 = \mathbf{T}_i^c\mathbf{T}_i^c \equiv C_i$ is the Casimir operator (colour factor) C_F for quark and C_A for gluon. An identity related with the colour conservation in state is shown in Ref. [63] as

$$\sum_{i=1}^{n} \mathbf{T}_i^c|1,...,n\rangle = 0, \tag{2.21}$$

or just $\sum_i \mathbf{T}_i^c = 0$. Trivial relations are

$$\langle c_1,...,c_i,...,c_n,c|\mathbf{T}_i^c|c_1',...,c_i',...,c_n'\rangle = \delta_{c_1 c_1'}\cdots T^c_{c_i c_i'}\cdots\delta_{c_n c_n'}. \tag{2.22}$$

Next let us consider a factorized amplitude for $i(p_i+k,s_i',c_i') \to i(p_i,s_i,c_i) + g(k,s,c)$, where variables in parenthesis for partons show those momentum, spin and colour. When parton i is quark, that is given by

$$\begin{aligned} \bar{u}(p_i,s_i)\epsilon_\mu^{s*} g_s\gamma^\mu u(p_i+k,s_i')\frac{1}{(p_i+k)^2}T^c_{c_i c_i'}\mathcal{M}_n^{c_1,...,c_i',...,c_n;s_1,...,s_i',...,s_n}(p_1,...,p_i+k,...,p_n), \\ \to g_s\epsilon_\mu^{s*}\frac{p_i^\mu}{p_i\cdot k}T^c_{c_i c_i'}\mathcal{M}_n^{c_1,...,c_i',...,c_n;s_1,...,s_i,...,s_n}(p_1,...,p_i,...,p_n), \end{aligned} \tag{2.23}$$

where ϵ_μ is polarization vector of emitted gluon. We used soft approximation (so called eikonal approximation), namely $k^\mu \to 0$. The factorized factor $p_i^\mu/(p_i\cdot k)$ is called as eikonal factor whose form is independent on the emitting flavour i. Feynman rules in the eikonal approximation is summarized in Ref. [64]. The eikonal factor take the form as

$$\frac{p_i^\mu}{p_i\cdot k} = \frac{p_i^\mu}{E_i\omega(1-\cos\theta_{ik})}, \tag{2.24}$$

where E_i and ω are energies of parton i and emitted gluon, and θ_{ik} is an opening angle between p_i and k. This factor has a soft singularity in $\omega \to 0$ and collinear singularity in $\theta_{ik} \to 0$.

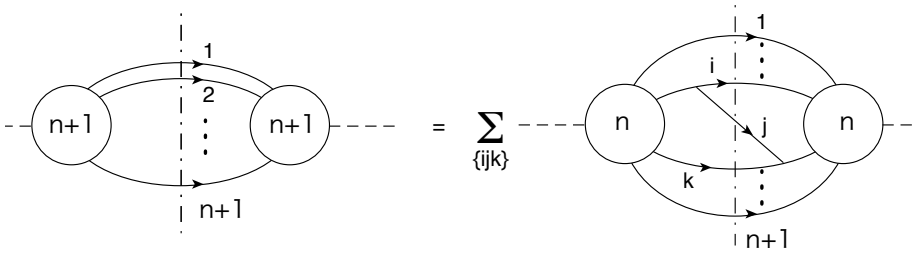

Figure 5: Diagrammatic representation of the external-leg insertion rule. The blobs denote the tree-level matrix elements and their complex conjugate. The dots on the right-hand side stand for non-singular terms both in the soft and collinear limits. From Ref. [63]

Amplitude square related to such emission from n-legs have a soft-enhance term $1/\omega^2$. By neglecting contributions whose contributions to amplitude square are weaker than $1/\omega^2$, a $(n+1)$-body amplitude is given by

$$\mathcal{M}_{n+1}^{c_1,...,c_{n+1};s_1,...,s_{n+1}}(p_1,...,p_{n+1}) \tag{2.25}$$

$$\simeq g_s \epsilon_\mu^{s*} \sum_{i=1}^{n} \frac{p_i^\mu}{p_i \cdot k} T^c_{c_i c_i'} \mathcal{M}_n^{c_1,...,c_i',...,c_n;s_1,...,s_n}(p_1,...,p_n), \tag{2.26}$$

$$= g_s \epsilon_\mu^{s*} \sum_{i=1}^{n} \frac{p_i^\mu}{p_i \cdot k} (\delta_{c_1 c_1'} \cdots T^c_{c_i c_i'} \cdots \delta_{c_n c_n'}) \mathcal{M}_n^{c_1',...,c_n';s_1,...,s_n}(p_1,...,p_n), \tag{2.27}$$

$$= g_s \epsilon_\mu^{s*} \sum_{i=1}^{n} \frac{p_i^\mu}{p_i \cdot k} \langle c_1,...,c_n,c|\mathbf{T}_i^c|c_1',...,c_n'\rangle \langle c_1',...,c_n'|\langle s_1,...,s_n|1,...,n\rangle, \tag{2.28}$$

$$= \langle c_1,...,c_n,c|\langle s_1,...,s_n| \sum_{i=1}^{n} g_s \epsilon_\mu^{s*} \frac{p_i^\mu}{p_i \cdot k} \mathbf{T}_i^c |1,...,n\rangle. \tag{2.29}$$

Therefore amplitude square in soft limit is given by

$$|\mathcal{M}_{n+1}|^2 \simeq -\frac{2g_s^2}{\omega^2} \sum_{i<j} W_{ij} \langle 1,...,n|\mathbf{T}_i^c \mathbf{T}_j^c|1,...,n\rangle, \tag{2.30}$$

$$W_{ij} = \frac{p_i \cdot p_j}{p_i \cdot \hat{k}\ p_j \cdot \hat{k}}, \qquad \hat{k} \equiv k/\omega \tag{2.31}$$

A relation $\sum_s \epsilon_\nu^s \epsilon_\mu^{s*} \to -g_{\mu\nu}$ is used. Hereinafter $\mathbf{T}_i^c$ will be just written by $\mathbf{T}_i$. W_{ij} is called as antenna function. Diagrammatic representation of the equation is shown in Fig. 5

Let us consider $n = 2$ system, and a gluon is emitted from the system. By using Eq. (2.21), non-Casimir operator product is written by

$$\mathbf{T}_1 \mathbf{T}_2 = -C_1^2 = -C_2^2 \equiv -C_{12}. \tag{2.32}$$

Then the amplitude square is given by

$$|\mathcal{M}_{2+1}|^2 = -\frac{2g_s^2}{\omega^2} W_{12} \langle 1,2|\mathbf{T}_1\mathbf{T}_2|1,2\rangle, \tag{2.33}$$

$$= \frac{2g_s^2}{\omega^2} C_{12} W_{12} |\mathcal{M}_2|^2. \tag{2.34}$$

We see that the colour part is factorized. The collinear singularities in W_{ij} can be disentangled by

$$W_{ij} = W_{ij}^{[i]} + W_{ij}^{[j]}, \tag{2.35}$$

where

$$W_{ij}^{[i]} = \frac{1}{2}\left(W_{ij} + \frac{1}{1-\cos\theta_{ik}} - \frac{1}{1-\cos\theta_{jk}} \right). \tag{2.36}$$

$W_{ij}^{[i]}$ contain the collinear singularity by a emission along i only, and vise verse. This function satisfy a relation as

$$\int_0^{2\pi} \frac{d\phi_{ik}}{2\pi} W_{ij}^{[i]} = \frac{1}{1-\cos\theta_{ik}} \Theta(\theta_{ij} - \theta_{ik}) \tag{2.37}$$

where the integral means that integration over an azimuthal angle of emitted gluon along the direction of p_i, and Θ is the Heaviside step function. Therefore azimuthal-angle-averaged radiation along parton i is limited in the region $\theta_{ik} < \theta_{ij}$. Again 3-body amplitude square is written by

$$|\mathcal{M}_{2+1}|^2 = \frac{2g_s^2}{\omega^2} (C_1 W_{12}^{[1]} + C_2 W_{12}^{[2]}) |\mathcal{M}_2|^2. \tag{2.38}$$

Interpretation of the equation is that the opening angles of azimuthal-angle-averaged radiation along parton i and j, θ_{ik} and θ_{jk} are limited, which are smaller than the opening angle between "parents" i and j. (In this case $i = 1$ and $j = 2$.) This emission property is called as angular ordering. The pictorial representation is shown in Fig. 6.

For $n = 3$, non-Casimir operator products are written by

$$\mathbf{T}_1\mathbf{T}_2 = C_3 - C_1 - C_2 \equiv -C_{12}, \tag{2.39}$$

$$\mathbf{T}_1\mathbf{T}_3 = C_2 - C_3 - C_1 \equiv -C_{13}, \tag{2.40}$$

$$\mathbf{T}_2\mathbf{T}_3 = C_1 - C_2 - C_3 \equiv -C_{23}. \tag{2.41}$$

Therefore

$$|\mathcal{M}_{n+1}|^2 = \frac{2g_s^2}{\omega^2} \sum_{i<j} C_{ij} W_{ij} |\mathcal{M}_n|^2. \tag{2.42}$$

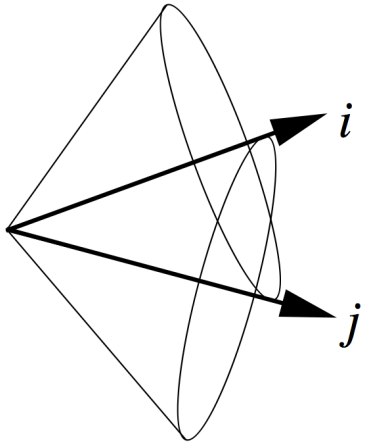

Figure 6: From Ref. [65]. The pictorial representation of angular ordering: Opening angles of azimuthal-angle-averaged radiation along parton i and j, i.e., θ_{ik} and θ_{jk} are limited, which are smaller than the opening angle between "parents" i and j.

We again see that the colour part is factorized. Now we assume a parton is soft and collinear respect to another parton. When p_3 is soft and collinear respect to p_1, colour and antenna term is written by

$$\sum_{i<j} C_{ij} W_{ij} = C_{12} W_{12} + C_{13} W_{13} + C_{23} W_{23} \tag{2.43}$$

$$\simeq C_1 W_{13}^{[1]} + C_3 W_{13}^{[3]} + C_2 W_{1'2}^{[2]} + C_{1'} \widetilde{W}_{1'2}^{[1']}, \tag{2.44}$$

where $1'$ show the direction respect to $p_1 + p_3$ ($\simeq p_1$) and

$$C_{1'} = -(\mathbf{T}_1 + \mathbf{T}_3)^2, \qquad \widetilde{W}_{1'2}^{[1']} \simeq W_{1'2}^{[1']} - W_{1'3}^{[1']}. \tag{2.45}$$

After averaging over the azimuthal angle with respect to $1'$:

$$\widetilde{W}_{1'2}^{[1']} \to \frac{1}{1 - \cos\theta_{1'k}} [\Theta(\theta_{1'2} - \theta_{1'k}) - \Theta(\theta_{1'3} - \theta_{1'k})], \tag{2.46}$$

$$= \begin{cases} \frac{1}{1-\cos\theta_{1'k}} & \text{for } \theta_{1'2} > \theta_{1'k} > \theta_{1'3}, \\ 0 & \text{for others.} \end{cases} \tag{2.47}$$

Therefore Eq. (2.44) has angular ordering property, and the pictorial representation is shown in Fig. 7. Angular ordered emissions labeled by $[I]$ in the figure correspond to the I-th term in Eq. (2.44).

For $n \geq 4$, non-Casimir operator products are not written by only Casimir operators, so colour part is not factorized [63]. However if we neglect sub-leading colour terms, colour part is factorized as in Eq. (2.42), and we can check angular ordering in all order.

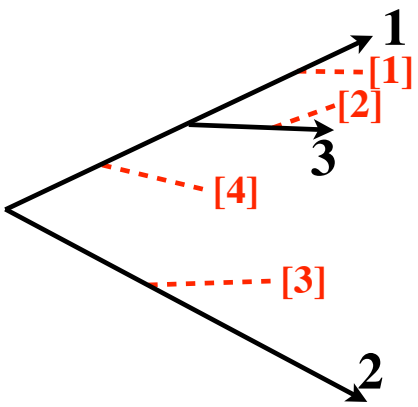

Figure 7: Angular ordered emissions labeled by $[I]$ in the figure correspond to the I-th term in Eq. (2.44).

I summarize this section. By imposing angular ordering on parton shower branchings which is generated by azimuthal-angle-averaged splitting functions like Eq. (2.6), the shower history can contain correct colour correlations for each partons in soft collinear approximation, but loosing sub-leading colour term which is proportional to $1/N_c$ after fifth emission.

3 Jet and its substructure

3.1 Jet definition

While the partons from the hard process fragments into hadrons, the branching of partons are mostly soft and/or collinear. By summing the momentum of the hadrons in the same direction, one can extract the information of the hard process. The procedure, called jet clustering is the key issue for the hadron collider physics. Required property for jet clustering is infrared and collinear (IRC) safety. It means that jet sets does not affect from soft and collinear emissions. In this section, we introduce sequential recombination jet algorithms, which are IRC safe and used well recently.

In e^+e^- collider, energy and angle between final state particles are used in the definition of the jets. A basic variable for the clustering is Durham-k_T, which is defined as

$$k_{ij}^2 = \min(E_i^2, E_j^2)(1 - \cos\theta_{ij}), \tag{3.1}$$

where E_i is the energy of particle labeled i, and θ_{ij} is angle between particle i and j. When the number of final states is n, we calculate $n(n-1)/2$ Durham-k_T for each

particle pair.[4] When k_{IJ}^2 is smallest, we combine four momenta of I and J, and new mock momentum p_{IJ} is produced. This operation stop when all Durham-k_T become larger than a given value $d_{\rm cut}$. We call remaining four momenta in the list as jets. Therefore, jets four momenta and number depend on the dimension-full variable $d_{\rm cut}$. A dimension less notation $y_{\rm cut}(= d_{\rm cut}/Q)$ is also used, where Q is total energy of the e^+e^- system. This jet clustering algorithm is called as (exclusive) Durham algorithm. QCD radiation has soft-collinear singularity, whose emission probability for $(ij) \to i + j$ is given by

$$d^2P \propto \frac{dz}{z}\frac{d\theta_{ij}}{\theta_{ij}} \propto \frac{dz}{\min(E_i, E_j)}\frac{d\theta_{ij}}{\theta_{ij}} \propto \frac{dz d\theta_{ij}}{k_{ij}}, \tag{3.2}$$

therefore emissions are enhanced as those k_t are small. In Durham algorithm, a particle pair which has the smallest k_t is combined preferentially, which lead to IRC safety of the algorithm.

A generalized k_T algorithm exists [66], whose basic variables are written as,

$$d_{ij}^2 = \min(E_i^{2p}, E_j^{2p})\frac{1-\cos\theta_{ij}}{1-\cos R}, \qquad d_i^2 = \min(E_i^{2p}, E_j^{2p}) \tag{3.3}$$

Left one is called as *measure*, and two additional parameter, p and R, are introduced. We can calculate $n(n-1)/2$ measures and n of d_i^2. When d_{IJ}^2 is smallest, we combine four momenta of I and J, and new mock momentum p_{IJ} is produced. This operation stop when all measures become larger than all d_i^2. We call remaining four momenta in the list as jets. Jet properties are depend on the p and R, and R is called as a jet radious parameter. This name stem from the fact that a pair of four momentum whose opening angle is larger than R is never combined in the definition.

In hadron colliders, variables which are invariant with respect to boost of a beam direction are used. A transverse momentum along with a beam direction and a distance in rapidity-azimuthal plain are used rather than energy and opening angle. A corresponding measure for the jet definition is described as

$$d_{ij}^2 = \min(p_{T,i}^{2p}, p_{T,j}^{2p})\frac{\Delta R_{ij}}{R}, \qquad d_i^2 = \min(p_{T,i}^{2p}, p_{T,j}^{2p}), \tag{3.4}$$

where the distance are mainly defined as

$$\Delta R_{ij} = \sqrt{(\eta_i - \eta_j)^2 + (\phi_i - \phi_j)^2}. \tag{3.5}$$

The variables $\eta_{i,j}$ and $\phi_{i,j}$ are the rapidity and azimuthal angle of particle i and j.

[4] For searching minimal measure d_{ij}, we need computation time which is propotional to $n(n-1)/2$. This increases rapidly as the number of final states n increases. `FastJet` program [66] for jet clustering achieves expected $N \ln N$ timing for many sequential recombination algorithms, and make it possible to utilize the modern jet algorithm for data analysis.

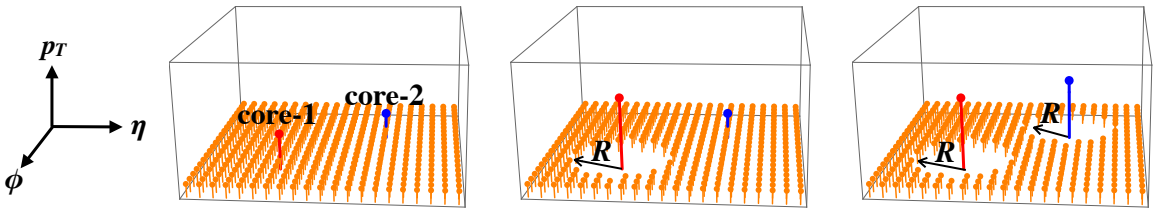

Figure 8: An example event to understand that anti-k_T jets are constructed by particles around the core. These orange, red, blue points show the final states in $\eta - \phi - p_T$ space. The orange points have smaller p_T, which are almost the same for each other. The red particle (core-1) have largest p_T, and blue one (core-2) have second p_T.

Jet algorithms with different power factors p in Eqs. (3.3) and (3.4) are called as:

$$p = \begin{cases} 1 & (k_T \text{ algorithm [67]}), \\ 0 & (\text{Cambridge-Aachen algorithm [68, 69]}), \\ -1 & (\text{anti-}k_T \text{ algorithm [70]}). \end{cases} \tag{3.6}$$

A cluster pare which has the smallest k_T (angle) is combined preferentially in k_T (Cambridge-Aachen algorithm) algorithm. While, the highest p_T cluster tend to be clustered in anti k_T algorithm. In hadron collider, anti-k_T algorithm is often used since jets defined the algorithm is not easily affected by contamination of underlying event compare to jets defined other algorithms. We can understand that by clustering test events in Fig. 8. These orange, red, blue points show the final states in $\eta - \phi - p_T$ space. The orange points have smaller p_T, which are almost the same for each other. The red particle (core-1) have largest p_T, and blue one (core-2) have second p_T. From the jet definition orange particles around red one within R are absorbed by core-1 in the first stage of the clustering when we set as $p = -1$. After that, orange particles around core-2 are absorbed by that and second jet are constructed. Some orange particles which are far from the core are actually contaminations from underlying and pile-up events. Anti-k_T jets are constructed by particles around the core, therefore, the contaminations effect in jets is minimal. Jets defined by k_T and Cambridge-Aachen algorithm can take the contaminations in jets more.

3.2 Jet substructure

Jet substructure techniques are particularly useful in identifying (tagging) a jet origin in hard processes. While original work of this thesis is on quark-gluon dis-

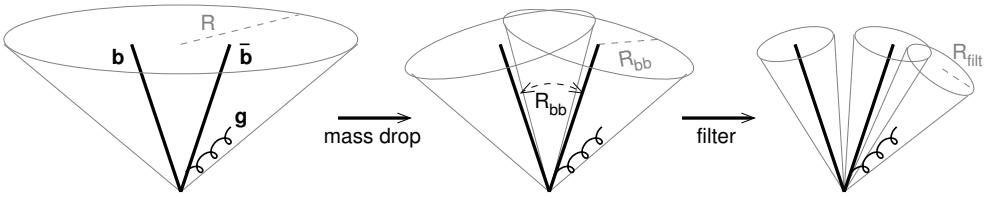

Figure 9: Pictorial representation of the boosted Higgs tagging in Ref. [4]. See text for details.

crimination, I also review two-prong and three-prong tagging in this section.

3.2.1 Two-prong and three-prong tagging

Two-prong tagging is used for boosted Z, W and Higgs boson. These *mother* bosons can decay to two *daughter* fermions, e.g., $H \to b\bar{b}$. When we neglect mass of daughters, mother mass m is described as

$$m^2 = (p_1 + p_2)^2 \simeq E_1 E_2 \theta_{12}^2 = z(1-z)E^2\theta_{12}^2, \tag{3.7}$$

where $p_{1,2}$ and $E_{1,2}$ are four momenta and energies of daughter particles, θ_{12} is a opening angle between daughters, E is the mother energy, and z is a energy fraction, $z = E_1/E$. When the mother is boosted enough, $m/E \ll 1$, the energies of daughters are tend to be balanced, $z \sim 1/2$. In this case, the typical opening angle is given as

$$\theta_{12} \sim \frac{2m}{E}. \tag{3.8}$$

The daughters are collimated as the mother is boosted. In hadron collider, transverse momentum p_T and distance ΔR_{12} rather than E and θ_{12} are used. Alternative relation is

$$\Delta R_{12} \sim \frac{2m}{p_T}. \tag{3.9}$$

Therefore, $b\bar{b}$-pairs from Higgs which have $p_T = 200$ GeV would be inside of jet defined by $R \sim 1.2$. We call such large-radious jet which contains decay products from a mother particle as *fat jet*. The four momentum of fat jet is similar with that of a mother particle. So, the mass of fat jet is cloth to the mother mass. We would see two subjets in the fat jet of signal, on the other hand, there is not such substructure in the QCD fat jet typically, which is the main idea of 2-prong tagging.

Pictorial representation of the idea is shown in Fig. 9. Left figure shows the fat jet, whose mass is around Higgs mass. Undoing the clustering, we again cluster objects in the fat jet until the jet splits into two subjets, which is shown in center figure. If the subjets come from the Higgs decay, we may observe two light subjets.

On the other hand, if the subjets come from the QCD radiation, one of the subjet is light since that stem from a soft radiation, however another one is heaver than it typically.[5] Likewise, the momenta of subjets from the Higgs decay may be balanced, on the other hand, those from the QCD radiation is not balanced due to the soft singularity. Continuing the clustering with a given radius parameter $R_{\rm filt}$, we look for $H \to b\bar{b}g$ configuration. The last operation shown in right figure is called as *filtering*. Most of QCD radiations from Higgs which is colour singlet should go into the three subjets due to the angular ordering. Neglecting objects outside the subjets, we can filter away the contaminations of underlying event.

Another difference between boosted objects from the Higgs/weak boson and the QCD jets is number of charged tracks in the jets. As the jet p_T increases, the energy scale of partons in the QCD jets become larger and the number of charged tracks increases [71, 72]. On the other hand, the energy scales of boosted objects are limited by their masses. So, the difference of number between signal and background would be significant especially in the high-p_T range.

For 3-prong tagging, idea is the same with 2-prong tagging. Three-prong tagging is especially used as boosted top tagging. Hadronic top decay is mainly following as $t \to W^+ b \to q\bar{q}'b$. So, we would see three subjets in the fat jet of top quark.

3.2.2 Quark-gluon discrimination

The boosted Z, W and Higgs jet have 2-prong substructure in there fat jets, and 3-prong substructure for top fat jets. Quark- and gluon-initiated jets have both 1-prong substructure since QCD radiations are soft and collinear dominantly. We review how the nature of the jets are predicted by QCD, emphasizing the difference between the quark and gluon jets.

One of the observables is the two-point energy correlation function $C_1^{(\beta)}$ [33, 73], which can be defined in the rest frame of a parton pair as

$$C_1^{(\beta)} = \sum_{i<j\in \text{jet}} z_i z_j \left(2\sin\frac{\theta_{ij}}{2}\right)^{\beta}, \quad z_i = \frac{E_i}{E_{\text{jet}}} \tag{3.10}$$

where $E_i$is the energy of the particles labeled by i in the jet, E_{jet} is the jet energy, θ_{ij} is the angle between i and j, and β is a power parameter. The sum runs over all distinct pairs of particles in the jet. We set $\beta > 0$ since the $C_1^{(\beta)}$ with $\beta \leq 0$ change the value by collinear emissoins. The angularity is calculated by the summation of weight $z_i z_j \theta_{ij}^{\beta}$. Since QCD radiation is soft and angular ordering suppresses diffuse

[5] Probability that both subjets by QCD radiation are light is strongly suppressed by the Sudakov form factor.

sequential-branching, QCD jet contains one most energetic core parton (labeled by 0) and many soft partons (labeled by $1, .., n$) which are close to the core parton.[6] So, the weights $z_i z_j \theta_{ij}^{\beta}$ $(i, j \geq 1)$ are negligible. In this approximation, $C_1^{(\beta)}$ is described as

$$C_1^{(\beta)} \simeq \sum_{i=1}^{n} z_i \theta_i^{\beta}, \quad \theta_i = \theta_{i0}. \tag{3.11}$$

We assume that a branching whose weight is largest in $\{z_i \theta_i^{\beta}\}$ gives dominant contribution to $C_1^{(\beta)}$ [74], and write $C_1^{(\beta)}$ as,

$$C_1^{(\beta)} \simeq \max(z_1 \theta_1^{\beta}, ..., z_n \theta_n^{\beta}), \tag{3.12}$$

where we assume that this jet contain n times branching.

Then, let's estimate $C_1^{(\beta)}$ distributions for quark jets and gluon jets analytically. We use the general scale as evolution variable, $t_i = f(z_i) q_i^2 \simeq z_i f(z_i) \theta_i^2$. Eq. (3.12) is written as

$$C_1^{(\beta)} \simeq \max(w_1, ..., w_n), \quad w_i = z_i \theta_i^{\beta} = z_i \left(\frac{t_i}{z_i f(z_i)} \right)^{\beta/2} \tag{3.13}$$

If a branching satisfy relation, $\max(w_1, ..., w_n) < x$, $C_1^{(\beta)}$ for the jet is smaller than a given value x. When the branching is associated with m-body hard process, the cross section that $C_1^{(\beta)}$ is smaller than x is

$$d\sigma_m \int_{\Omega_x^{(2n)}} d^2\mathcal{P}_F(z_1, t_1) \cdots d^2\mathcal{P}_F(z_n, t_n), \tag{3.14}$$

where $d\sigma_m$ is the differential cross section of hard part, and

$$\Omega_x^{(2n)} = \{(z_1, t_1, ..., z_n, t_n) \in \mathbf{R}^{2n} \mid \theta_i < R,\ t_1 > \cdots > t_n,\ \max(w_1, ..., w_n) < x\}, \tag{3.15}$$

$$d^2\mathcal{P}_X(z, t) = \frac{dt}{t} dz \frac{\alpha_S(t)}{2\pi} \hat{P}_F(z), \tag{3.16}$$

where R is jet radius. We don't need to consider wider emissions ($\theta > R$). X denote flavors of the core parton, i.e., $X =$ q (quark) or g (gluon), and explicitly

$$\hat{P}_q = C_F \frac{1 + z^2}{1 - z}, \tag{3.17}$$

$$\hat{P}_g = 2C_A \left(\frac{z}{1 - z} + \frac{1 - z}{z} + z(1 - z) \right). \tag{3.18}$$

[6] This is clear difference between QCD jet substructure and boosted W, Z, H and top quark jet substructure.

We denote $\Sigma_X(x)$ as the probability that $C_1^{(\beta)}$ is smaller than a given value x. This cumulative distribution function (CDF) is given by

$$\Sigma_X(x) = \frac{1}{\sigma_X}\int_0^x de_\beta \frac{d\sigma_X}{de_\beta} = \frac{d\sigma_m + \sum_{n=1}^{\infty} d\sigma_m \int_{\Omega_x^{(2n)}} \prod_{i=1}^{n} d^2\mathcal{P}_X(z_i,t_i)}{d\sigma_m + \sum_{n=1}^{\infty} d\sigma_m \int_{\Omega^{(2n)}} \prod_{i=1}^{n} d^2\mathcal{P}_X(z_i,t_i)}, \tag{3.19}$$

$$\Omega^{(2n)} = \{(z_1,t_1,...,z_n,t_n) \in \mathbf{R}^{2n} \mid \theta_i < R, t_1 > \cdots > t_n\}. \tag{3.20}$$

The denominator in Eq. (3.19) is the cross section for whole events, and the numerator is the summation of cross section that $C_1^{(\beta)}$ is smaller than x at all order. By using relations in appendix C, we can write as

$$\Sigma_X(x) = \frac{\exp\left[\int_{\Omega_x^{(2)}} d^2\mathcal{P}_X(z,t)\right]}{\exp\left[\int_{\Omega^{(2)}} d^2\mathcal{P}_X(z,t)\right]}, \qquad (z=z_1, t=t_1) \tag{3.21}$$

$$= \exp\left[-\int_{\Omega^{(2)}\setminus\Omega_x^{(2)}} d^2\mathcal{P}_X(z,t)\right], \tag{3.22}$$

$$= \exp\left[-\int_{\Omega^{(2)}\setminus\Omega_x^{(2)}} \frac{dt}{t}dz\frac{\alpha_S}{2\pi}\hat{P}_X(z)\right]. \tag{3.23}$$

We note that the right hand side in Eq. (3.23) is not depend on the choice of evolution variable function $f(z)$.

Let us calculate $\Sigma_X(x)$ in soft limit. In the limit, the splitting function become

$$\hat{P}_X = \frac{2C_X}{z}, \quad C_X = \begin{cases} C_F & (X=q), \\ C_A & (X=g). \end{cases} \tag{3.24}$$

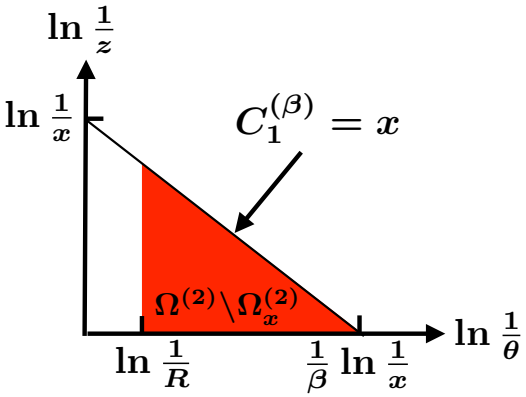

Figure 10: Set difference $\Omega^{(2)}\setminus\Omega_x^{(2)}$ in $\ln\frac{1}{\theta}$-$\ln\frac{1}{z}$ plain.

We choose as $f(z) = 1/z$ for simplicity, then

$$\Sigma_X(x) \simeq \exp\left[-\int_{\Omega^{(2)}\backslash\Omega_x^{(2)}} \left(d\ln\frac{1}{\theta}\right)\left(d\ln\frac{1}{z}\right)\frac{2\alpha_S C_X}{\pi}\right], \tag{3.25}$$

$$\Omega_x^{(2)} = \{(z,\theta) \in \mathbf{R}^2 \mid \theta < R,\ \omega_1 = z\theta^\beta < x\}, \tag{3.26}$$

$$\Omega^{(2)} = \{(z,\theta) \in \mathbf{R}^2 \mid \theta < R\}. \tag{3.27}$$

Therefore the set difference $\Omega^{(2)}\backslash\Omega_x^{(2)}$ is represented by

$$\Omega^{(2)}\backslash\Omega_x^{(2)} = \{(z,\theta) \in \mathbf{R}^2 \mid \theta < R,\ \ln\frac{1}{z} + \beta\ln\frac{1}{\theta} \geq \ln\frac{1}{x}\}, \tag{3.28}$$

which is the red region in Fig. 10. We get the CDF in soft limit as

$$\Sigma_X(x) = \exp\left(-\frac{\alpha_S C_X}{\pi\beta}\ln^2\frac{R^\beta}{x}\right). \tag{3.29}$$

The difference between quark jet and gluon jet on the cumulative distribution function come from the difference of the colour factors. The probability distribution function (PDF) for $C_1^{(\beta)}$ is given by the differential of CDF,

$$\frac{1}{\sigma_X}\frac{d\sigma_X}{dC_1^{(\beta)}} = \frac{d}{dC_1^{(\beta)}}\Sigma_X(C_1^{(\beta)}), \tag{3.30}$$

$$= \frac{2\alpha_S C_X}{\pi\beta}\frac{1}{C_1^{(\beta)}}\ln\frac{R^\beta}{C_1^{(\beta)}}\exp\left(-\frac{\alpha_S C_X}{\pi\beta}\ln^2\frac{R^\beta}{C_1^{(\beta)}}\right). \tag{3.31}$$

The factor prior to exponential in Eq. (3.31) has a singularity at $e_\beta = 0$, and actually correspond to the differential cross section for $C_1^{(\beta)}$ at lowest fixed order. The singularity is suppressed by the exponential factor, which is called as *Sudakov suppression*. The term of $\alpha_S\ln^2(\cdots)$ is in the exponent, which is called as leading logarithmic (LL) term. When we take into account finite terms in the splitting functions, the running of α_S, and so on, next-to-leading logarithmic (NLL) terms appear, which has a form of $\alpha_S\ln(\cdots)$.

In Fig. 11, the red and blue curves show $C_1^{(\beta)}$ distribution for quark jets and gluon jets in Eq. (3.31). We can see that $C_1^{(\beta)}$ for gluon jets is larger than that for quark jets statistically. The colour factor for the gluon decay is larger that for the quark's one, therefore, branchings from gluon tend to happen at a higher scale. The high scale branchings correspond to wide and/or hard emissions, so $C_1^{(\beta)}$ becomes larger.

Let us assume that the quark jets are signal and gluon jets are background. We can collect more quark jets than gluon jets by collecting jets whose $C_1^{(\beta)}$ are small. The CDF $\Sigma_q(x)$ and $\Sigma_g(x)$ show the remaining probability (efficiency) with cut $C_1^{(\beta)} < x$ (see in Eq. (3.19)). Therefore, larger value of CDF ratio like $\Sigma_q(x)/\Sigma_g(x)$

or $\ln\Sigma_g(x)/\ln\Sigma_q(x)$ means that the performance of quark-gluon discrimination is better. The ratio is given by

$$\frac{\ln\Sigma_g}{\ln\Sigma_q} = \begin{cases} \frac{C_A}{C_F} & \text{(LL)}, \\ \frac{C_A}{C_F}\left[1+\frac{n_F-C_A}{3C_A}\sqrt{\frac{\alpha_S C_F}{\pi\beta\ln\frac{1}{\Sigma_q}}}+\frac{n_F-C_A}{C_A}\frac{\alpha_S}{36\pi}\frac{b_0}{\beta}(2-\beta)+\cdots\right] & \text{(LL+NLL)}. \end{cases} \tag{3.32}$$

We can see that the ratio is not depend on β in LL approximation, however it depends on β by taking into account NLL contributions. The first and second terms come from the finite term of splitting function, and the running coupling constant. We can see more details of the NLL terms in Ref. [33]. We note that the ratio become larger as β increase, in other words, $C_1^{(\beta)}$ with smaller β more separate quark jets from gluon jets.

In Fig. 12, the β dependence of the quark-gluon discrimination with $C_1^{(\beta)}$ by using a Monte Carlo event generator `Pythia8` is shown [33]. This is a quark efficiency ($\Sigma_q(x)$) versus gluon efficiency ($\Sigma_g(x)$) plot. The curves are drawn by changing the cut value of x. Larger quark efficiency and smaller gluon efficiency means better discrimination, therefore we can see that the smaller choice of β give the better discrimination. We use $C_1^{(\beta)}$ in the following studies.

3.3 Subjet rates: Generating function method

There are several methods to calculate jet observables. Here, we introduce generating function method, which is especially useful to calculate subjet rates $R_n^f(E_j, t_{\max})$ [75,

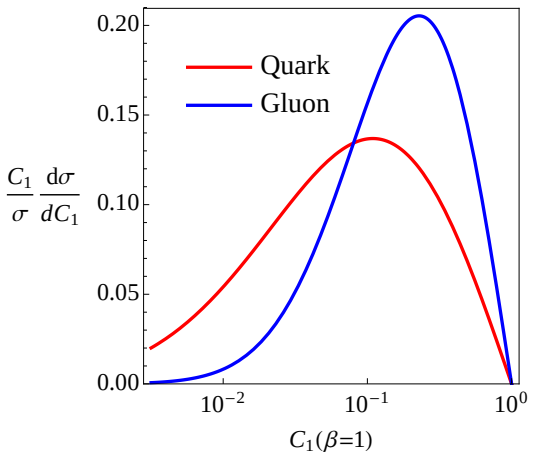

Figure 11: The red and blue curves show $C_1^{(\beta)}$ distribution for quark jets and gluon jets in Eq. (3.31). ($R = 1.0, \alpha_S = 0.12$.)

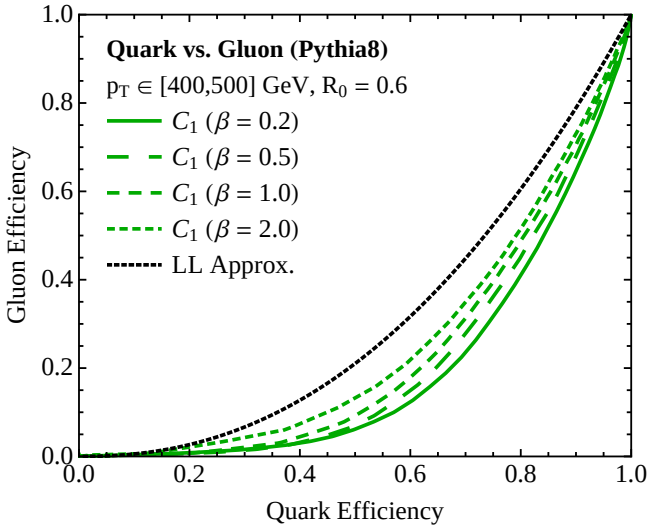

Figure 12: From Ref. [33]. The β dependence of the quark-gluon discrimination with $C_1^{(\beta)}$ by using a Monte Carlo event generator `Pythia8`. This is a quark efficiency ($\Sigma_q(x)$) versus gluon efficiency ($\Sigma_g(x)$) plot. The curves are drawn by changing the cut value of x. Larger quark efficiency and smaller gluon efficiency means better discrimination, therefore we can see that the smaller choice of β give the better discrimination.

76, 77, 78]. The subjet rates $R_n^f(E_j, t_{\max})$ show the probability that a primary parton whose flavour, energy and scale are f, E_j and $t_{\max}$ produces n jet(s). Using these subjet rates, we define generating function as

$$\phi_f(u, E_j, t_{\max}) \equiv \sum_{n=1}^{\infty} u^n R_n^f(E_j, t_{\max}). \tag{3.33}$$

We can recover n subjet rate by

$$R_n^f(E_j, t_{\max}) = \frac{1}{n!} \left. \frac{d^n \phi_f}{du^n} \right|_{u=0}. \tag{3.34}$$

Let us consider a situation that there are N primary partons in a system. For example, there are five primary partons in the situation in Fig. 13. *Whole* generating function for a given system X is just defined by the product of each generating functions:

$$\Phi_X \equiv \prod_{i=1}^{N} \phi_{f_i}(u, E_{j,i}, t_{\max,i}), \tag{3.35}$$

where f_i, $E_{j,i}$ and $t_{\max,i}$ are flavour, energy and appropriate starting scale of i-th primary partons. For example, whole generating function for $e^+e^- \to q\bar{q}$ system may be simply given by

$$\Phi_{e^+e^-} = \phi_q(u, \sqrt{s}/2, t_{\max})\phi_{\bar{q}}(u, \sqrt{s}/2, t_{\max}), \tag{3.36}$$

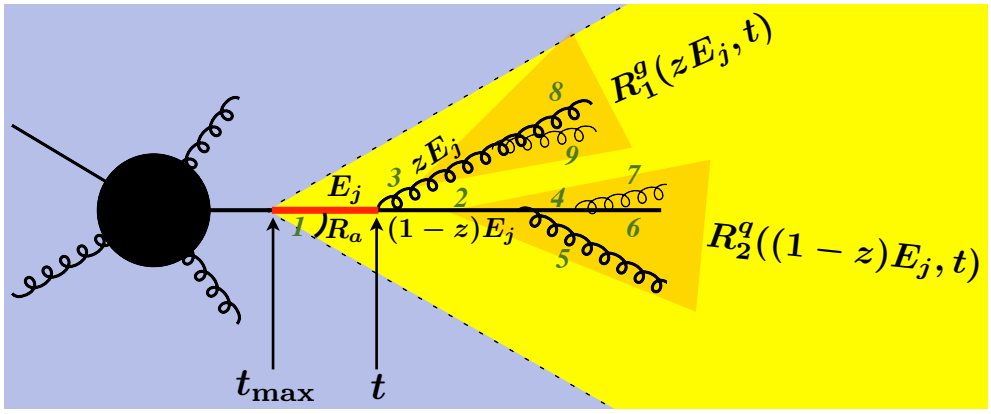

Figure 13: An example of two associated jet event. The emissions $1 \to 2, 3$ and $2 \to 4, 5$ are *resolved* emissions, and $4 \to 6, 7$ and $3 \to 8, 9$ are unresolved emissions.

where $\sqrt{s}$ is center of mass energy of e^+e^- collision. $t_{\max}$ is depend on the choice of evolution variable.[7] In the definition, we get following relation:

$$\Phi_{e^+e^-} = u^2(R_1^q R_1^{\bar{q}}) + u^3(R_1^q R_2^{\bar{q}} + R_2^q R_1^{\bar{q}}) + u^4(R_1^q R_3^{\bar{q}} + R_2^q R_2^{\bar{q}} + R_3^q R_1^{\bar{q}}) + \cdots . \quad (3.37)$$

The parenthesis of i-th term corresponds to the probability that the system has i jets. Therefore we can again recover n jet rate in the whole system by

$$\frac{1}{n!} \frac{d^n \Phi_{e^+e^-}}{du^n}\bigg|_{u=0} . \quad (3.38)$$

Let us consider $R_n^f(E_j, t_{\max})$ to deduce a basic equation for the generating function. In Fig. 13, we illustrate an example of three subjet event. The emissions $1 \to 2, 3$ and $2 \to 4, 5$ are *resolved* emissions, and $4 \to 6, 7$ and $3 \to 8, 9$ are unresolved emissions. The resolved emission mean that its emission angle is $\theta \in [R, R_a]$ and energy fraction is $z \in [E_a/E_j, 1 - E_a/E_j]$. There are three resolved subjet in the yellow region. Emitted particles generated by sequential decays can go inside another subjet. For example, emitted gluon 5 can go inside subjet whose core is gluon 3. In the case, number of subjet decrease from three to two. Such effect called as *non-global logarithms* [79]. The order of non-global logarithms is at NLL, and we neglect that in this thesis.

First, let us consider one subjet rate from a flavor i and whose energy and starting scale are E_j and $t_{\max}$, i.e., $R_1^q(E_j, t_{\max})$. This correspond to the probability that any emissions do not happen in resolved region. By recalling in Sec. 2.1 and 3.2.2, such

[7] The maximal scale will be discussed in Sec. 5, which is given by Eq. (5.5) for a general evolution variable defined by Eq. (5.1).

probability is described by the inverse of the exponentiate of total cross section over the resolved region, i.e.,

$$R_1^i(E_j, t_{\max}) = \Delta_i(E_j, t_{\max}), \tag{3.39}$$

$$\Delta_i(E_j, t) = \exp\left[-\int_{t_{\min}}^{t} \frac{dt'}{t'} \int_{\frac{E_a}{E_j}}^{1-\frac{E_a}{E_j}} dz \frac{\alpha_S(k_t^2)}{2\pi} \hat{P}_i(z) \right. \tag{3.40}$$
$$\left. \times \Theta(\theta(t,z) - R)\Theta(R_a - \theta(t,z)) \right],$$

where $t_{\max}$ and $t_{\min}$ are the maximal and minimum values of scale t. For example, when we use the virtuality, $t = q^2 = 2z(1-z)E_j^2(1-\cos\theta)$, as scale,

$$t_{\max} = \frac{E_j^2}{2}(1 - \cos R_a), \tag{3.41}$$

$$t_{\min} = 2\frac{E_a}{E_j}\left(1 - \frac{E_a}{E_j}\right)(1 - \cos R). \tag{3.42}$$

The differential three subjet rate for the configuration in Fig. 13 is described as

$$\frac{\Delta_q(E_j, t_{\max})}{\Delta_q(E_j, t)} \times \frac{dt}{t} dz \frac{\alpha_S(k_t^2)}{2\pi} \hat{P}_q(z) \times R_2^q((1-z)E_j, t) R_1^g(zE_j, t). \tag{3.43}$$

The ratio show the probability that any emissions do not happen between t and $t_{\max}$. $R_2^q((1-z)E_j, t)$ show the probability that a quark, whose energy is $(1-z)E_j$ and starting scale is t, emits two resolved partons. Then, three subjet rate have the form,

$$R_3^q(E_j, t_{\max}) = \int_{t_{\min}}^{t_{\max}} \frac{dt}{t} \int_{\frac{E_a}{E_j}}^{1-\frac{E_a}{E_j}} dz \frac{\Delta_q(E_j, t_{\max})}{\Delta_q(E_j, t)} \frac{\alpha_S(k_t^2)}{2\pi} \hat{P}_q(z) \tag{3.44}$$
$$\times [R_2^q((1-z)E_j, t) R_1^g(zE_j, t) + R_1^q((1-z)E_j, t) R_2^g(zE_j, t)].$$

For $n(>1)$ jet, we get easily as,

$$R_n^q(E_j, t_{\max}) = \sum_{k+m=n} \int_{t_{\min}}^{t_{\max}} \frac{dt}{t} \int_{\frac{E_a}{E_j}}^{1-\frac{E_a}{E_j}} dz \frac{\Delta_q(E_j, t_{\max})}{\Delta_q(E_j, t)} \frac{\alpha_S(k_t^2)}{2\pi} \hat{P}_q(z) \tag{3.45}$$
$$\times R_k^q((1-z)E_j, t) R_m^g(zE_j, t).$$

By using the generating function in Eq. (3.33), Eq. (3.39) and (3.45) are described uniformly by

$$\phi_q(u, E_j, t_{\max}) = u\Delta_q(E_j, t_{\max}) + \int_{t_{\min}}^{t_{\max}} \frac{dt}{t} \int_{\frac{E_a}{E_j}}^{1-\frac{E_a}{E_j}} dz \tag{3.46}$$
$$\times \frac{\Delta_q(E_j, t_{\max})}{\Delta_q(E_j, t)} \frac{\alpha_S(k_t^2)}{2\pi} \hat{P}_q(z) \phi_q(u, (1-z)E_j, t) \phi_g(u, zE_j, t).$$

For brevity, we use angle function as scale, i.e., $t = q^2/[2z(1-z)E_j^2] = 1-\cos\theta = \xi$. In the soft limit $(1-z)E_j \to E_j$, the equations of generating functions for quark and gluon are written by

$$\phi_q(u, E_j, \xi_a) = u\Delta_q(E_j, \xi_a) + \int_{\xi_j}^{\xi_a} \frac{d\xi}{\xi} \int_{\frac{E_a}{E_j}}^{1} dz \frac{\Delta_q(E_j, \xi_a)}{\Delta_q(E_j, \xi)} \tag{3.47}$$
$$\times \frac{\alpha_S(k_t^2)}{2\pi} \hat{P}_{qg}(z) \phi_q(u, E_j, \xi) \phi_g(u, zE_j, \xi),$$
$$\phi_g(u, E_j, \xi_a) = u\Delta_g(E_j, \xi_a) + \int_{\xi_j}^{\xi_a} \frac{d\xi}{\xi} \int_{\frac{E_a}{E_j}}^{1} dz \frac{\Delta_g(E_j, \xi_a)}{\Delta_g(E_j, \xi)} \tag{3.48}$$
$$\times \frac{\alpha_S(k_t^2)}{2\pi} \{\hat{P}_{gg}(z) \phi_g(u, E_j, \xi) \phi_g(u, zE_j, \xi) + \hat{P}_{gq}(z)[\phi_q(u, E_j, \xi)]^2\},$$

where $\xi_j = 1-\cos R$, $\xi_a = 1-\cos R_a$, and $\hat{P}_{qg}$, $\hat{P}_{gg}$ and $\hat{P}_{gq}$ are splitting functions for $q \to qg$, $g \to gg$ and $g \to q\bar{q}$ in Eq. (2.6). We use a relation $\phi_q = \phi_{\bar{q}}$. In the choice of scale, Sudakov form factor in Eq. (3.40) is simply written by

$$\Delta_q(E_j, \xi) = \exp\left[-\int_{\xi_j}^{\xi} \frac{d\xi'}{\xi'} \int_{\frac{E_a}{E_j}}^{1} dz \frac{\alpha_S(k_t^2)}{2\pi} \hat{P}_{qg}(z) \right], \tag{3.49}$$

$$\Delta_g(E_j, \xi) = \exp\left[-\int_{\xi_j}^{\xi} \frac{d\xi'}{\xi'} \int_{\frac{E_a}{E_j}}^{1} dz \frac{\alpha_S(k_t^2)}{2\pi} \{\hat{P}_{gg}(z) + n_f \hat{P}_{gq}(z)\} \right], \tag{3.50}$$

where n_f is number of active flavors. We can eliminate Sudakov factors from the equations as

Eq. (3.47)

$$\Leftrightarrow \frac{\phi_q(u, E_j, \xi)}{\Delta_q(E_j, \xi)} = u + \int_{\xi_j}^{\xi} \frac{d\xi'}{\xi'} \int_{\frac{E_a}{E_j}}^{1} dz \frac{\alpha_S(k_t^2)}{2\pi} \hat{P}_{qg}(z) \frac{\phi_q(u, E_j, \xi')}{\Delta_q(E_j, \xi')} \phi_g(u, zE_j, \xi'),$$

$$\Rightarrow \frac{d}{d\xi}\left(\frac{\phi_q(u, E_j, \xi)}{\Delta_q(E_j, \xi)} \right) = \frac{1}{\xi} \int_{\frac{E_a}{E_j}}^{1} dz \frac{\alpha_S(k_t^2)}{2\pi} \hat{P}_{qg}(z) \left(\frac{\phi_q(u, E_j, \xi)}{\Delta_q(E_j, \xi)} \right) \phi_g(u, zE_j, \xi),$$

$$\Rightarrow \ln \frac{\phi_q(u, E_j, \xi_a)}{\Delta_q(E_j, \xi_a)} - \ln \frac{\phi_q(u, E_j, \xi_j)}{\Delta_q(E_j, \xi_j)} = \int_{\xi_j}^{\xi_a} \frac{d\xi}{\xi} \int_{\frac{E_a}{E_j}}^{1} dz \frac{\alpha_S(k_t^2)}{2\pi} \hat{P}_{qg}(z) \phi_g(u, zE_j, \xi),$$

Then we get

$$\phi_q(u, E_j, \xi_a) = u \exp\left\{ \int_{\xi_j}^{\xi_a} \frac{d\xi}{\xi} \int_{\frac{E_a}{E_j}}^{1} dz \frac{\alpha_S(k_t^2)}{2\pi} \hat{P}_{qg}(z)[\phi_g(u, zE_j, \xi) - 1] \right\}, \tag{3.51}$$

where we use a trivial relation $\phi_q(u, E_j, \xi_j) = u$, which means that any primary partons whose starting angular-scale is ξ_j never emit resolved emissions. Likewise,

we get a following equation for the gluon generating function:

$$\phi_g(u, E_j, \xi_a) = u \exp\left\{ \int_{\xi_j}^{\xi_a} \frac{d\xi}{\xi} \int_{\frac{E_a}{E_j}}^{1} dz \frac{\alpha_S(k_t^2)}{2\pi} \Big(\hat{P}_{gg}(z)[\phi_g(u, zE_j, \xi) - 1] + \hat{P}_{gq}(z)[\frac{\phi_q(u, zE_j, \xi)^2}{\phi_g(u, zE_j, \xi)} - 1] \Big) \right\}. \tag{3.52}$$

We can solve the gluon generating function by iteration, and then substitute in this equation to get the complete solution.

3.3.1 Double logarithmic accuracy

In this subsection, we solve subjet rates at double logarithmic accuracy (DLA). DLA means that we consider only terms which have the form $\alpha_S^m \ln^{2m}(\cdots)$.

For brevity we define the following logarithms:

$$\kappa = \ln(E_j/E_a), \quad \kappa' = \ln(zE_j/E_a), \tag{3.53}$$

$$\lambda = \ln(\xi_a/\xi_j), \quad \lambda' = \ln(\xi/\xi_j), \tag{3.54}$$

We set a reference relative transverse momentum $\overline{k_t}^2 \equiv E_j^2 \xi_a$, and strong coupling constant by

$$\overline{\alpha}_S \equiv \frac{\alpha_S(\overline{k_t}^2)}{\pi} = \frac{1}{b_0 \ln(E_j^2 \xi_a / \Lambda^2)}. \tag{3.55}$$

By using this, we expand coupling constant by

$$\frac{\alpha_S(k_t^2 = z^2 E_j^2 \xi)}{\pi} = \frac{1}{b_0 \ln(z^2 E_j^2 \xi / \Lambda^2)}, \tag{3.56}$$

$$\simeq \overline{\alpha}_S - b_0 \overline{\alpha}_S^2 [2 \ln z + \ln(\xi/\xi_j)], \tag{3.57}$$

$$= \overline{\alpha}_S - b_0 \overline{\alpha}_S^2 [2(\kappa' - \kappa) + \lambda']. \tag{3.58}$$

In DLA, we neglect the non-singular terms of splitting functions, i.e., $\hat{P}_{qg,gg} \simeq 2C_{q,g}/z$, $\hat{P}_{gq}$, and $\overline{\alpha}_S^2$ term in the coupling constant, where $C_{q,g} = C_{F,A}$. Then, from Eq. (3.47, 3.48),

$$\phi_i(u, \kappa, \lambda) \equiv \phi_i(u, E_j, \xi_a) \tag{3.59}$$

$$\simeq u \exp\left\{ \int_{\xi_j}^{\xi_a} \frac{d\xi}{\xi} \int_{E_a/E_j}^{1} dz \frac{\overline{\alpha}_S}{2} \frac{2C_i}{z} [\phi_g(u, zE_j, \xi) - 1], \right\}, \tag{3.60}$$

$$= u \ \mathrm{e}^{-a_i \kappa \lambda} \mathrm{e}^{f_i}, \tag{3.61}$$

where

$$a_i = C_i \overline{\alpha}_S, \qquad f_i = a_i \int_0^\lambda d\lambda' \int_0^\kappa d\kappa' \phi_g(u, \kappa', \lambda'). \tag{3.62}$$

We want to know the differentiate of generating functions. We write as:

$$f_i^{(n)} \equiv \frac{\partial^n}{\partial u^n} f_i, \qquad \phi_i^{(n)} \equiv \frac{\partial^n}{\partial u^n} \phi_i, \tag{3.63}$$

Then,

$$\phi_i^{(1)} = \mathrm{e}^{-a_i \kappa \lambda} [1 + u f_i^{(1)}] \mathrm{e}^{f_i}, \tag{3.64}$$

$$\phi_i^{(2)} = \mathrm{e}^{-a_i \kappa \lambda} [1 + u f_i^{(1)}] \mathrm{e}^{f_i} f_i^{(1)} + \mathrm{e}^{-a_i \kappa \lambda} [f_i^{(1)} + u f_i^{(2)}] \mathrm{e}^{f_i}. \tag{3.65}$$

Using trivial relations $\phi_i(u = 0, \kappa, \lambda) = 0$ and $f_i|_{u=0} = 0$,

$$\phi_i^{(1)}|_{u=0} = \mathrm{e}^{-a_i \kappa \lambda}, \tag{3.66}$$

$$\phi_i^{(2)}|_{u=0} = 2\mathrm{e}^{-a_i \kappa \lambda} f_i^{(1)}|_{u=0}, \tag{3.67}$$

where

$$f_i^{(1)}|_{u=0} = a_i \int_0^\lambda d\lambda' \int_0^\kappa d\kappa' \phi_g^{(1)}(u, \kappa', \lambda')|_{u=0}, \tag{3.68}$$

$$= a_i \int_0^\lambda d\lambda' \int_0^\kappa d\kappa' \mathrm{e}^{-a_g \kappa' \lambda'}, \tag{3.69}$$

$$= \frac{a_i}{a_g} \mathrm{Ein}(a_g \kappa \lambda), \tag{3.70}$$

where Ein is the entire exponential integral function

$$\mathrm{Ein}(z) = \int_0^z \frac{dt}{t} (1 - \mathrm{e}^{-t}) = -\sum_{k=1}^\infty \frac{(-z)^k}{k \; k!}. \tag{3.71}$$

Therefore we get subjet rates for $n = 1$ and 2 at DLA:

$$R_1^i(E_j, \xi_a) = \mathrm{e}^{-a_i \kappa \lambda}, \tag{3.72}$$

$$R_2^i(E_j, \xi_a) = \mathrm{e}^{-a_i \kappa \lambda} \frac{a_i}{a_g} \mathrm{Ein}(a_g \kappa \lambda). \tag{3.73}$$

3.3.2 Next-to-double logarithmic accuracy

In this subsection, we solve subjet rates at next-to-double logarithmic accuracy (NDLA). NDLA means that we consider terms which have the form not only $\alpha_S^m \ln^{2m}(\cdots)$ but also $\alpha_S^m \ln^{2m-1}(\cdots)$.

First we define three Γ_X functions:

$$\Gamma_q(\kappa',\lambda',\kappa,\lambda) \equiv \frac{\alpha_S(k_t^2)}{2\pi} z\hat{P}_{qg}(z), \tag{3.74}$$

$$\Gamma_g(\kappa',\lambda',\kappa,\lambda) \equiv \frac{\alpha_S(k_t^2)}{2\pi} z\hat{P}_{gg}(z), \tag{3.75}$$

$$\Gamma_f(\kappa',\kappa) \equiv n_f \frac{\alpha_S(k_t^2)}{2\pi} z\hat{P}_{gq}(z). \tag{3.76}$$

These have the following forms

$$\begin{aligned}\Gamma_q(\kappa',\lambda',\kappa,\lambda) &= \frac{C_F\overline{\alpha}_S}{2}[1+(1-z)^2] - \frac{b_0 C_F\overline{\alpha}_S^2}{2}[2\ln z + \ln(\xi/\xi_a)][1+(1-z)^2], \\ &\simeq C_F\overline{\alpha}_S[1-\mathrm{e}^{\kappa'-\kappa}+\mathrm{e}^{2(\kappa'-\kappa)}/2] - C_F b_0\overline{\alpha}_S^2[2(\kappa'-\kappa)+\lambda'-\lambda],\end{aligned} \tag{3.77}$$

where we neglect the sub-leading term of splitting function in $\overline{\alpha}_S^2$ term, namely $1-z\to 1$. Likewise,

$$\begin{aligned}\Gamma_g(\kappa',\lambda',\kappa,\lambda) \simeq C_A\overline{\alpha}_S[1-\mathrm{e}^{\kappa'-\kappa}+\mathrm{e}^{2(\kappa'-\kappa)}/2-\mathrm{e}^{3(\kappa'-\kappa)}/2] \\ - C_A b_0\overline{\alpha}_S^2[2(\kappa'-\kappa)+\lambda'-\lambda],\end{aligned} \tag{3.78}$$

where we use

$$P_{gg}(z) = \frac{1-z}{z} + \frac{z}{1-z} + z(1-z), \tag{3.79}$$

$$\to 2\frac{1-z}{z} + z(1-z), \tag{3.80}$$

to shift the singularity on second term to first term. P_{gq} doesn't have singularity, so Γ_f start from NLL term. Then we neglect $\overline{\alpha}_S^2$ term, and get

$$\Gamma_f(\kappa',\kappa) \simeq \frac{n_f}{4}\overline{\alpha}_S[\mathrm{e}^{\kappa'-\kappa} - 2\mathrm{e}^{2(\kappa'-\kappa)} + 2\mathrm{e}^{3(\kappa'-\kappa)}]. \tag{3.81}$$

Using Γ_X, the Sudakov form factors in Eq. (3.49) and (3.50) are written by

$$\Delta_q(\kappa,\lambda) = \exp\left\{-C_F\overline{\alpha}_S\lambda\left[\kappa - \frac{3}{4} + \mathrm{e}^{-\kappa} - \frac{1}{4}\mathrm{e}^{-2\kappa}\right] - C_F b_0\overline{\alpha}_S^2\kappa\lambda\left[\kappa+\frac{1}{2}\lambda\right]\right\} \tag{3.82}$$

$$\begin{aligned}\Delta_g(\kappa,\lambda) = \exp\Bigg\{-C_A\overline{\alpha}_S\lambda\left[\kappa - \frac{11}{12} + \mathrm{e}^{-\kappa} - \frac{1}{4}\mathrm{e}^{-2\kappa} + \frac{1}{6}\mathrm{e}^{-3\kappa}\right] - C_A b_0\overline{\alpha}_S^2\kappa\lambda\left[\kappa+\frac{1}{2}\lambda\right] \\ -\frac{n_f}{4}\overline{\alpha}_S\lambda[\frac{2}{3} - \mathrm{e}^{-\kappa} + \mathrm{e}^{-2\kappa} - \frac{2}{3}\mathrm{e}^{-3\kappa}]\Bigg\}.\end{aligned} \tag{3.83}$$

Using Γ_X and Sudakov form factor, the generating function for quark in Eq. (3.51) is written by

$$\phi_q(u,\kappa,\lambda) = u\Delta_q(\kappa,\lambda)\mathrm{e}^F, \tag{3.84}$$

$$F = \int_0^\lambda d\lambda' \int_0^\kappa d\kappa' \Gamma_q(\kappa',\lambda',\kappa,\lambda)\phi_g(u,\kappa',\lambda'). \tag{3.85}$$

The generating function for gluon in Eq. (3.52) is expanded by

$$\begin{aligned}
\phi_g(u,\kappa,\lambda) &= u\Delta_g(\kappa,\lambda)\exp\left[\int_0^\lambda d\lambda'\int_0^\kappa d\kappa'\Big\{\Gamma_g(\kappa',\lambda',\kappa,\lambda)\phi_g(u,\kappa',\lambda')\right.\\
&\qquad\left.+\Gamma_f(\kappa',\kappa)\frac{[\phi_q(u,\kappa,\lambda')]^2}{\phi_g(u,\kappa,\lambda')}\Big\}\right],\\
&= u\Delta_g(\kappa,\lambda)\left[1+\int_0^\lambda d\lambda'\int_0^\kappa d\kappa'\Big\{\Gamma_g(\kappa',\lambda',\kappa,\lambda)\phi_g(u,\kappa',\lambda')\right.\\
&\qquad\left.+\Gamma_f(\kappa',\kappa)\frac{[\phi_q(u,\kappa,\lambda')]^2}{\phi_g(u,\kappa,\lambda')}\Big\}+\mathcal{O}(u^2)\right],\\
&= u\Delta_g(\kappa,\lambda)\left[1+\int_0^\lambda d\lambda'\int_0^\kappa d\kappa'\Big\{\Gamma_g(\kappa',\lambda',\kappa,\lambda)[u\Delta_g(\kappa',\lambda')+\mathcal{O}(u^2)]\right.\\
&\qquad\left.+\Gamma_f(\kappa',\kappa)\frac{[u\Delta_q(\kappa,\lambda')+\mathcal{O}(u^2)]^2}{u\Delta_g(\kappa,\lambda')+\mathcal{O}(u^2)}\Big\}+\mathcal{O}(u^2)\right],\\
&= u\Delta_g(\kappa,\lambda)\left[1+u\int_0^\lambda d\lambda'\int_0^\kappa d\kappa'\Big\{\Gamma_g(\kappa',\lambda',\kappa,\lambda)\Delta_g(\kappa',\lambda')\right.\\
&\qquad\left.+\Gamma_f(\kappa',\kappa)\Delta_f(\kappa,\lambda')\Big\}+\mathcal{O}(u^2)\right],
\end{aligned}\tag{3.86}$$

where $\Delta_f \equiv \Delta_g^2/\Delta_q$. Therefore we get subjet rates for $n=1$ and 2 at NDLA:

$$R_1^i(\kappa,\lambda) = \phi_i^{(1)}(u,\kappa,\lambda)|_{u=0} = \Delta_i(\kappa,\lambda), \tag{3.87}$$

$$\begin{aligned}
R_2^q(\kappa,\lambda) &= \frac{1}{2!}\phi_q^{(2)}(u,\kappa,\lambda)|_{u=0}, \qquad (3.88)\\
&= \Delta_q(\kappa,\lambda)\int_0^\lambda d\lambda'\int_0^\kappa d\kappa'\Gamma_g(\kappa',\lambda',\kappa,\lambda)\Delta_g(\kappa',\lambda'),
\end{aligned}$$

$$\begin{aligned}
R_2^g(\kappa,\lambda) &= \frac{1}{2!}\phi_g^{(2)}(u,\kappa,\lambda)|_{u=0}, \qquad (3.89)\\
&= \Delta_q(\kappa,\lambda)\int_0^\lambda d\lambda'\int_0^\kappa d\kappa'[\Gamma_g(\kappa',\lambda',\kappa,\lambda)\Delta_g(\kappa',\lambda')+\Gamma_g(\kappa',\lambda',\kappa,\lambda)\Delta_g(\kappa',\lambda')],
\end{aligned}$$

For $n \geq 2$, we need numerical integration.

3.3.3 Results: subjet rates

In Fig. 14, the analytical and numerical calculations of subjet rates at DLA (black curves) and NDLA (red curves) are shown. We set $R = 0.4$, $R_a = 0.8$ and $E_a = 20$ GeV. The difference between DLA and NDLA is up to 5% in the energy range. These results say that gluon emits much of jets compare to quark. This mainly stems from the colour factor of gluon branching is larger than that of quark's one.

In Sec. 4, we compare the results obtained by generating function methods and those by Monte Carlo event generators, and demonstrate that the performance of

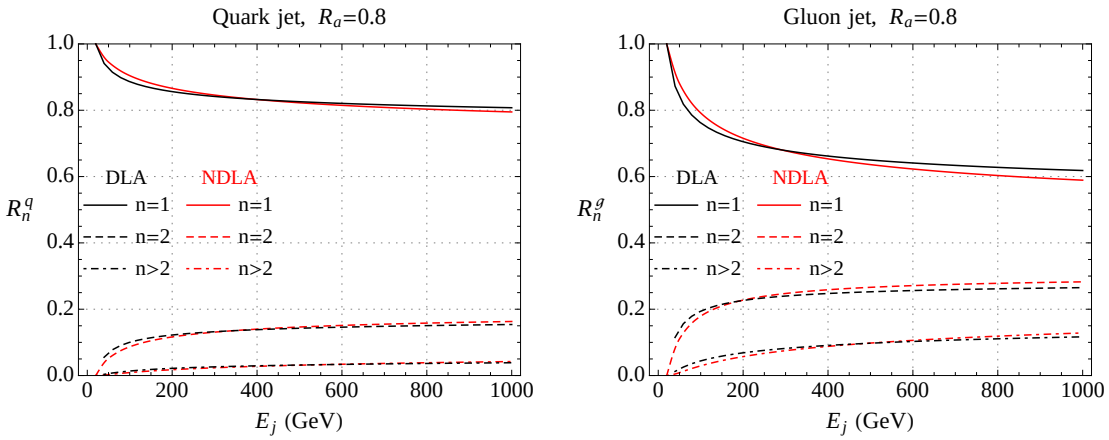

Figure 14: The analytical and numerical calculations of subjet rates at DLA (black curves) and NDLA (red curves) are shown. We set $R = 0.4$, $R_a = 0.8$ and $E_a = 20$ GeV. The difference between DLA and NDLA is up to 5% in the energy range.

quark-gluon discrimination improves by using not only jet substructure variables but also subjet information.

4 Associated jet and subjet rates in light-quark and gluon jet discrimination

In the LHC environment, in order to keep the contribution of the underlying event and multiple proton-proton collisions at a minimum, for multijet processes the standard choice is an anti-k_t algorithm with radius parameter $R = 0.4$. In addition, in the ATLAS study mentioned above, jets are required to satisfy an isolation criterion: a jet is considered isolated if there is no other reconstructed jet within a cone of size $\Delta R < 0.7$ (where $\Delta R = \sqrt{(\Delta\eta)^2 + (\Delta\phi)^2}$ is the standard distance measure in the pseudorapidity-azimuthal angle plane). An optimum choice for the jet radius parameter was discussed in Refs. [80, 81] for quark and gluon jets as a function of their transverse momenta (p_T), and it was observed that one usually requires a larger radius for a gluon jet in order for the parton p_T to be close to the jet p_T. However, for experimental purposes it is advantageous to use a fixed and small radius parameter for the jets, for reasons mentioned above. Therefore, we propose to recover the missed information on radiation from the parent parton outside the chosen jet radius by including softer reconstructed jets that can be present (with a calculable probability) around a certain radius of a primary hard jet. These softer jets are referred to as "associated jets" in this study. It is important to note here that imposing an isolation criterion as above while studying quark and gluon jet properties might not be appropriate, since it leads to rejecting a fraction of the jet candidates beforehand, and thus biasing the sample to ones where the initial quark or gluon has not radiated outside the adopted jet radius.

We first define the associated jet rates and compare the analytical results with those from different parton shower MC's in Sec. 4.1. Using the information on the presence (or absence) of associated jets can improve the discrimination of quarks and gluons. We demonstrate this through a multivariate analysis in Sec. 4.2. Several combinations of jet discrimination variables are tried out, and an attempt is made to determine an optimum choice. Even though we include standard discrimination variables like the number of charged tracks as inputs to our multivariate analysis, it should be emphasized that they are subject to MC ambiguities stemming from parton shower algorithms and their associated parameters, and tunings of hadronization and underlying event (UE) models. However, in order to judge the improvement in tagger performance on using the associated jet rates, we compare the performance of different sets of variables within the same MC.

In Secs. 4.3 and 4.4 we study the use of the number of subjets of a jet (defined with an exclusive k_t algorithm) in place of the number of charged tracks, since the

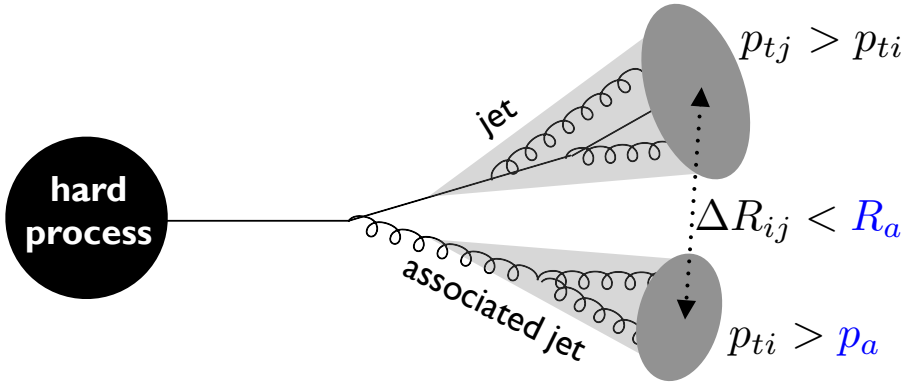

Figure 15: A schematic illustration of associated jets, and the relevant variables which determine the associated jet rate (see text for details).

different MC prediction tend to be similar for the former observable. We compute the subjet rates upto NDLA as well, and compare the NDLA results with predictions from different MC generators. Our results on both associated jets and subjets are summarized in Sec. 6. We discuss the 2-dimensional joint distributions of the three discrimination variables used as inputs in the multivariate analysis in an App. A.

4.1 Associated jet rates

Once a primary jet j has been defined, say using the anti-k_t algorithm with radius parameter R, we define a nearby jet i with $p_{tj} > p_{ti} > p_a$ and $R < \Delta R_{ij} < R_a$ as an *associated jet*. Thus the associated jet rates are functions of the primary jet $p_t = p_j$, its radius R, the association radius R_a and the minimum associated jet $p_t = p_a$. In Fig. 15 we illustrate the idea of an associated jet schematically, and show the relevant variables that determine the associated jet rate.

In perturbative QCD, the rate of n-jet production from a primary object of type i ($i = q, g$ in this case), R^i_n, can be obtained from the associated generating function as discussed in Sec. 3.3

$$\phi_i(u) = \sum_n R^i_n u^n \,. \tag{4.1}$$

We can recover the jet rates by differentiating at $u = 0$,

$$R^i_n = \frac{1}{n!} \left. \frac{d^n \phi_i}{du^n} \right|_{u=0} \,. \tag{4.2}$$

The jet rates $R^i_n = R^i_n(p_j, \xi)$ are functions of the trigger jet transverse momentum p_j, and the evolution scale for parton showering, which, for hadron-hadron collisions is taken as $\xi = \Delta R^2/2$. This is equivalent to the evolution scale for coherent parton showering, $\xi \equiv 1 - \cos\theta$, with θ being the emission angle ($\Delta R^2/2 \approx \theta^2/2 \approx 1 - \cos\theta$).

To be resolved, an emission must have $\xi > \xi_j = R^2/2$ and $p_t > p_a$. Since the jet rates R^i_n include the trigger jet j, the probability of n *associated jets* for a jet of type i with transverse momentum p_j is

$$P^i_n = R^i_{n+1}(p_j, \xi_a) \; . \tag{4.3}$$

Here, $\xi_a = R_a^2/2$, with R_a being the association radius defined above. We have already calculated the subjet rates in Sec. 3.3. The argument was energy rather than transverse momentum. Recalling the calculation, the argument have been used for the definition of fraction variable z, see Eq. (3.46), and scale of strong coupling constant in Eq. (3.55). Energy and transverse momentum fraction are similar for collinear emissions and scale of strong coupling constant is transverse momentum rather than energy in hadron collisions. Therefore it is a good approximation to use the subjet rates in Eqs. (3.87)-(3.89) by substituting $E_j \to p_j$ in the case of hadron collisions.

We are now in a position to compare the NDLA predictions for associated jet rates discussed in the previous section with the results obtained using the `Herwig++` [41] and `Pythia8` [39] event generators [8], where the quark- and gluon-initiated jets are simulated using the $Z + q$ and $Z + g$ processes at leading order in QCD (with the Z boson subsequently decayed to $\nu\bar{\nu}$). The event samples were generated for proton-proton collisions at the 13 TeV LHC, using the `CTEQ6L1` [82] parton distribution functions (PDF) for the `Pythia` generators and the default `MRST LO**` [83] PDF and UE model for `Herwig++`. Subsequently, we used a modified version of `DELPHES2` [84] for including detector effects. For observables based on charged tracks to be discussed in the following, we use a minimum p_T threshold of 1 GeV for each track. All jets are reconstructed with an anti-k_t algorithm [66, 70] with radius parameter $R = 0.4$, and are required to have $p_T > 20$ GeV. In addition, the leading jet is required to be central with $|\eta| < 2$.

In Fig. 16 we show the probability of obtaining n associated jets P_n as a function of the jet p_T for $n = 0, 1$ and $n > 1$, for quark- and gluon-initiated jets, in the left and right columns respectively. The association radius is set to be $R_a = 0.8$ and the minimum associated jet transverse momentum is $p_a = 20$ GeV. In the MC simulations, P_n has been computed as a function of $p_T(j_s)$, which is the vector sum of the leading jet and associated jet p_T's. The jet rates are studied as a function of $p_T(j_s)$, as it is closer to the transverse momentum of the parton that initiates the final state shower.

We see that the functional behaviour with respect to the jet p_T in the MC compu-

[8] To be specific, we use `Herwig++ 2.7.0` and `Pythia 8.201` (tune `4C`) for all our calculations.

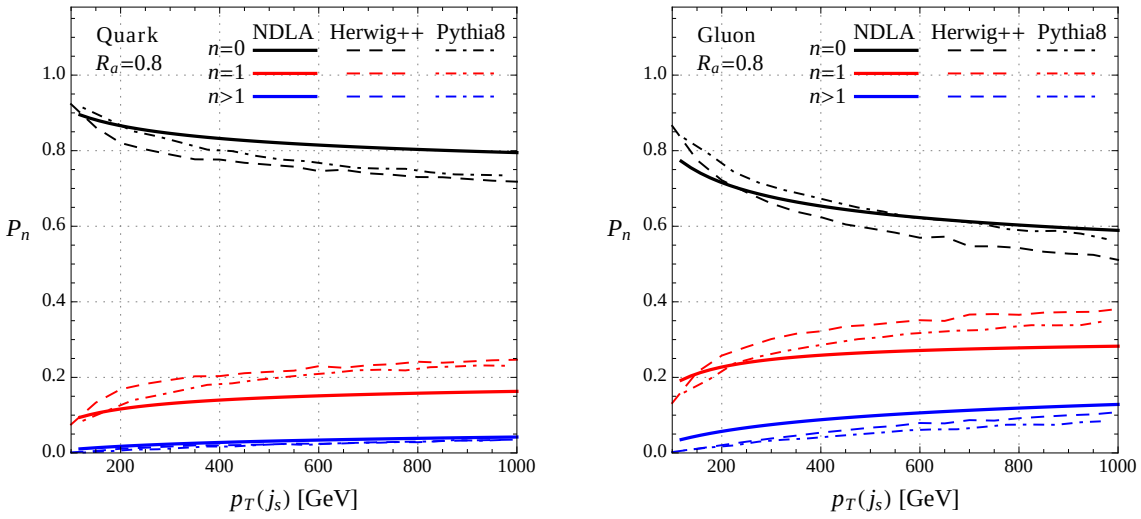

Figure 16: Comparison of the `Herwig++` and `Pythia8` MC predictions for associated jet rates with the NDLA results, as a function of $p_T(j_s)$: for quark jets (left), and gluon jets (right), with $R_a = 0.8$ and $p_a = 20$ GeV. Here, $p_T(j_s)$ is the vector sum of the leading jet and associated jet p_T's.

tation [9] and the NDLA calculation are similar, although there are some differences in the values of P_n. In particular, the MC prediction of P_1 for quark and gluon jets is higher than the NDLA result, especially at higher $p_T(j_s)$, with `Herwig++` giving rise to a slightly larger P_1 compared to `Pythia8`. For a quark jet, the probability of having at least one associated jet ranges from around 15% to 25% as we go from $p_T(j_s) = 200$ GeV to $p_T(j_s) = 500$ GeV and at higher $p_T(j_s)$ the probability essentially remains the same. For gluon jets, the corresponding probability ranges from around 30% to 40% as we go from $p_T(j_s) = 200$ GeV to $p_T(j_s) = 500$ GeV. The larger probability to have an associated jet around a gluon can thus be utilized to better discriminate it from quarks, as we shall see in the next section.

The NDLA computation includes only the time-like showering of the final state partons, and ignores some power-suppressed effects due to momentum conservation and hadronization. On the other hand, the MC results shown above include momentum conservation and hadronization as well as the effects of initial state radiation (ISR) and multiple interaction (MPI). In order to quantify the effect of ISR and MPI, we compare the predictions for P_n with and without ISR and MPI in `Herwig++`, `Pythia8` as well as in `Pythia6` [38] (we use the version `Pythia 6.4.28`

[9] For the associated jet rate calculations, we generated MC event samples with a statistics of 20,000 events each fixing the threshold for the minimum leading jet p_T at $50 \times (i+1)$ GeV, for $i \in [0, 19]$. Only events with the leading jet $p_T(j_s)$ above the generation threshold are used in the analysis. This ensures uniform MC statistics in the whole range of $p_T(j_s)$.

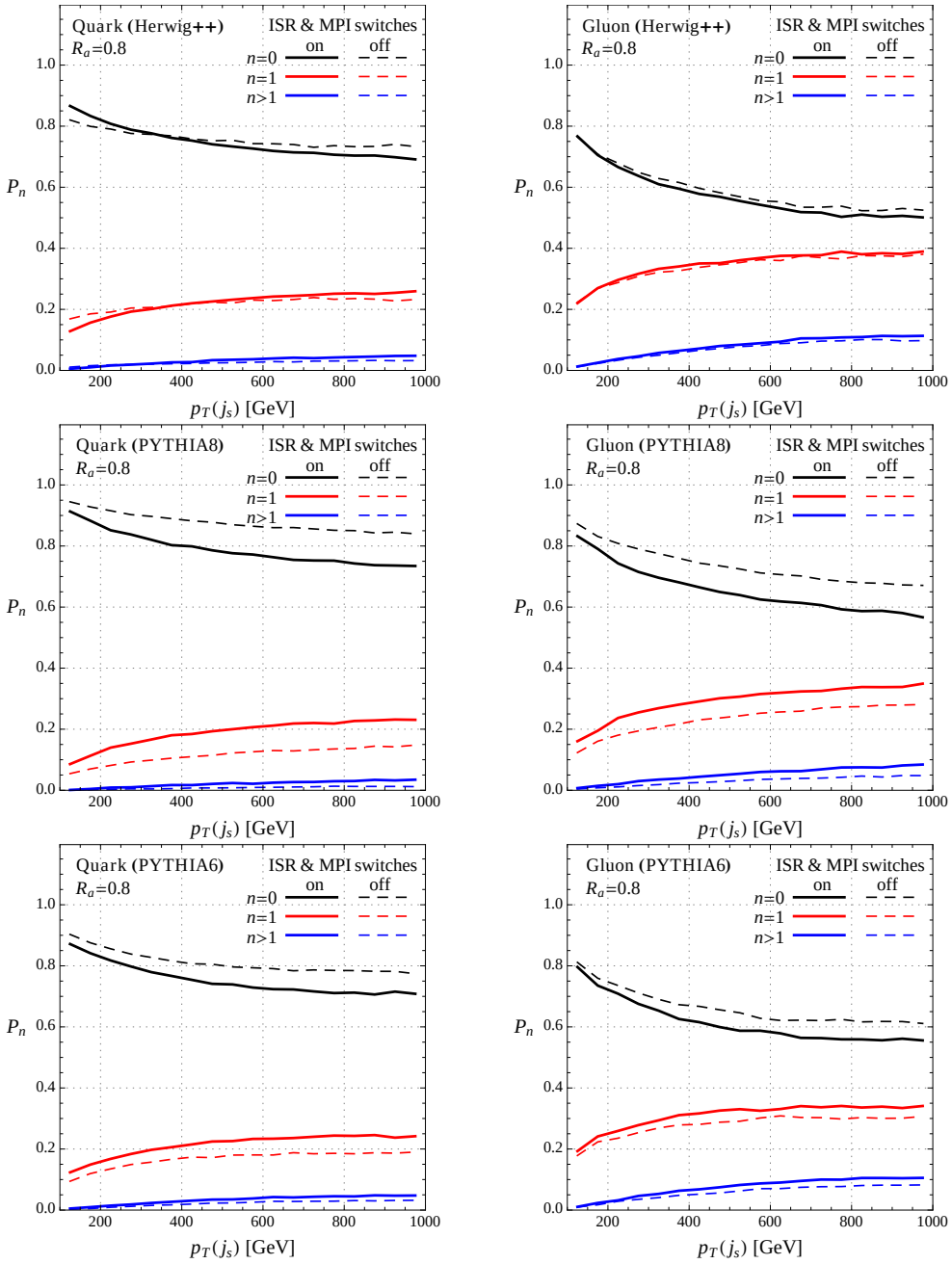

Figure 17: Comparison of the `Herwig++`, `Pythia8` and `Pythia6` predictions for associated jet rates with and without ISR and MPI, as a function of $p_T(j_s)$: for quark jets (left), and gluon jets (right). Here, $p_T(j_s)$ is the vector sum of the leading jet and associated jet p_T's.

with the `AUET2B-CT6L` tune) in Fig. 17. It is clear from this figure that the impact of ISR and MPI is rather small for our choice of the association radius $R_a = 0.8$, thereby making the predictions stable against such effects. For this choice of R_a, we can see that `Pythia8` shows the highest variation against such effects, followed by

Pythia6, while the effects are indeed negligible for the case of Herwig++ [10]. Furthermore, the MC results become closer to the NDLA ones when ISR and MPI effects are switched off.

We also investigated the effects of momentum conservation, by changing the recombination scheme in the anti-k_t jet algorithm from the default E-scheme to the "winner-take-all" scheme introduced in [85], which is less sensitive to recoils in the parton shower [73]. Such a change increases the MC associated jet rates very slightly. We believe this is because the axis of the leading jet is moved away from the overall momentum vector of the system. The effects are roughly proportional for quark and gluon jets, so they would not affect discrimination significantly.

4.2 Quark-gluon separation: multivariate analysis

4.2.1 Variables for quark-gluon separation

A large number of variables have been surveyed in the context of quark-gluon discrimination, constructed out of either track based observables or calorimeter based ones [27, 28, 29, 33, 34]. While the former category has the practical advantage of being more accurate due to better track momentum resolution as well as being less prone to pile-up contamination, the latter category can be used for jets with larger rapidities outside the tracker coverage. The most widely studied variables include the number of charged tracks inside the jet cone ($n_{\rm ch}$), the jet width [27] and two-point energy correlation function [33]. The jet width is defined as

$$w = \frac{\sum_i p_{T,i} \times \Delta R(i,\ \text{jet})}{\sum_i p_{T,i}} \tag{4.4}$$

where the sum goes over all the tracks associated to the jet. For hadron collider, the two-point energy correlation function variable $C_1^{(\beta)}$ introduced in Sec. 3.2.2 can be defined as

$$C_1^{(\beta)} = \frac{\sum_i \sum_j p_{T,i} \times p_{T,j} \times (\Delta R(i,j))^\beta}{(\sum_i p_{T,i})^2}. \tag{4.5}$$

Here again the sum over i and j run over all the tracks associated to the jet with $j > i$, while β is a tunable parameter. It has been demonstrated in Ref. [29, 33] that smaller values of the exponent β leads to a better quark-gluon separation, and $\beta = 0.2$ is found to be optimal from perturbative calculations and MC studies based on Herwig++ and Pythia8 generators. We have compared the performance of the jet width variable w and the variable $C_1^{(\beta=0.2)}$ in the multivariate analyses (MVA) to

[10] However, we have checked that if we take a larger association radius, $R_a > 1.2$, the ISR effects become appreciable in Herwig++.

be discussed below, and find that in all cases $C_1^{(\beta=0.2)}$ leads to a better separation of gluons from quarks. Therefore, in the following, we only show results based on $n_{\rm ch}$ (with each charged track having $p_T > 1$ GeV) and $C_1^{(\beta=0.2)}$. In addition, we shall include the associated jet information as well as the jet mass variable and compare the performance of the different MVA methods. As seen in the previous section, for $n = 1$ or $n > 1$, the probability of finding n associated jets, P_n, is significantly larger for gluon jets compared to quark-initiated ones across the whole p_T range of interest. Therefore, the presence (or absence) of an associated jet within a certain distance R_a of a high-p_T jet can be used to further improve the separation.

As the boundary between the signal and background regions in the hyper-surface spanned by the variables is non-linear, it is beneficial to adopt a multivariate analysis strategy as compared to a cut-based one. For this purpose, we employed a Boosted Decision Tree (BDT) algorithm with the help of the `TMVA-Toolkit` [86] in the `ROOT` framework. The training of the classifier was performed with Z+$q-$jet and Z+$g-$jet samples, and we generated the above MC samples uniformly distributed in jet-p_T [11]. The input variables for the two variable training are taken to be $n_{\rm ch}$ and $C_1^{(\beta=0.2)}$, while for three-variable trainings we further include the variable $m_J/p_{T,J}$, where m_J is the jet mass and $p_{T,J}$ is the transverse momentum of the leading jet. The information on the number of associated jets is included in the form of two categories ($n = 0$ or $n \geq 1$) in the MVA.

It should be emphasized that the MC prediction of the discrimination variables, especially the number of charged tracks $n_{\rm ch}$ is quite sensitive not only to the parton shower (PS) algorithm adopted and the related parameters, but also to the tuning of the hadronization and underlying event models. This is expected, since $n_{\rm ch}$ is not an infrared safe quantity, and only the ratio $n_{\rm ch}^{\rm gluon}/n_{\rm ch}^{\rm quark}$ converges rather slowly to the ratio of the colour factors C_A/C_F for high jet p_T [87]. The disagreement between different MC generators can therefore be reduced only by appropriate tuning at the LHC energies. With this limitation of the MC predictions in view, in this study, we compare the performance of different MVA methods within the same MC generator to estimate the improvement in adding associated jet related observables. We also show the quark-gluon separation as predicted by the different MC generators for comparison. In App. A we present details of the distributions of the discrimination variables and the differences between the MC predictions for them.

[11] The MC event samples for the training of the classifier were generated in the same manner as for the associated jet rate computation in the previous section, but with a smaller step size of 10 GeV for the minimum $p_T(j_s)$ thresholds.

4.2.2 Performance in MVA

Based on the BDT analysis, we obtain the efficiencies of tagging quark (ϵ_q) and gluon jets (ϵ_g) as a function of the cut on the BDT score. It is more useful to compare the ratio of the tagging efficiencies as a function of ϵ_q, in order to judge the separation power of a "quark-rich signal" from a "gluon-rich" background. In Figs. 18-20 (left column) we show the ratio of the quark and gluon tagging efficiencies, ϵ_q/ϵ_g as a function of ϵ_q, for $400 < p_T(j_s) < 500$ GeV, with the event samples generated with all the three MC codes. Four different MVA methods are shown corresponding to different choices for the discrimination variables:

- **Method-1:** Two variables, $n_{\rm ch}$ and C_1 with $\beta = 0.2$.
- **Method-2:** Two variables, $n_{\rm ch}$ and C_1 with $\beta = 0.2$, with two categories determined in terms the number of associated jets ($n = 0$ or $n \geq 1$).
- **Method-3:** Three variables, $n_{\rm ch}$, C_1 with $\beta = 0.2$ and $m_J/p_{T,J}$.
- **Method-4:** Three variables, $n_{\rm ch}$, C_1 with $\beta = 0.2$ and $m_J/p_{T,J}$, with two categories determined in terms the number of associated jets ($n = 0$ or $n \geq 1$).

We can quantify the improvement in quark-gluon separation using ϵ_g(Method-1)/ϵ_g(Method-$\{2,3,4\}$) as a function of ϵ_q, as shown in Figs. 18-20 (right). For e.g., for an operating point of $\epsilon_q = 0.4$, we can obtain an improvement of around 10%, 15% and 20% using Methods-2,3 and 4 respectively, when compared to Method-1. The differences between the improvement factors obtained using the three MC generators are found to be small.

In order to estimate the change in tagger performance as we consider lower p_T jets, we show in Fig. 21 the same results as in Fig. 18, but now with $150 < p_T(j_s) < 200$ GeV. The improvement on adding associated jet rates is still appreciable, although it is somewhat reduced compared to the higher p_T range. The fluctuations in the ϵ_g ratio for lower values of ϵ_q in Fig. 21 are due to low MC statistics.

We can see in Figs. 18-20 that there is an improvement in going from a two variable analysis to a three variable one by including the variable $m_J/p_{T,J}$. This can be understood as follows. The jet mass variable is related to $C_1^{(\beta=2)}$, as can be seen by writing both of them in terms of the z, θ variables for the hardest emission inside the jet cone: $m_J^2 \simeq z(1-z)\theta^2 p_{TJ}^2$. Furthermore, $C_1^{(\beta=2)}$ and $C_1^{(\beta=0.2)}$ are two independent variables belonging to the C_1 class which carry all the information on this hardest emission, and including both of them improves the tagger performance. For this reason, further addition of a third variable in the C_1 class does not change the performance appreciably, a fact that we explicitly checked by a separate MVA

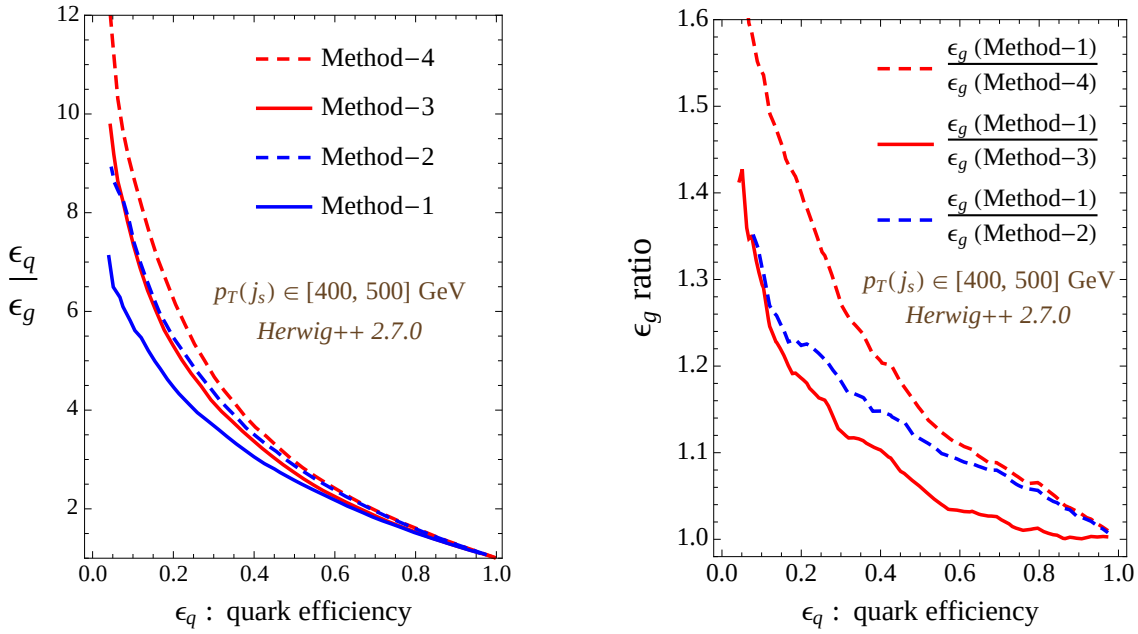

Figure 18: The ratio of the quark and gluon tagging efficiencies, ϵ_q/ϵ_g as a function of ϵ_q, for $400 < p_T(j_s) < 500$ GeV, as determined by MC simulations with `Herwig++` (left column). The different MVA methods, determined in terms of the input variables are explained in the text. To quantify the improvement in quark gluon separation as we go to Methods 2,3 and 4, we show ϵ_g(Method-1)/ϵ_g(Method-{2,3,4}) as a function of ϵ_q as well (right column).

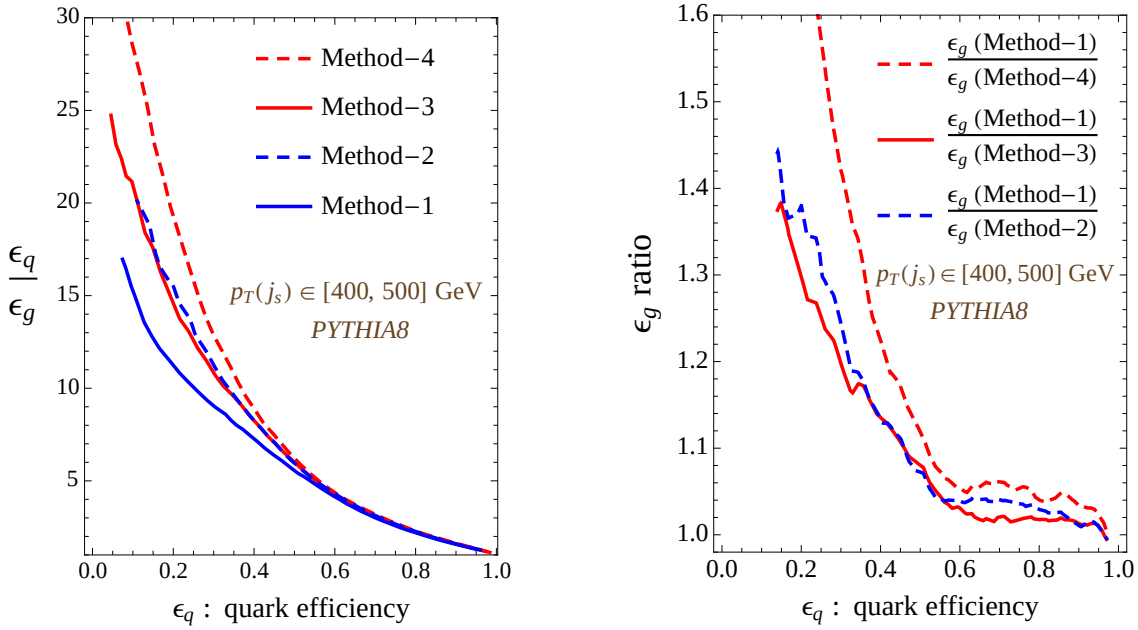

Figure 19: Same as Fig. 18, with MC simulations using `Pythia8`.

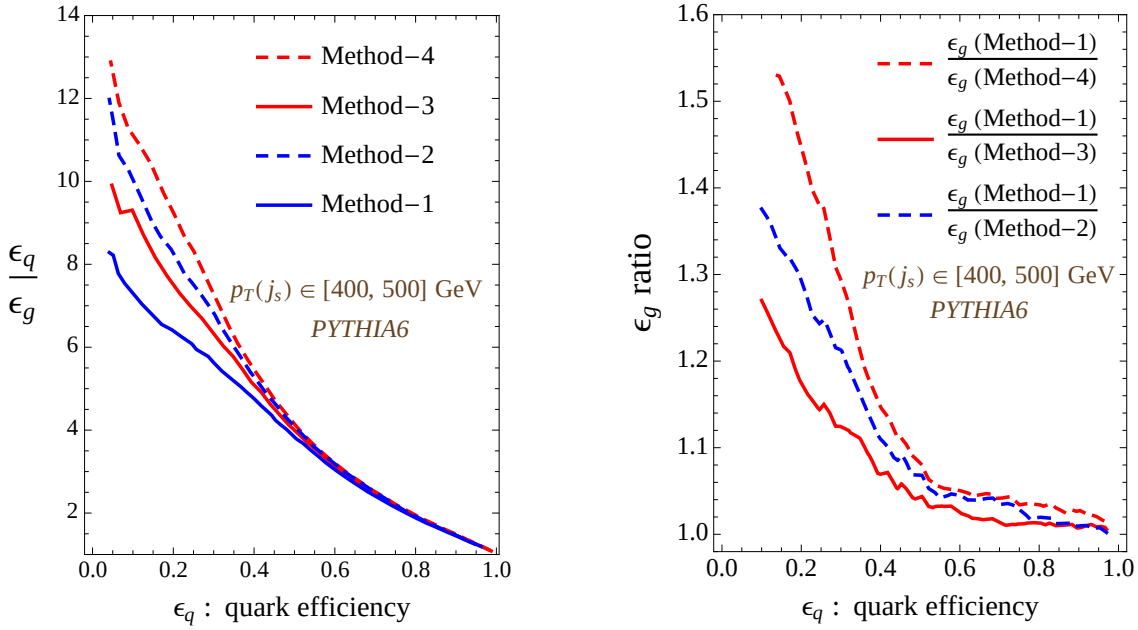

Figure 20: Same as Fig. 18, with MC simulations using `Pythia6`.

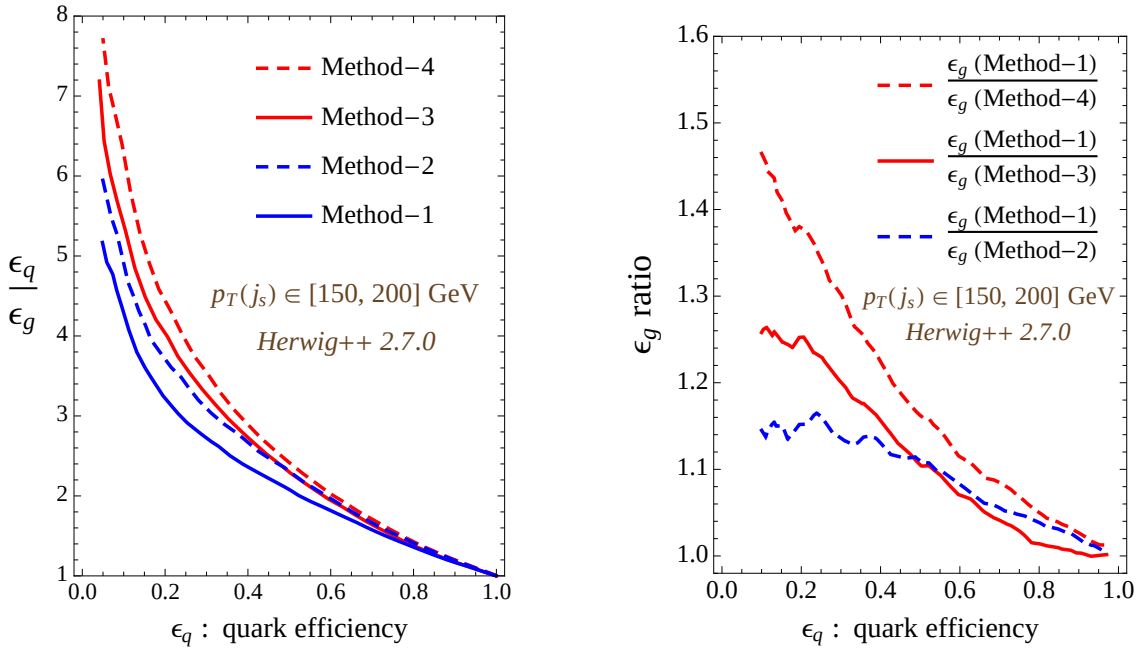

Figure 21: Same as Fig. 18, for a lower range of jet p_T, $150 < p_T(j_s) < 200$ GeV. Results using only `Herwig++` are shown.

analysis. There is a further improvement in the quark-gluon separation when the number of associated jets information is included at the level of categories in both the two and three variable MVA analyses. Since the associated jet rates carry the additional information of radiation outside the jet cone, Methods 2 and 4 lead to further improvements as compared to Methods 1 and 3, respectively.

Method 4 leads to the best performance out of the four different MVA's considered. In fact, we find that there is an alternative way to include the associated jet rates information in Method 4 by using the modified jet mass variable $m(j_s)/p_{T,J}$ in Method 3. Here, $m(j_s)$ is the jet mass computed by adding the leading jet and associated jet four momenta. Because of a larger associated jet rate, for the same $p_T(j_s)$, $m(j_s)$ is higher for a gluon jet compared to a quark, while $p_{T,J}$ is lower. Therefore, using either associated jet rate categories and $m_J/p_{T,J}$, or using only the variable $m(j_s)/p_{T,J}$ leads to the same MVA performance, as shown in Fig. 22.

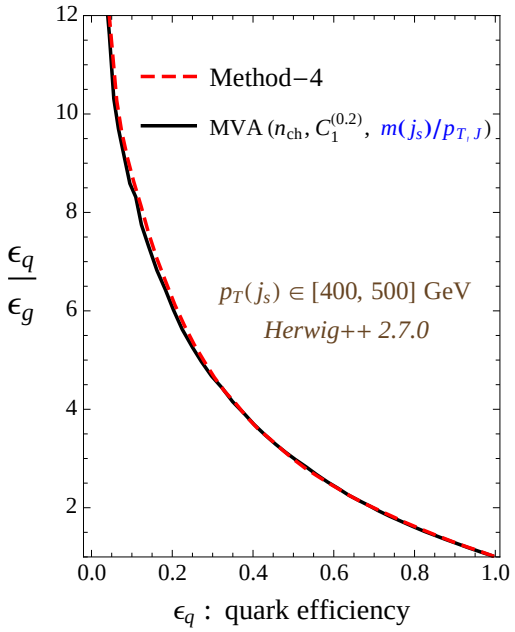

Figure 22: Comparison of Method 4 which includes $m_J/p_{T,J}$ and the associated jet rates as categories in the MVA, and the alternative method of including the associated jet rate information by using the modified jet mass variable $m(j_s)/p_{T,J}$. Both methods lead to the same MVA performance.

4.3 Subjet rates in jets: analytical calculations

The number of charged tracks inside a jet cone, $n_{\rm ch}$ (with each track having transverse momentum above a threshold, usually taken to be around 1 GeV) is often used as a good discriminating variable. However, as mentioned earlier, the MC predictions for this observable are quite sensitive not only to the parton shower (PS) algorithm and the related parameters, but also to the tuning of the hadronization and underlying event models. On the otherhand, we find that the number of subjets of a primary jet leads to a more uniform prediction across the MC generators, and thus can be better suited in quark gluon separation studies. The number of

subjets as a quark-gluon separation variable was considered earlier in Ref. [27]. In this study, we compute the subjet rates to NDLA accuracy, and show a detailed comparison with different MC generators.

We find the *subjets* of jet j with the *exclusive* k_t *algorithm*, which applies the dimensionless distance measure

$$y_{ik} = \min\{p_{ti}^2, p_{tk}^2\} \frac{\Delta R_{ik}^2}{R^2 p_j^2} \,, \tag{4.6}$$

to its constituent objects and clusters them as discussed for a generalized k_t algorithm in Sec. 4.1, until the smallest y_{ik} is above $y_{\rm cut}$. Thus the subjet rates are functions of the jet $p_t = p_j$, the jet radius R, and $y_{\rm cut}$.

In this section, we compute the subjet rates to NDLA, i.e. considering double and next-to-double logarithms, $\alpha_{\rm S}^n L^{2n}$ and $\alpha_{\rm S}^n L^{2n-1}$, where now $L = \ln(1/y_{\rm cut})$. The relevant generating functions in this case are those given in Refs. [67, 77]:

$$\phi_q(u,Q) = u\,\Delta_q(Q) \exp\left(\int_{Q_0}^{Q} dq\,\Gamma_q(Q,q)\phi_g(u,q)\right) , \tag{4.7}$$

$$\phi_g(u,Q) = u\,\Delta_g(Q) \exp\left(\int_{Q_0}^{Q} dq \left[\Gamma_g(Q,q)\phi_g(u,q) + \Gamma_f(q)\frac{\phi_q(u,q)^2}{\phi_g(u,q)}\right]\right) \tag{4.8}$$

where $Q = R\,p_j$ is the jet scale, $Q_0 = R\,p_j\sqrt{y}_{\rm cut}$ is the resolution scale,[12]

$$\Gamma_q(Q,q) = \frac{2C_F}{\pi}\frac{\alpha_{\rm S}(q^2)}{q}\left(\ln\frac{Q}{q} - \frac{3}{4} + \frac{q}{Q} - \frac{1}{4}\frac{q^2}{Q^2}\right) , \tag{4.9}$$

$$\Gamma_g(Q,q) = \frac{2C_A}{\pi}\frac{\alpha_{\rm S}(q^2)}{q}\left(\ln\frac{Q}{q} - \frac{11}{12} + \frac{q}{Q} - \frac{1}{4}\frac{q^2}{Q^2} + \frac{1}{6}\frac{q^3}{Q^3}\right) , \tag{4.10}$$

$$\Gamma_f(q) = \frac{n_f}{3\pi}\frac{\alpha_{\rm S}(q^2)}{q}\left(1 - \frac{3}{2}\frac{Q_0}{q} + \frac{3}{2}\frac{Q_0^2}{q^2} - \frac{Q_0^3}{q^3}\right) . \tag{4.11}$$

The Sudakov factors for no resolvable emission are now

$$\Delta_q(Q) = \exp\left(-\int_{Q_0}^{Q} dq\,\Gamma_q(Q,q)\right) , \tag{4.12}$$

$$\Delta_q(Q) = \exp\left(-\int_{Q_0}^{Q} dq\,[\Gamma_g(Q,q) + \Gamma_f(q)]\right) . \tag{4.13}$$

Hence the rates for 1, 2 or 3 subjets in a quark jet are:

$$\begin{aligned} R_1^q &= \Delta_q(Q)\,, \\ R_2^q &= \Delta_q(Q)\int_{Q_0}^{Q} dq\,\Gamma_q(Q,q)\Delta_g(q)\,, \\ R_3^q &= \Delta_q(Q)\int_{Q_0}^{Q} dq \int_{Q_0}^{q} dq'\,\Gamma_q(Q,q)\Delta_g(q) \times \\ &\quad \{[\Gamma_q(Q,q') + \Gamma_g(q,q')]\,\Delta_g(q') + \Gamma_f(q')\Delta_f(q')\}\,, \end{aligned} \tag{4.14}$$

[12] Here again we keep power-suppressed corrections in order to satisfy boundary conditions.

where $\Delta_f = \Delta_q^2/\Delta_g$, and for a gluon jet we have

$$
\begin{aligned}
R_1^g &= \Delta_g(Q)\,, \\
R_2^g &= \Delta_g(Q)\int_{Q_0}^{Q} dq\,[\Gamma_g(Q,q)\Delta_g(q)+\Gamma_f(q)\Delta_f(q)]\,, \\
R_3^g &= \Delta_g(Q)\int_{Q_0}^{Q} dq\int_{Q_0}^{q} dq'\Big[\Gamma_g(Q,q)\Delta_g(q)\times \\
&\quad \{[\Gamma_g(Q,q')+\Gamma_g(q,q')]\,\Delta_g(q')+\Gamma_f(q')\Delta_f(q')\}+\Gamma_f(q)\Delta_f(q)\times \\
&\quad \{[\Gamma_g(Q,q')-\Gamma_g(q,q')]\,\Delta_g(q')+2\Gamma_q(q,q')\Delta_q(q')\}\Big]\,.
\end{aligned}
\tag{4.15}
$$

4.4 Subjet rates in jets: comparison with Monte Carlo

We now compare the above results with Monte Carlo predictions. MC samples of quark and gluon jets were prepared for the subjet analysis using the same setup as in the associated jet study in Sec. 4.1, however, detector effects and minimum p_T cuts for the charged and neutral hadrons were not included for this analysis. In this sense, our study of the subjet rates should be taken as illustrative, and we do not include the subjet rates in an MVA analysis in this paper. As we shall see in the following, one needs to go down to at least $L = 4$ to have some discrimination power. This corresponds to going down to 0.1 for ΔR resolution, which is the typical size of calorimeter cells, although the ΔR separation of subjets would be larger when the subjet p_T is smaller compared to the primary jet p_T. Therefore, in a proper analysis, combining track and calorimeter information is essential, and a detailed experimental study is necessary, which is beyond the scope of this paper.

Figure 23 shows comparisons between the resummed results of Eqs. (4.14, 4.15) and the MC results for jets with $p_{T,J} \in [500, 600]$ GeV and $R = 0.4$. For quark jets the different MC generators agree quite well with each other and with the resummed calculations, the MC predictions being somewhat below the resummed 1-subjet rate for $L > 4$, and vice-versa for 2 subjets. Hadronization effects are small for $L < 7$, after which the 1- and 2-subjet rates are suppressed and the higher subjet rates are therefore enhanced. At this value of $R\,p_{Tj}$, $L = 7$ corresponds to resolving subjets with $\min\{p_{ti}, p_{tj}\}\Delta R_{ij} \sim 6$ GeV.

For gluon jets the agreement between the resummed results and the Monte Carlos is still quite close for 1 subjet. For 2 and 3 subjets the peak rates are in roughly the same place but have higher values than the resummed ones, with the effect that the rate for 4 or more subjets is substantially suppressed. Once again the hadronization effects are small for $L < 7$, after which the 1- and 2-subjet rates are suppressed and the higher subjet rates are enhanced, actually bringing the latter into close agreement with the analytical calculations.

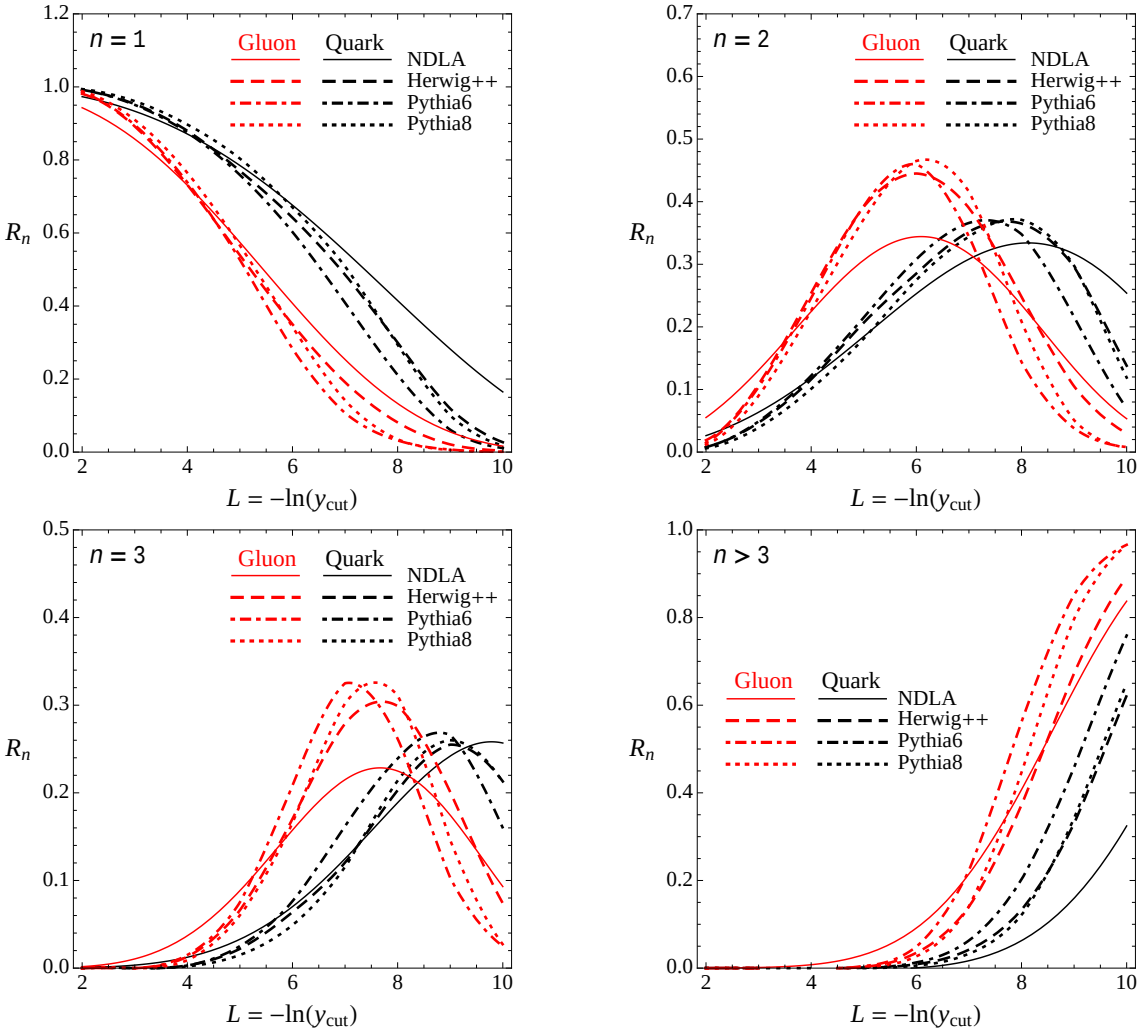

Figure 23: Subjet rates R_n with $n = 1, 2, 3$ and $n > 3$ as a function of $L = -\ln(y_{\rm cut})$, for quark jets (black) and gluon jets (red), with $p_{T,J} \in [500, 600]$ GeV, $R = 0.4$. Curves are `Herwig++` (dashed), `Pythia6` (dot-dashed), `Pythia8` (dotted) and NDLA resummed (solid).

In conclusion, the fairly good agreement between the Monte Carlos and the resummed 1-, 2- and 3-subjet rates for $R = 0.4$ and L not too large ($L < 5$, subjet resolution above about 15 GeV) suggests that in this range those subjet rates can be used for quark-gluon discrimination. At larger jet radii, the agreement remains similar, as we have checked using $R = 0.8$.

5 Evolution variable dependence of jet substructure

Through the study in Sec. 4, we noticed that the predictions of QCD jet substructure are different between `Pythia` and `Herwig++`. Main purpose of this section is to consider the differences by focusing on the parton shower algorithm. With this goal in mind, we simulate QCD jet substructure related observables with the following generalized evolution variable:

$$Q_\alpha^2 = [4z(1-z)]^\alpha q^2, \tag{5.1}$$

where, α is treated as a free parameter. For final state radiation, the above variable with $\alpha = 1$ and -1 correspond to the evolution variables employed in `Pythia8` and `Herwig++` respectively. In Sec. 5.1, we provide further details on the framework used to implement this evolution variable in our parton shower program. In Sec. 5.2, we show properties of QCD radiations generated by a given Q_α, and discuss the correlation pattern between such radiation properties and the resulting behaviour of the jet shape variable, $C_1^{(\beta)}$ [33]. In Sec. 5.3, we show α-dependence of $C_1^{(\beta)}$ distributions and the associated jet rate observable [88] with tuned values of the parton shower parameters. We summarize our findings in Sec. 6.

5.1 Modification of the parton shower formalism

The evolution variable for the final state radiation of light partons used in our analysis is defined in Eq. (5.1), where z is the momentum fraction of one of the daughter partons and q^2 is the virtuality of the mother parton. The daughter partons are taken to be on-shell. The variable Q_α is parametrized by a continuous parameter α, and we take the range as $\alpha \in [-1, 1]$ in this study. Q_α with $\alpha = 1$ and -1 correspond to `Pythia8`'s evolution variable (i.e., relative transverse momentum) and `Herwig++`'s one respectively. QCD radiations are governed by the DGLAP equation [45, 46]. When we use Q_α as a scale variable, the evolution equation takes on a equivalent form for each α due to the following relation,

$$\frac{dQ_\alpha^2}{Q_\alpha^2} dz = \frac{dq^2}{q^2} dz. \tag{5.2}$$

We implement the general evolution variable Q_α for arbitrary α in a parton shower program, and calculate jet substructure observables. Even though there are various recent parton shower formalisms, e.g., dipole shower in `Pythia8` [89] or dipole-antenna shower in `Vincia` [90, 91], we use in this study a traditional formalism

based on Refs. [41, 92], which is used in `Herwig++`. In the following subsection, we describe the modification to the formalism in Refs [41, 92] required to have a parton shower with arbitrary α.

5.1.1 Phase space

Consider an emission where a mother parton a branches off into light or massless partons b and c ($a \to bc$). We give an effective mass $m_{\rm qg}$ to the daughter partons to avoid singularities in the splitting functions. Then, upper and lower values of the *energy* fraction of one daughter parton z_E^+ and z_E^- are given by

$$z_E^{\pm} = \frac{1}{2}\left(1 \pm \sqrt{1-\frac{q^2}{E_a^2}}\sqrt{1-\frac{4m_{\rm qg}^2}{q^2}}\right), \tag{5.3}$$

where q^2 is the virtuality of a when b and c are on-shell, and E_a is the energy of a. This gives a condition for the allowed region on the energy fraction z_E and Q_α as

$$\frac{Q_{\rm min}^2}{Q_\alpha^2}w^\alpha + \frac{Q_\alpha^2}{Q_{\rm max}^2}w^{-\alpha} \le w + \frac{Q_{\rm min}^2}{Q_{\rm max}^2}, \qquad w = 4z_E(1-z_E), \tag{5.4}$$

where $Q_{\rm max}$ and $Q_{\rm min}$ are the maximal and minimal values for Q_α. These are independent of α, and given as

$$Q_{\rm max} = E_a, \qquad Q_{\rm min} = 2m_{\rm qg}. \tag{5.5}$$

Here, z describes not the energy fraction but the light-cone momentum fraction as in Refs. [41, 92]. However, we have explicitly checked that these are approximately the same. Hence we use Eq. (5.4) with a substitutions, $z_E \to z$ in the generation of Q_α and z. The energy of the partons are known at the end of all branchings. So, we set $Q_{\rm max}$ in Eq. (5.4) to the energy of the initial hard scattering process, i.e., $\sqrt{s}/2$ for the first branching, and calculate by taking z as the energy fraction for subsequent branchings. These choices ensure the required relation $\mathbf{p}_\perp^2 = Q_1^2 - Q_{\rm min}^2 \ge 0$, where $\mathbf{p}_\perp$ is the spatial component of the *relative transverse momentum* for each branchings, as defined in Ref. [41, 92].

The allowed phase spaces in the $\ln z - \ln Q_\alpha$ plane for each choice of α is illustrated in Fig. 24, where the parton energy E_a is fixed at 500 GeV. At leading order, the parton branchings occur almost uniformly on this plane. The partons start from a high scale and evolve to low scale in timelike branchings, and the smaller α is, the larger the phase space becomes in the high scale region. So, when the evolution starts from a high scale, initial emissions tend to choose a high scale and soft emission for small α.

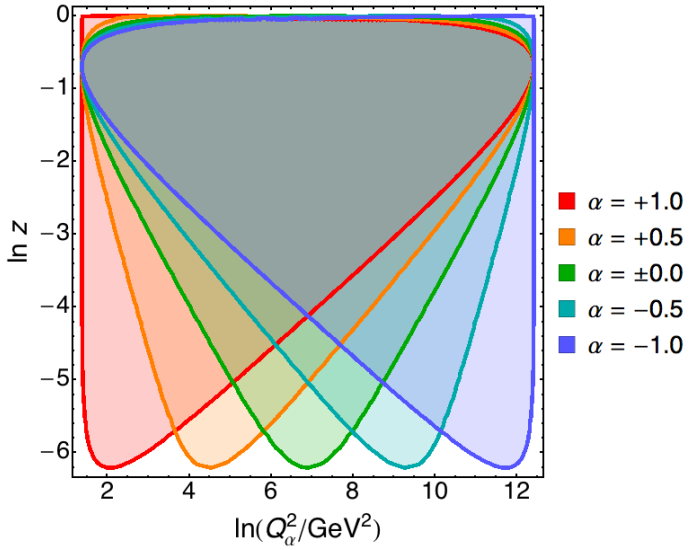

Figure 24: The allowed phase space in the $\ln z - \ln Q_\alpha$ plane for each choice of α, with E_a fixed at 500 GeV.

5.1.2 Starting scale

We consider final states of either a light quark pair ($q\bar{q}$) or a gluon pair (gg), with a center of mass energy of $\sqrt{s}$, and set the starting scale for the initial partons to their energy in the rest frame of the final state, i.e., $\sqrt{s}/2$. This is the maximal choice for the starting scale, see Eq. (5.5).

Next, consider the sequential branchings $a \to bc$ and $b \to de$, with the scales of the branching given by Q_α and $Q_{\alpha,b}$ as;

$$Q_\alpha^2 \simeq [4z(1-z)]^\alpha \times 2z(1-z)E_a^2(1-\cos\theta_a), \tag{5.6}$$

$$Q_{\alpha,b}^2 \simeq [4z_b(1-z_b)]^\alpha \times 2z_b(1-z_b)E_b^2(1-\cos\theta_b), \tag{5.7}$$

where θ_a and θ_b are the angle between b and c, and d and e respectively. The momentum fractions for the branchings $a \to bc$ and $b \to de$ are given by z and z_b, and the energy of a and b are E_a and $E_b \simeq z_b E_a$. By imposing the angular ordering $\theta_a > \theta_b$, we get

$$Q_{\alpha,b} < Q_\alpha z \left[\frac{4z(1-z)}{4z_b(1-z_b)}\right]^{-(\alpha+1)/2}, \tag{5.8}$$

$$\leq Q_\alpha z[4z(1-z)]^{-(\alpha+1)/2}. \tag{5.9}$$

The right-hand side in Eq. (5.9) can be greater than the previous scale Q_α. To avoid this wrong of ordering the scale, we set the starting scale of the daughter parton b as

$$Q_{\alpha,b}^S = Q_\alpha \min(1, z[4z(1-z)]^{-(\alpha+1)/2}). \tag{5.10}$$

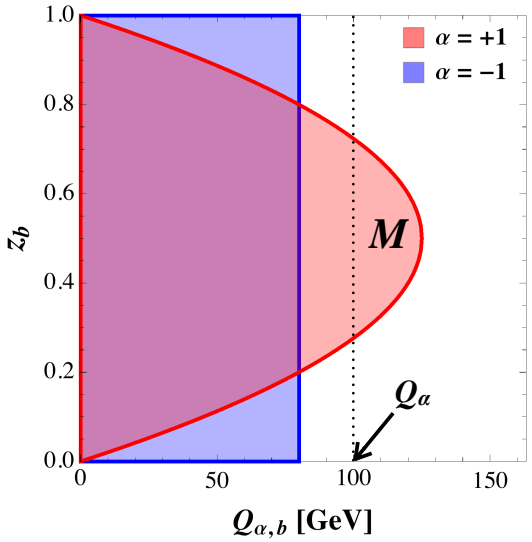

Figure 25: Red and blue regions satisfy the angular-ordered condition in Eq. (5.9) for $\alpha = 1$ and -1, where previous scale and momentum fraction are set to $Q_\alpha = 100$ GeV and $z = 0.8$. The region M is in red region and above Q_α. Sequential emissions in M are prohibited since the scale $Q_{\alpha,b}$ does not ordered. Such missing phase space make the difference of emissions for each α essentially.

The angular ordering is ensured by using this starting scale for $\alpha = -1$. However, angular ordered emission is not ensured for $\alpha \neq -1$. Such emissions are vetoed by hand as in `Pythia6` [38].

In Fig. 25, red and blue regions satisfy the angular-ordered condition in Eq. (5.9) for $\alpha = 1$ and -1, where previous scale and momentum fraction are set to $Q_\alpha = 100$ GeV and $z = 0.8$. The region M is in red region and above Q_α. Sequential emissions in M are prohibited since the scale $Q_{\alpha,b}$ does not ordered. Such missing phase space make the difference of emissions for each α essentially.

5.1.3 Tunable parameters and other modifications

We use three parameters $\alpha_S(m_Z)$, $m_{\rm qg}$, and $r_{\rm cut}$ in our parton shower program. The first one is the strong coupling constant at the scale of the Z boson mass. We use one loop running of α_S in our code. The argument of α_S is set to $p_\perp = 2^{-\alpha}[z(1-z)]^{(1-\alpha)/2}Q_\alpha$ thereby including the effects of subleading terms in the splitting functions. The value of α_S is significant to the predictions of jet substructure. Larger values of α_S lead to high scale emissions, and jet shape distributions, e.g., the jet mass distribution shift to higher value regions. The value of $\alpha_S(m_Z)$ is set to 0.118 in `Herwig++`, and about $0.136 - 0.139$ for the final state radiation in `Pyhtia8`.

The second variable $m_{\rm qg}$ is the effective mass of the light partons and gluons to avoid soft-collinear singularities, which was introduced in Sec. 5.1.1. The third one is defined as

$$r_{\rm cut} = \frac{Q_{\rm cut}}{Q_{\rm min}} = \frac{Q_{\rm cut}}{2m_{\rm qg}}, \tag{5.11}$$

where $Q_{\rm cut}$ is a given scale where the evolution terminates.

We note in passing that, in our analysis, we neglect $g \to q\bar{q}$ branchings for simplicity, which affect distributions at the NLL order.

5.2 Emission property

Jet shape observables are important in examining the substructure of QCD jets. One of the recently studied jet shape observable is the two-point energy correlation function $C_1^{(\beta)}$ [33, 73], which can be defined in the rest frame of a parton pair as

$$C_1^{(\beta)} = \sum_{i<j\in{\rm jet}} \frac{E_i E_j}{E_{\rm jet}^2} \left(2\sin\frac{\theta_{ij}}{2}\right)^{\beta}, \tag{5.12}$$

where E_i and E_j are the energies of the particles labeled by i and j in the jet, $E_{\rm jet}$ is the jet energy, and θ_{ij} is the angle between i and j. The sum runs over all distinct pairs of particles in the jet. The dominant contribution to this observable comes from the hardest emission in the jet, which is also the first emission in the jet [74]. Neglecting all other emissions except for the hardest one, we get in the soft limit

$$\ln C_1^{(\beta)} \simeq \ln z + \beta \ln\left(2\sin\frac{\theta}{2}\right), \tag{5.13}$$

where z and θ are the smaller energy fraction and the angle of the hardest emission, respectively. Evidently from the above equation, studying the properties of the first emission in the jet on the $z-\theta$ plane will lead to an understanding of the behaviour of this jet shape.

Figs. 26 and 27 show the emission probability on the $\ln z - \ln(2\sin(\theta/2))$ plane for quark and gluon jets respectively. The top, center and bottom rows show the results for the first, second and third emissions. Here, the second and third emissions refer to the emissions from the harder of the two partons produced by the first and second emissions respectively. We find that the equal-probability curves for the first emission plots are roughly given by the contours described by

$$\text{Const.} = \frac{\alpha+1}{2}\ln z + \ln\left(2\sin\frac{\theta}{2}\right). \tag{5.14}$$

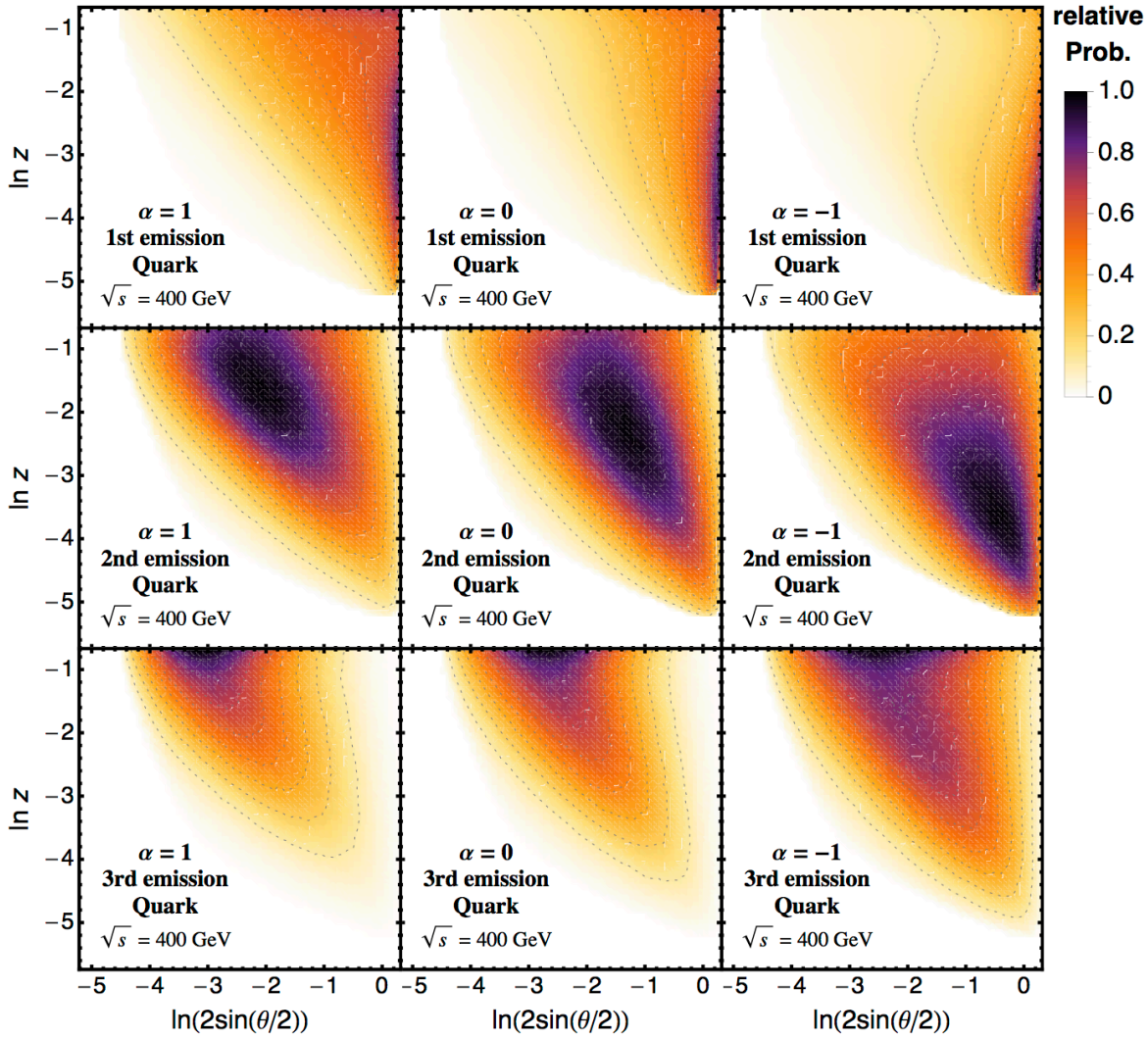

Figure 26: Emission probability in the $\ln z - \ln(2\sin(\theta/2))$ plane for quark jets. The top, center and bottom rows show the results for the first, second and third emissions, respectively. The second and third emission refer to the emissions from the harder parton produced by the first and second emissions respectively.

This is because, the evolution variable, in other words, the *ordering* variable, in Eq. (5.1) can be written in the soft limit as

$$\ln Q_\alpha = \frac{\alpha+1}{2}\ln z + \ln\left(2\sin\frac{\theta}{2}\right) + \text{Const.} \tag{5.15}$$

It should be mentioned that the small z regions are more favourable due to larger values of the strong coupling constant, α_S. In the case of $\alpha = -1$, the evolution variable is given by $Q_{-1} \simeq E \times 2\sin(\theta/2)$, where E is the energy of the mother parton. So, high scales also imply larger angles. As mentioned above, the emissions tend to prefer high scales and soft emissions for smaller values of α. This is consistent

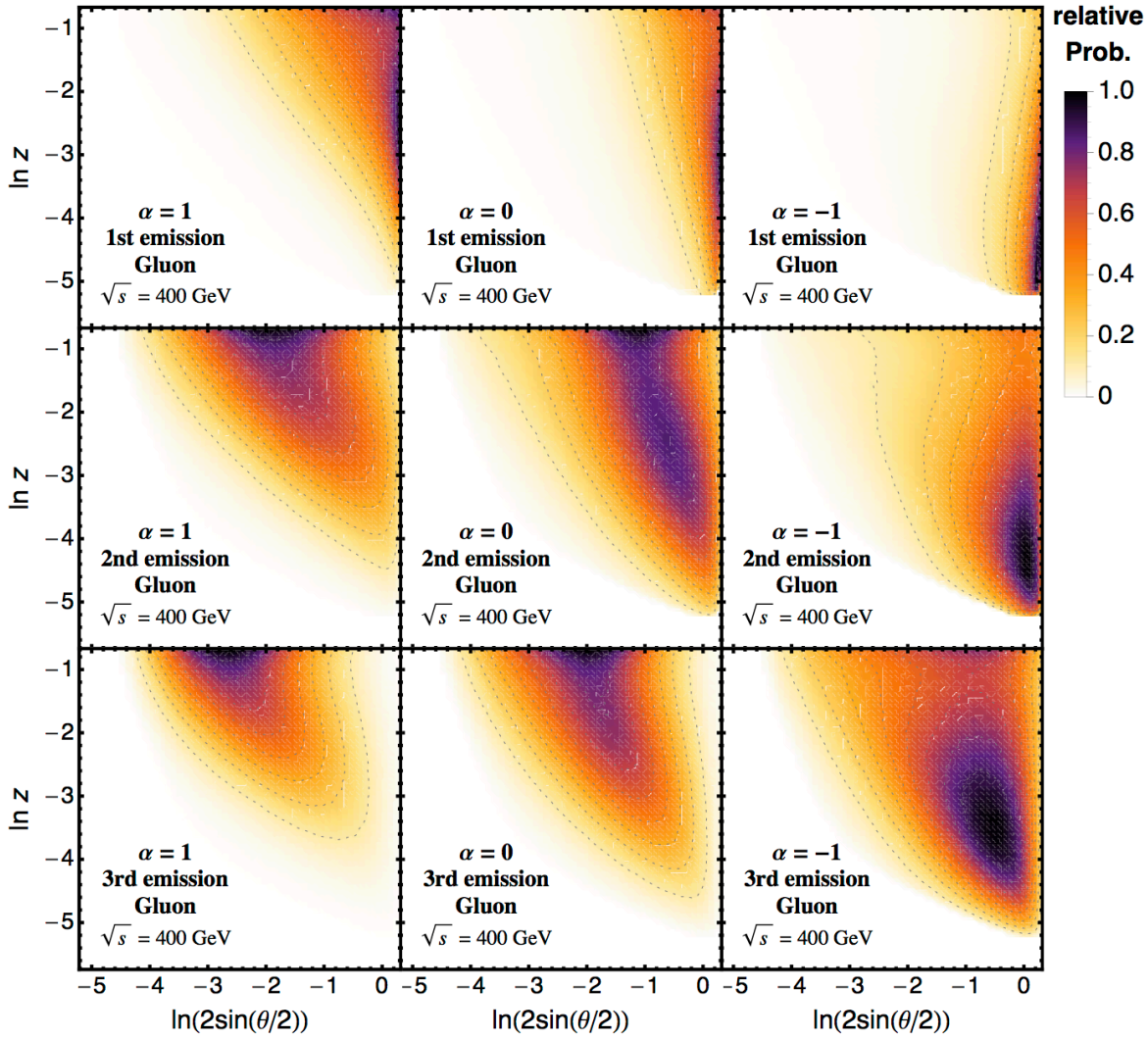

Figure 27: Same as Fig. 26, for gluon jets.

with the results for the first emission with $\alpha = -1$ in Figs. 26 and 27.

Clearly, for the jet shape observable in question, we are mostly interested here in the first emission in a jet. When we set the jet radius to $R = 0.4$, such emissions are distributed in the region described by $\ln(2\sin(\theta/2)) < -0.9$. The first emissions often fall outside a narrow jet, especially for small α. Also, such emissions tend to be vetoed out in the parton shower-matrix element matching algorithms. Therefore, it is also important to look into the subsequent emissions. We find that the second and the third emissions also have a different distribution for each value of α. This fact indicates that parton shower algorithms implementing different evolution variables would have different predictions for jet substructure. However, the results in Figs. 26 and 27 are obtained with the same set of inputs for the tunable parameters described

in the previous section [13] for all values of α. In the next section, we employ a procedure to fit the values of these parameters for each α separately, and show our results with the fitted values of the parton shower parameters for completeness.

5.3 The α dependence

5.3.1 Jet shape distribution

Jet shape distributions depend on the parameters $\alpha_S(m_Z)$, $m_{\rm qg}$, and $r_{\rm cut}$ introduced in Sec. 5.1.3. These parameters are determined by performing a fit of the MC predictions to experimental data on several jet observables, for which the $e^+e^- \to n$ jets data from LEP are particularly useful. Performing such a fit to the experimental data is, however, beyond the scope of the present study as this would require the implementation of a hadronization model in our parton shower code. Since the primary goal of this study is to examine between difference between parton shower algorithms using different evolution variables, as an alternative to real data, we utilize the $e^+e^- \to q\bar{q}$ events generated by `Herwig++` with hadronization switched off as our *data* [14].

The $C_1^{(0.5)}$, $C_1^{(2.0)}$ and $C_1^{(3.0)}$ distributions have been used to tune the above parameters. As mentioned in Sec. 5.2, the first emission in the jet has a significant effect on the jet shape, which can be parametrized by the momentum fraction z and the angle θ. Therefore, two independent $C_1^{(\beta)}$ distributions contain the necessary information about the jet shapes. Here, we use three variables in order to further examine the β dependence of the QCD jet substructure.

Throughout this paper, jets are clustered using the generalized k_t algorithm for e^+e^- collisions using `FastJet 3.1.1` [66], the distance measure for which is defined as

$$d_{ij} = \min(E_i^{2p}, E_j^{2p}) \frac{1-\cos\theta_{ij}}{1-\cos R}, \tag{5.16}$$

where R is the jet radius parameter, and we use $p = -1$.

We firstly generate events using five choices for the evolution variable, Q_1, $Q_{0.5}$, Q_0, $Q_{-0.5}$ and Q_{-1} at $\sqrt{s} = 200$GeV, where $\sqrt{s}$ denotes the center of mass energy in the e^+e^- collisions. We calculate $\ln C_1^{(0.5)}$, $\ln C_1^{(2.0)}$ and $\ln C_1^{(3.0)}$ distributions with $R = 0.4$, and find the values of the parameters that minimize the χ^2 variable computed using our results and the mock data generated by `Herwig++`. Theoretical

[13] The distributions in Figs. 26 and 27 are obtained with $\alpha_S(m_Z) = 0.12$, $m_{\rm qg} = 1$GeV, and $r_{\rm cut} = 1$.

[14] To be specific, we use `Herwig++ 2.7.1` with default tune, for the $u\bar{u}$ and $d\bar{d}$ parton level final states.

α	$\alpha_S(m_Z)$	$m_{\rm qg}$[GeV]	$r_{\rm cut}$
$+1.0$	0.132	0.94	1.00
$+0.5$	0.126	0.90	1.00
± 0.0	0.121	0.84	1.05
-0.5	0.119	0.83	1.16
-1.0	0.119	0.85	1.25

Table 1: Tuned values of the parton shower parameters for each choice of α, obtained by fitting the $\ln C_1^{(0.5)}$, $\ln C_1^{(2.0)}$ and $\ln C_1^{(3.0)}$ distributions for quark jets with $R = 0.4$ with an e^+e^- centre of mass energy of $\sqrt{s} = 200$GeV. The reference distributions are calculated by using $e^+e^- \to q\bar{q}$ events generated by `Herwig++`

errors are assigned using a flat distribution for each bin. The best fit values of the parameters are shown in Table 1. We see that the larger α is, the larger the tuned value of $\alpha_S(m_Z)$ becomes. In other words, the `Pythia8`-like case with Q_1 prefers a higher value of $\alpha_S(m_Z)$ compared to the `Herwig`-like case with Q_{-1}. This qualitative behaviour is in agreement with the actual implementations found in `Pythia8` and `Herwig++`. It should be emphasized that the outcomes of this tuning procedure do not entirely reflect the Monte Carlo difference between `Pythia8` and `Herwig++`, as the the parton shower algorithm implemented in `Pythia8` is different from ours.

In Fig. 28, the top row shows the fitted results, and hence the distributions are in good agreement with `Herwig++` predictions. We also obtained the distributions for a fat jet (with $R = 1.2$) and for gluon jets using the fitted values of the parameters shown in Table 1. For the same energy, the gluon jet distributions with $R = 0.4$ are similar for each choice of the evolution variable. Small differences appear in the shapes predicted by different choices of α for the fat quark and gluon jets ($R = 1.2$). Fig. 29 shows the same distributions as in Fig. 28, with a higher value of the center of mass energy, $\sqrt{s} = 1000$ GeV. As we can see, the α-dependence of the shapes is found to be higher for higher energy jets.

5.3.2 Wideness of soft emissions in jets

The larger the parameter β in $C_1^{(\beta)}$ is, the larger the differences become in Fig. 29. This implies that the wideness of the emissions, especially for the hardest emission in the jets, is different for each α. This is because, the larger β is, the larger the contribution to $C_1^{(\beta)}$ from the emission angle of the hardest emission becomes, which is understood from Eq. (5.13).

Associated jet rates defined in Ref. [88] directly reveal the wideness of the emissions in jets. Associated jets are jets nearby a hard jet, and are defined by two

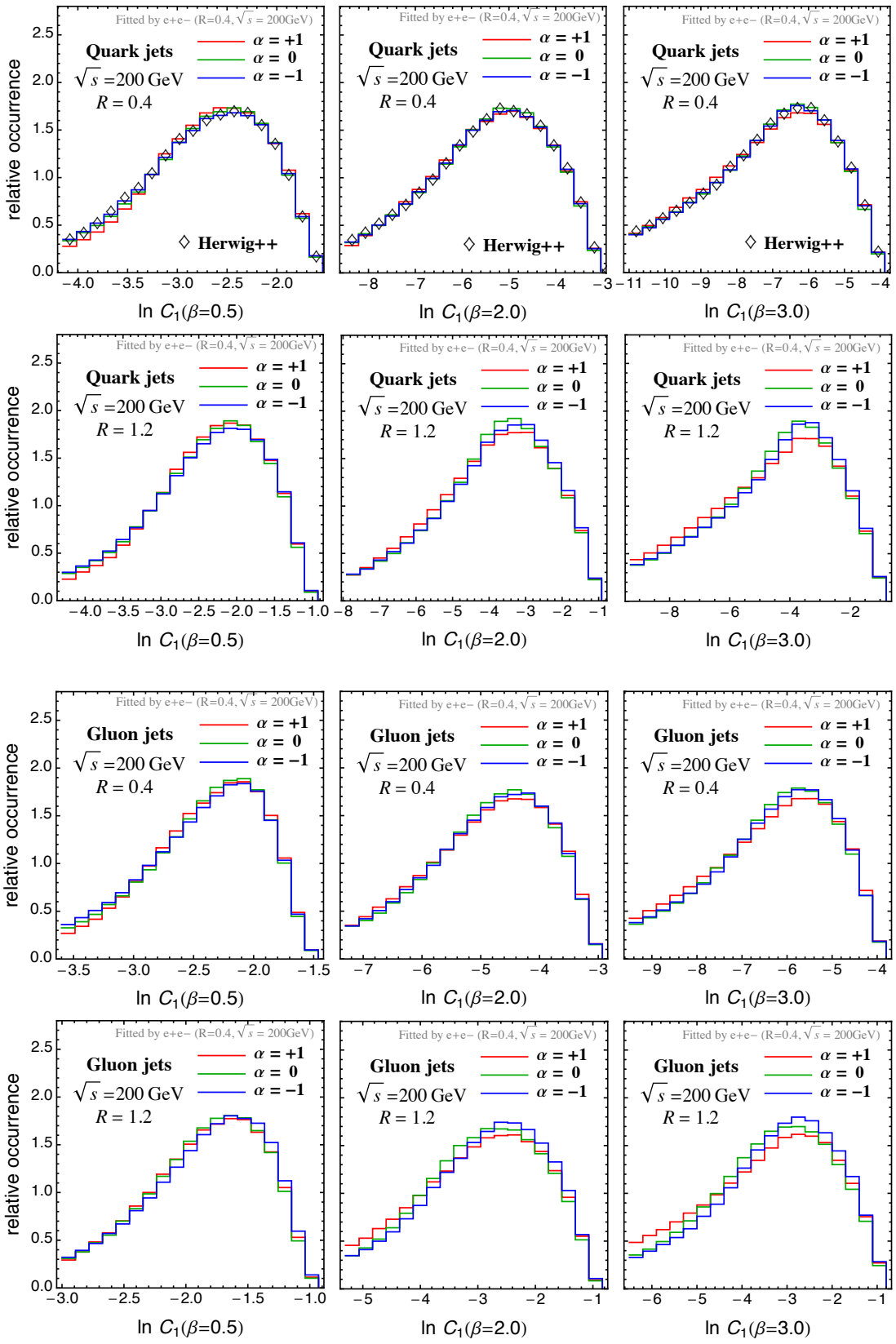

Figure 28: Distributions of $\ln C_1^{(0.5)}$, $\ln C_1^{(2.0)}$ and $\ln C_1^{(3.0)}$ for quark and gluon jets, with $R = 0.4$ and 1.2, at $\sqrt{s} = 200$ GeV, as obtained using the parameter values shown in Table 1.

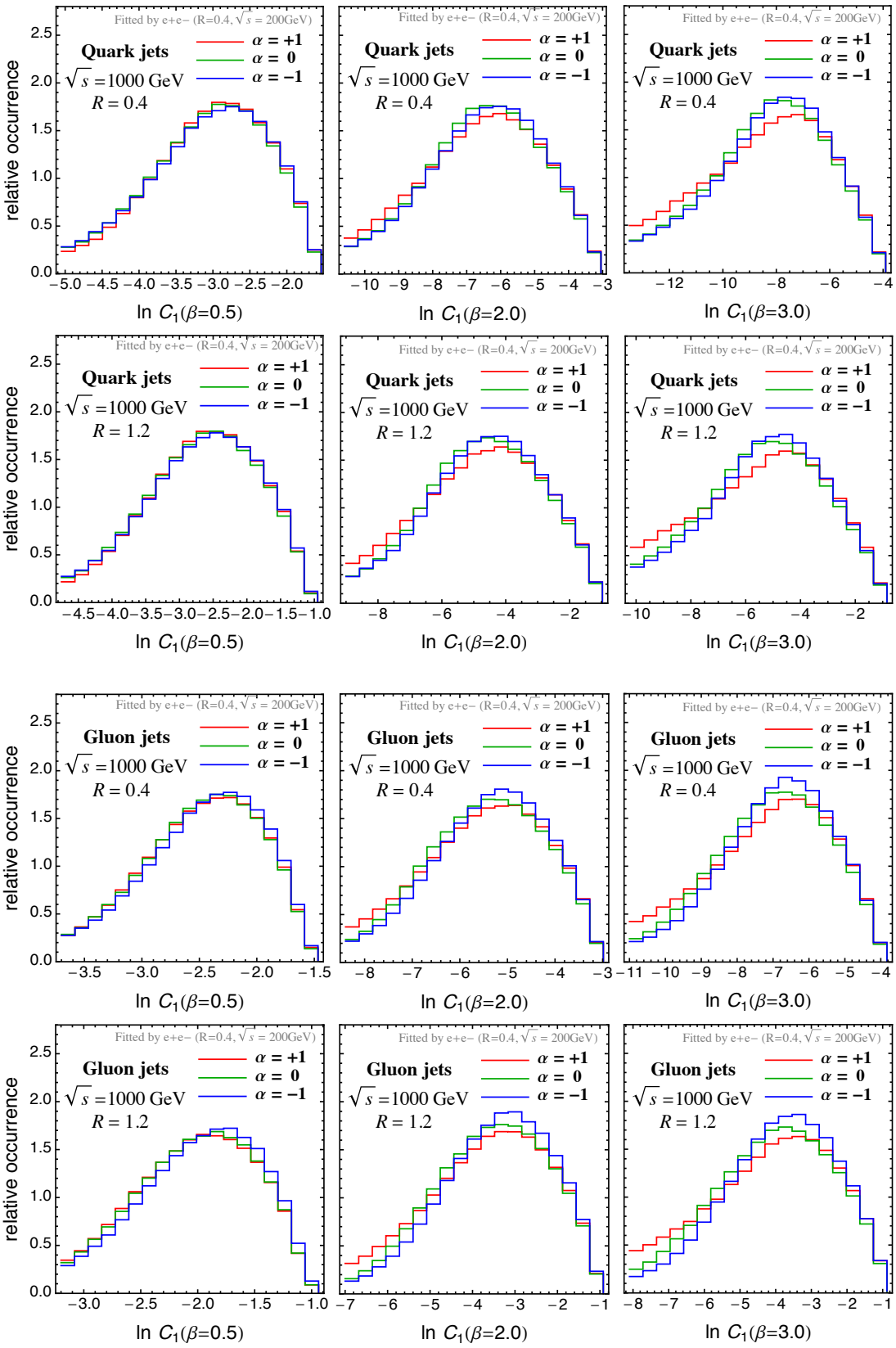

Figure 29: Same as Fig. 28, with a higher center of mass energy, $\sqrt{s} = 1000$ GeV.

parameters, R_a and E_a. Here, R_a is the maximum allowed angle between the momentum directions of the hard jet and the associated jet, and E_a is the minimum energy of the associated jets[15]. We set the value to $E_a = 20$ GeV in this study.

A high probability for having no associated jet implies that the probability of wide emissions occurring around the hard jet is low. Such probabilities have been obtained by using `Pythia8`, `Pythia6`, and `Herwig++`, and it has been found that the no associated jet probability predicted by `Pythia` is higher than the one obtained with `Herwig++` [88].

The no associated jet probabilities calculated with Q_1, $Q_{0.5}$, Q_0, $Q_{-0.5}$ and Q_{-1} are shown in Fig. 30, where, the fitted values of the parameters in Table 1 have been used. We can see that no associated jet probabilities are similar for each α at the low energy range. This is expected as the parameters have been tuned at $\sqrt{s} = 200$ GeV. The α dependence is enhanced at the high energy range. The larger α is, the larger the no associated jet probabilities become. Therefore, an angular ordered shower ($\alpha = -1$) predicts wider jets, while a $p_\perp$ ordered shower ($\alpha = 1$) predicts narrower jets. This result is qualitatively in agreement with the missing phase space of the $p_\perp$ ordered shower [93]. The wideness of the emissions in the jets are thus tunable by changing the parameter α in the evolution variable continuously.

Fig. 31 is similar to Fig. 30, with the tuning parameters obtained by fitting $\ln C_1^{(\beta)}$ distributions for quark jets in $e^+e^- \to q\bar{q}$ events at $\sqrt{s} = 2000$ GeV. The no associated jet probabilities are similar for each α around $\sqrt{s} = 2000$ GeV for the quark jets. The α dependence now appears at other energy ranges. The energy scaling of the wideness seems to be inherent in the choice of the evolution variable for the same modelling of the parton shower.

[15] In Ref. [88], for studies in hadron collisions, the parameter p_a has been used to define associated jets instead of E_a, where p_a is the minimum transverse momentum of the associated jets. However, for the e^+e^- collisions studied in our paper, it is more suitable to use the energy variable.

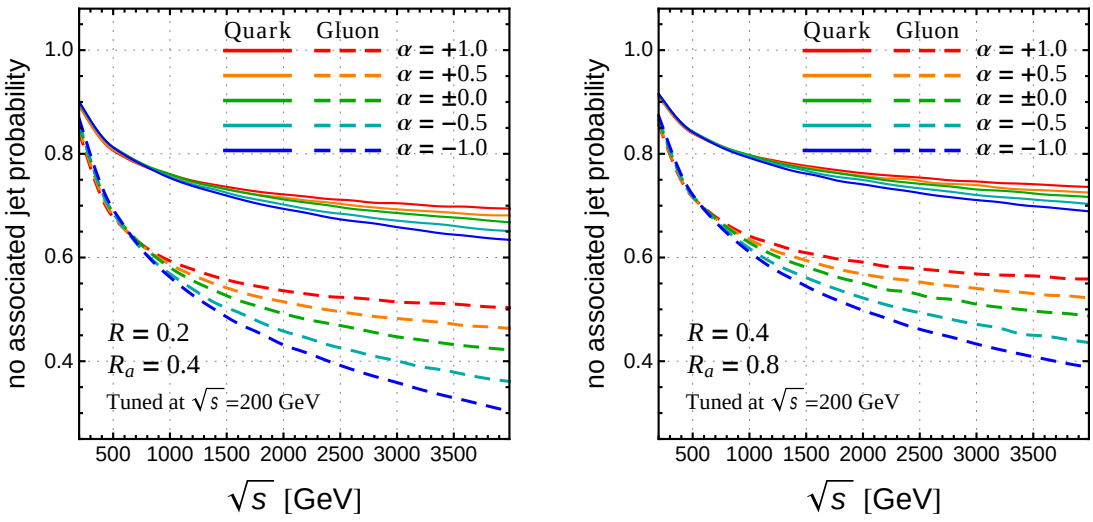

Figure 30: No associated jet probabilities for $(R, R_a) = (0.2, 0.4)$ and $(0.4, 0.8)$, computed with the input parameters as in Table 1.

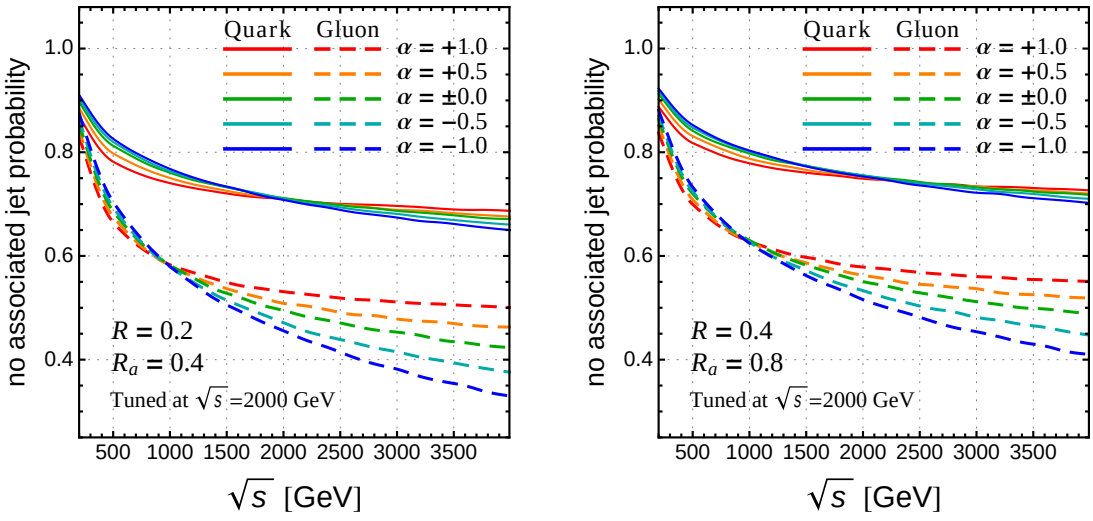

Figure 31: Same as Fig. 30, with the input parameters obtained by fitting the $\ln C_1^{(0.5)}$, $\ln C_1^{(2.0)}$ and $\ln C_1^{(3.0)}$ distributions for quark jets in $e^+e^- \to q\bar{q}$ events at $\sqrt{s} = 2000$ GeV.

6 Summary

To summarize our findings in Sec. 4, we show that in studies of light quark and gluon jet discrimination at the LHC, it is important to include the information on associated jet rates around a primary hard jet. Associated jet rates are defined as the probability of finding at least one softer reconstructed jet around the primary hard jet under consideration. This probability is found to be substantially higher for a gluon-initiated jet compared to a quark-initiated one. Since commonly a small jet radius parameter is adopted in LHC studies of hadronic jets, the associated jet rates carry the information on the radiation outside the chosen jet radius.

We compute the associated jet rates up to NDLA accuracy in perturbative QCD, as a function of the primary jet and minimum associated jet p_T's, as well as the jet radius and association radius parameters. The NDLA results are thereafter compared with predictions from different parton shower MC generators. Since the NDLA predictions include only the time-like showering of the final state partons, we demonstrate the effects of ISR and MPI in the MC predictions as well, and it is observed that the NDLA predictions are closer to the MC's when ISR and MPI are switched off. Overall, the associated jet rates are not very sensitive to these effects as long as the association radius is not too large.

The probability of having at least one associated jet for a primary gluon jet is roughly a factor of two larger than for a quark jet, with a small variation in this number as a function of the jet p_T. This fact makes the presence or absence of associated jets a good variable for quark-gluon discrimination studies. We demonstrate the impact of including the associated jet rate information by including this variable in an MVA analysis, along with the well-studied variables of number of charged tracks, energy-energy-correlation angularities and jet mass. Comparing different two and three variable MVA's with and without the associated jet information, we find that including the associated jets leads to an improvement of around 10% in rejecting gluons, for a fixed quark selection efficiency of 0.4. We also show that using a three variable MVA with associated jet categories leads to the best performance, with an improvement of 20% in rejecting gluons, for the same quark efficiency as above.

Since for the number of charged tracks variable the MC predictions tend to differ, and are dependent on the parton shower and underlying event parameter tunes, we explore the number of k_t subjets of an anti-k_t jet as a quark-gluon discrimination variable. We compute the number of subjets to NDLA accuracy, and compare the resummed predictions with different MC's. The different MC predictions are found to be rather uniform, with the resummed predictions being broadly in agreement with them. However, for gluon jets the peak rates for 2 and 3 subjets are found

to be lower in the resummed computation, which might arise due to higher-order effects that are in general bigger for gluons.

In Sec. 5, we have introduced a generalized evolution variable Q_α which is a function of the free parameter α taking continuous values. Although the evolution equation governing the QCD radiation in jets takes an equivalent form for each α, jet substructure depends on α even in the same parton shower formalism. We have examined the α-dependence of $C_1^{(\beta)}$ distributions and the associated jet probability for quark and gluon jets. This is motivated by the differences found in the prediction for jet substructure observables between often-used Monte Carlo generators, and also by the fact that recent LHC data related to QCD jet substructure lies between the predictions of the MC generators. The angular-ordered parton shower formalism used in this study is built upon the one implemented in `Herwig++`. We leave further studies based on other recent parton shower formalisms to a future work.

We have studied the distributions of the first, second and third emissions in the momentum fraction z and emission angle θ plane. These distributions are of importance as the beginning emissions in the jets have a significant impact on $C_1^{(\beta)}$ and other jet shape observables. The distributions show a unique emission pattern for each choice of α.

We have tuned the parameters in the parton shower to $e^+e^- \to q\bar{q}$ mock data generated using `Herwig++`, with center of mass energies of $\sqrt{s} = 200$ GeV and 2000 GeV. Observables used in the tuning are $\ln C_1^{(0.5)}$, $\ln C_1^{(2.0)}$ and $\ln C_1^{(3.0)}$ distributions with the jet cone angle $R = 0.4$. From this fit, we observe that larger values of the strong coupling are preferred as we vary the values of α from -1 to 1. This is qualitatively in agreement with previous findings regarding the difference between the parton shower phase-space covered by the $p_\perp$ ordered and angular ordered showering algorithms. Using the best fit parameters, we have calculated the $\ln C_1^{(\beta)}$ distributions of the quark and gluon jets, with $R = 0.4$ and 1.2, for e^+e^- collisions at $\sqrt{s} = 200$ and 1000 GeV. As we move away from the setup used for the fits (namely, quark jets, $R = 0.4$, $\sqrt{s} = 200$ GeV), the α-dependence becomes more apparent, especially for larger values of β in $C_1^{(\beta)}$.

The α-dependence for large β implies that wideness of the soft emissions, especially the first ones in a jet are different for each α. We can examine this wideness directly by studying the associated jet probability. A high probability for having no associated jet simply means that the probability of wide emissions occurring around a hard jet is low. We have found that the larger α is, the larger the no associated jet probability becomes. This gives us a qualitative understanding of the generator

dependence of associated jet rates, especially between `Pythia8` and `Herwig++`. Our results open up the possibility that we might be able to reproduce the wideness of jets observed in real data by varying the value of α in the evolution variable continuously.

謝辞

私は、近代的な教育システムの発展、特に日本におけるそれに関わってこられた全ての方々に感謝します。また、教育課程の終わりに位置する博士後期課程を KEK で過ごせた事は、私にとって、物理研究の面だけでなく他の面から見ても非常にプラスとなりました。

指導教官である野尻美保子氏に感謝します。私は、KEK に来る前の M1 の頃に本論文の主題であるジェットに興味を持ちました。しかし、論文等の形にすることはできませんでした。KEK に移る際、当時在籍していた立教大学のポスドクの木村哲士氏に野尻さんを指導教官にしたらいいのではないかと言われました。結果、ジェットに関する二つの仕事をする事ができました。それぞれの仕事において、$C_1^{(\beta)}$ という物理量を用いましたが、野尻さんにそれに関する論文を読むよう進められたのがきっかけです。はじめ、読み進める事ができなかったのですが、彼女がオーガナイザーの一人として関わった国際会議 MC4BSM 2014 において、その論文の著者の一人である Andrew J. Larkoski 氏に偶然出くわし、かなり親切な指導をして頂きました。一つ目の仕事に関して、私は熱心に、計算は、しましたが、主要なアイデアの出所は、論文になるだいぶ前に野尻さんが gg 課程における second jet の p_T が parton のものと随分違っている事に着目した事と、Zg 課程の $p_T(j_s)$ は parton p_T に近くなる事に気付いた事あたりで尽きていると思います。また、本格的な collider 解析を理論サイドから日本に広めて頂いた事に感謝します。共同研究者である Satyanarayan Mukhopadhyay 氏、Bryan R. Webber 氏と非常に有益な議論をすることができました。Satya には二つ目の論文のとても注意深い推敲もしてもらいました、ありがとうございます。

B の物理に関しても四つの仕事をすることが出来ました。出発点は、2011 年度原子核三者若手夏の学校における吉永尊洸氏のショートレビューです。良いレビュー論文もいくつか紹介して頂きました。当時 SG-L の存在を知らなかった私ですが、第 8 回 B ファクトリー物理勉強会の存在をネットのどこかで知りました。初の研究会参加で緊張していたのですが、清裕一郎氏に B decay の form factor に関して丁寧に教えて頂き、KEK-FF 2012 に参加する事を奨めてもらいました。その研究会への参加は自分にとって大きな意味を持ちました。そこで渡邉諒太郎氏に B の semi-leptonic decay に関して教えてもらい、かなり詳しいノートも頂きました。そして、主にそれを参考にして初めての論文を書く事が出来ました。そこで出会った Paul Posch 氏に総研大への進学を勧めてもらいました。田中実氏、Andrey Tayduganov 氏、後藤亨氏からも B の研究を通じて良い指導を受ける事ができました。

萩原薫氏には、B の物理とジェットの両方に関して指導して頂きました、感謝します。萩原さんの物理、またはそれ以外に対する考えは非常におもしろく、また勇気を与えてくれるものでした。

私は共同研究者、キーパーソン、KEK の人々との出会い、そして教育制度に恵まれました。それら全てに感謝します。

Acknowledgements

I am grateful to all people who have involved the development of the modern education system, especially in japanese society. And I feel happy that I can visit KEK in doctor course, which is the most last term of education system.

I am grateful to my adviser Mihoko. M. Nojiri. When I was in first degree of master course in Rikkyo university, I had interested in jet physics, which is a central theme in this thesis. But I could not write paper. When I moved to KEK, Dr. Tetsuji Kimura suggested to me that I choose Mihoko as adviser. This choice lead to our two papers concerned with jet physics. I used a variable $C_1^{(\beta)}$ for both paper. This cue is Mihoko. I met Dr. Andrew J. Larkoski who is one of authors of C_1's paper at MC4BSM2014, and he taught many things me very kindly. Although I calculated hardly in the first paper about jet, main concept come from Mihoko's past calculations and findings actually. Also I am grateful to Dr. Satyanarayan Mukhopadhyay and Prof. Bryan R. Webber for many useful discussion. Satya also read and correct the second paper about jet very carefully, thanks.

I could write four papers about B physics. The starting point is a short review about B physics by Dr. Takahiro Yoshinaga at a meeting in Young Nuclear and Particle Physicist Group of Japan in 2011. He taught me good references about B physics. Although I did not know SG-L mailing list then, I found B factory workshop 8th somewhere in internet. I met Prof. Yuichiro Kiyo at the meeting, and he taught me about form factor of B decay. Also He recommend to attend KEK-FF 2012. The attendance in KEK-FF 2012 was very good for me. I met Dr. Ryotarou Watanabe, and he taught me about semi-leptonic B decay very carefully, and also gave me his note. By using the note, I wrote my first paper. I met Dr. Paul Posch, and he recommended KEK and Sokendai. Prof. Minoro Tanaka, Dr. Andrey Tayduganov, and Dr. Toru Goto also taught me many things through B physics. Thank you very much.

I am grateful to Prof. Kaoru Hagiwara. I enjoyed discussion with him about jet and B physics both. His convictions for not only Physics but also other things encourage me so much.

I am blessed with my collaborators, the key person, encounters with people in KEK, and the modern education system in Japan. I am very grateful to all of them.

A Distributions of discrimination variables

In Figs. 32-34 we show 2-dimensional plots of the joint distributions of the three discrimination variables used in the MVA presented in Section 4.2, for the two Monte Carlo event generators `Herwig++` and `Pythia8`. The following features may be observed:

- There are differences between the distributions predicted by the two Monte Carlos, those of `Pythia8` being somewhat narrower for quark jets and substantially narrower for gluon jets.
- The distributions of the infrared-unsafe variable n_{ch} show the greatest differences, with those of `Pythia8` being larger at high n_{ch}. This could be due to differences in tuning of the non-perturbative parameters of the generators.
- The above features are reflected in the likelihood plots, showing the probability ratio $P_q/(P_q + P_g)$, and account for the higher discrimination efficiency predicted by `Pythia8` (Fig. 19 vs Fig. 18).
- The quark-gluon discrimination in the events with associated jets is weaker than that for $n_{\mathrm{Ajet}} = 0$. This is expected because the events are selected according to $p_T(j_s)$, the sum of leading and associated jet p_T's. Therefore those with associated jets have leading jets with lower p_T's, which have lower discriminating power.
- Nevertheless the inclusion of the associated jet category improves the MVA performance, because the probability of an associated jet is lower for quark jets.

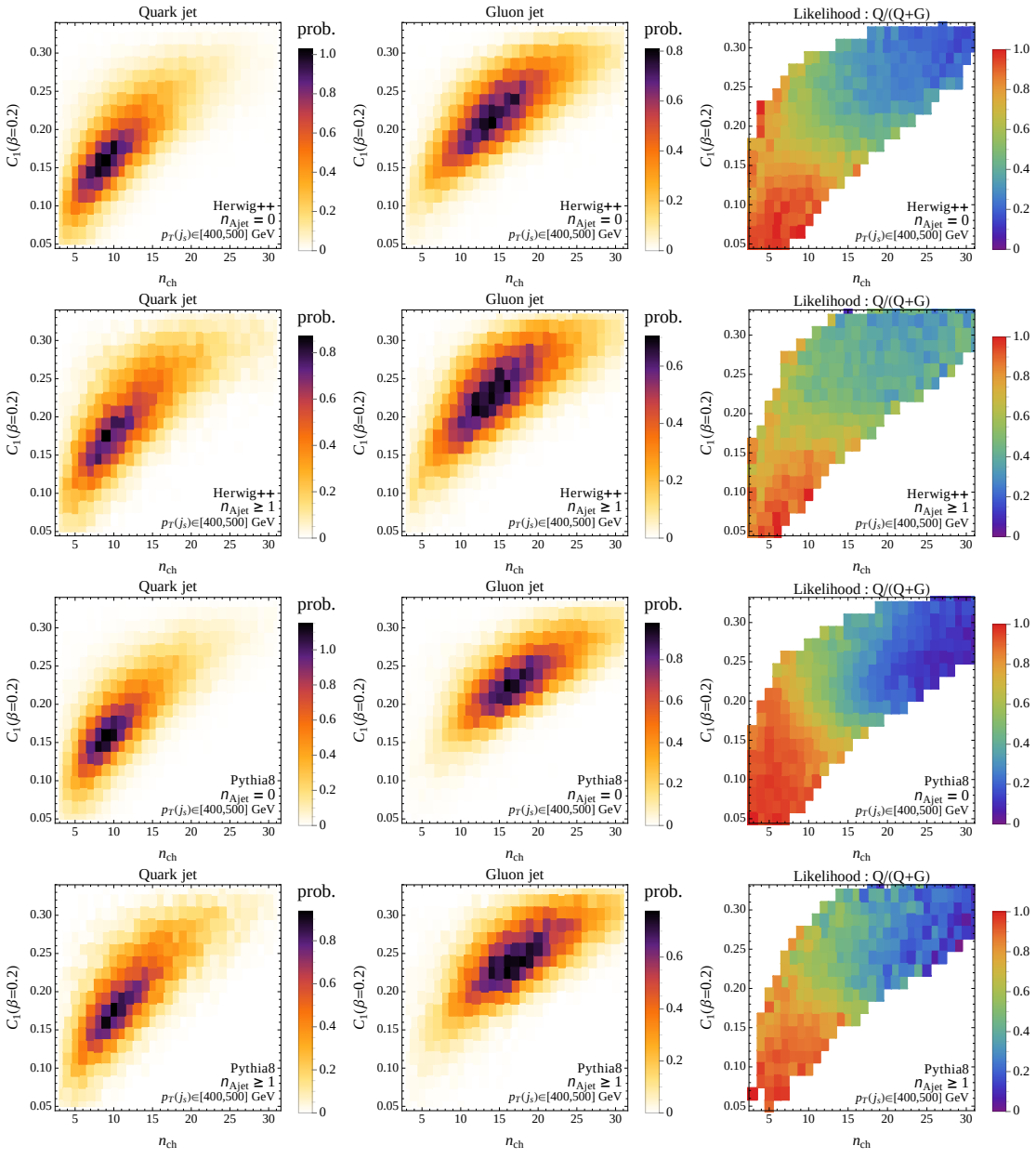

Figure 32: Joint distributions of $n_{\rm ch}$ and $C_1^{(\beta=0.2)}$ in `Herwig++` and `Pythia8`, for quark and gluon jets with $p_T(j_s) \in [400, 500]$ GeV having $n_{\rm Ajet} = 0$ and ≥ 1 associated jets.

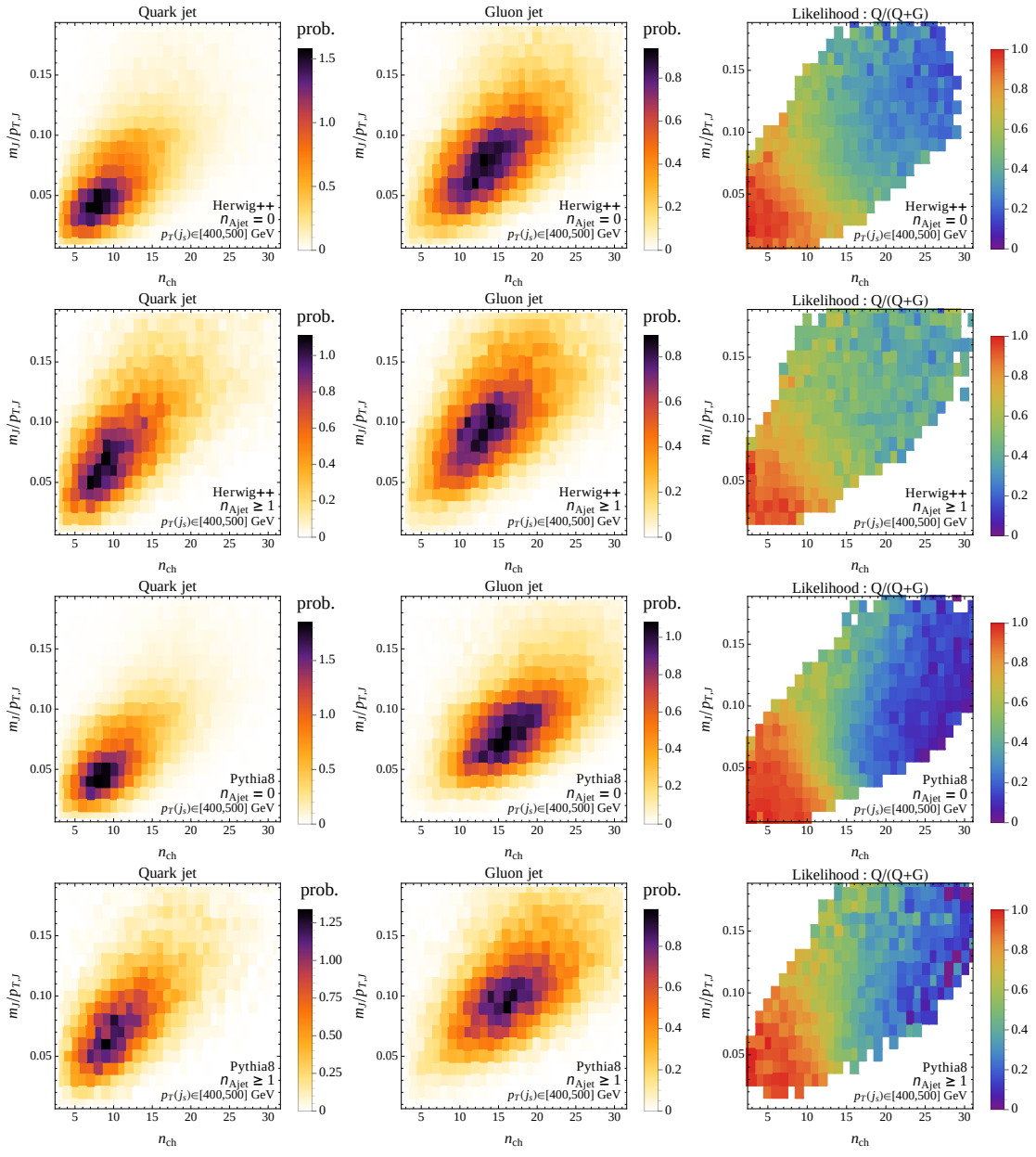

Figure 33: Joint distributions of $n_{\rm ch}$ and $m_J/p_{T,J}$ in `Herwig++` and `Pythia8`, for quark and gluon jets with $p_T(j_s) \in [400, 500]$ GeV having $n_{\rm Ajet} = 0$ and ≥ 1 associated jets.

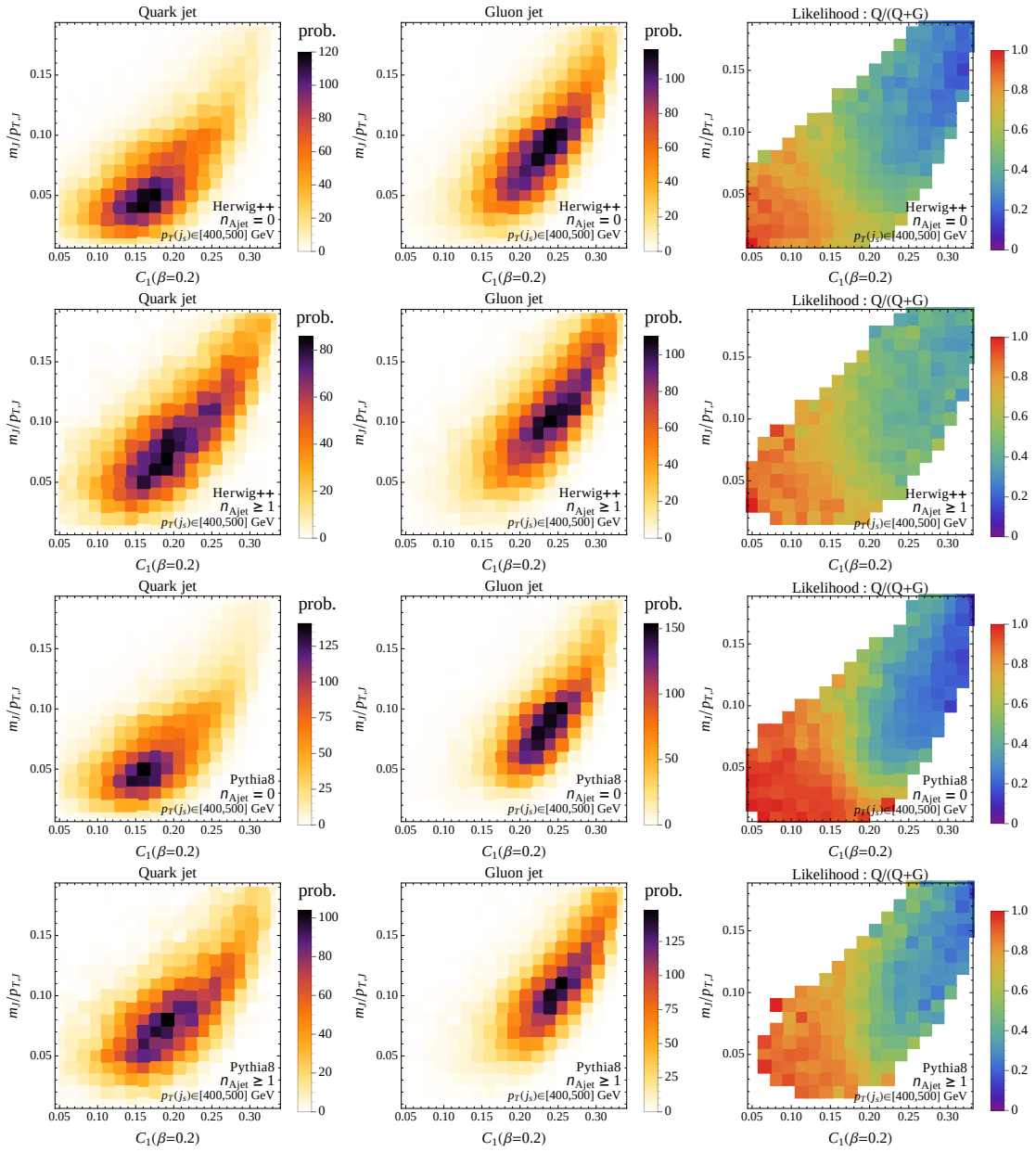

Figure 34: Joint distributions of $C_1^{(\beta=0.2)}$ and $m_J/p_{T,J}$ in `Herwig++` and `Pythia8`, for quark and gluon jets with $p_T(j_s) \in [400, 500]$ GeV having $n_{\mathrm{Ajet}} = 0$ and ≥ 1 associated jets.

B Veto algorithm

Developers of simulation tools should employ several techniques for optimal simulation, e.g., fast simulation. We introduce an useful technique to generate variables in Markov chain, which is called as veto algorithm.

A function $f(t)dt$ show a probability that something will happen (we call the happening as "emission" later for brevity) from time (or a scale) t to $t + dt$. The probability does not depend on what happened past. A probability that any emission doesn't happen from 0 to t is given as

$$\Delta(t) = \exp\left[-\int_0^t f(t')dt'\right]. \tag{B.1}$$

A probability that an emission happen in $[t, t + dt]$ for the first time is

$$P(t)dt = \Delta(t) \times f(t)dt. \tag{B.2}$$

We can generate next time by solving an equation:

$$\Delta(t) = R, \tag{B.3}$$

where R is random number which is generated flatly in $[0, 1]$. If the integral of f (F) and the inverse of integrant (F^{-1}) are known, we can solve Eq. B.3:

$$t = F^{-1}(F(0) - \ln R). \tag{B.4}$$

When we don't know F and/or F^{-1}, we may need to solve Eq. (B.3) numerically for each emissions. More efficient way is as follow. First we look for $\tilde{f}(t)$, which satisfy $\tilde{f}(t) \geq f(t)$ for all t and integral $\tilde{F}$ and its inverse $\tilde{F}^{-1}$ are known. By using the function, next emission time t is generated tentatively by,

$$t = \tilde{F}^{-1}(\tilde{F}(0) - \ln R). \tag{B.5}$$

If $f(t)/\tilde{f}(t) < R'$ is true, t is accepted as next time, where $R' \in [0, 1]$ is other flat random number. If it is false, t is rejected and the generation start from t. We continue that until accepted time is found. The distribution of accepted time t by the procedure (called as veto algorithm) is the same what we want, i.e., $P(t)$.

We show that the probability that next time is accepted in t by veto algorithm, $\tilde{P}(t)$, is equivalent to $P(t)$. The probability is repented as

$$\tilde{P}(t) = \sum_{n=0}^{\infty} \tilde{P}_n(t), \tag{B.6}$$

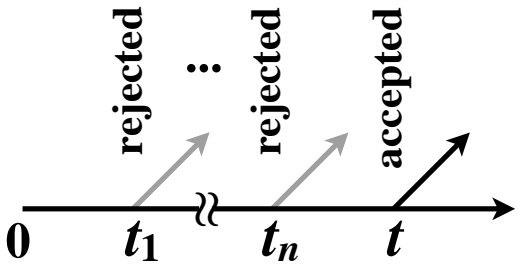

Figure 35: CAPTION

where $\tilde{P}_n(t)$ is the probability that an emission is accepted at t after emissions are rejected n times. Evaluation of $\tilde{P}_0(t)$ is trivial:

$$\tilde{P}_0(t) = \exp\left[-\int_0^t \tilde{f}(t')dt'\right] \tilde{f}(t) \times \frac{f(t)}{\tilde{f}(t)}, \tag{B.7}$$

$$= \exp\left[-\int_0^t \tilde{f}(t')dt'\right] f(t). \tag{B.8}$$

The ratio factor in Eq. (B.7) shows accepted probability at t. For $n \geq 1$, it is written as

$$\begin{aligned}\tilde{P}_n(t) = \int_0^t dt_1 \cdots \int_{t_{n-1}}^t dt_n \exp\left[-\int_0^{t_1} \tilde{f}(t')dt'\right] \tilde{f}(t_1)\left(1 - \frac{f(t_1)}{\tilde{f}(t_1)}\right) \\ \times \cdots \times \exp\left[-\int_{t_{n-1}}^{t_n} \tilde{f}(t')dt'\right] \tilde{f}(t_n)\left(1 - \frac{f(t_n)}{\tilde{f}(t_n)}\right) \\ \times \exp\left[-\int_{t_n}^t \tilde{f}(t')dt'\right] \tilde{f}(t)\frac{f(t)}{\tilde{f}(t)},\end{aligned} \tag{B.9}$$

$$= \exp\left[-\int_0^t \tilde{f}(t')dt'\right] f(t) \int_0^t dt_1 \cdots \int_{t_{n-1}}^t dt_n \prod_{i=1}^n [\tilde{f}(t_i) - f(t_i)], \tag{B.10}$$

$$= \tilde{P}_0(t)\frac{1}{n!}\left\{\int_0^t dt'[\tilde{f}(t') - f(t')]\right\}^n. \tag{B.11}$$

The factors $(1 - f(t_i)/\tilde{f}(t_i))$ show the rejected probability at t_i. See Fig. 35 for your understanding. We get relation which we wished,

$$\tilde{P}(t) = \tilde{P}_0(t) \int_0^t dt' \exp[\tilde{f}(t') - f(t')], \tag{B.12}$$

$$= P(t). \tag{B.13}$$

The function $f(t)$ sometime contain additional variable, e.g., it is the momentum fraction z in the parton shower. A probability that any emission doesn't happen from 0 to t is given as

$$\Delta(t) = \exp\left[-\int_0^t dt' f(t)\right], \qquad f(t) = \int_{z_-(t)}^{z_+(t)} f(t,z)dz, \tag{B.14}$$

where $z_-(t)$ and $z_+(t)$ show a minimal and maximal allowed region for z at t. We generate z in probability of $f(t,z)/f(t)$ after generating t. So, a probability that an emission at t and z for the first time is written as

$$P(t,z) = \Delta(t) \times f(t) \times \frac{f(t,z)}{f(t)}, \tag{B.15}$$

$$= \Delta(t) f(t,z). \tag{B.16}$$

Now we prepare a function $\tilde{f}$ which satisfies $\tilde{f}(t,z) > f(t,z)$ for all t and z, and its integral and inverse of integral are known, also defined as

$$\tilde{f}(t) = \int_{\tilde{z}_-(t)}^{\tilde{z}_+(t)} \tilde{f}(t,z')dz', \qquad \tilde{z}_-(t) < z_-(t) < z_+(t) < \tilde{z}_+(t). \tag{B.17}$$

We get next time t tentatively by Eq. (B.5), and z by

$$\frac{\int_{\tilde{z}_-(t)}^{z} dz' \tilde{f}(t,z')}{\tilde{f}(t)} = R'. \tag{B.18}$$

If $f(t,z)/\tilde{f}(t,z) < R''$ is true, t is accepted as next time, where $R'' \in [0,1]$ is other flat random number, and note that

$$f(t,z) = 0, \qquad \text{for} \quad \tilde{z}_-(t) < z < z_-(t) \quad \text{or} \quad z_+(t) < z < \tilde{z}_+(t) \tag{B.19}$$

If it is false, t is rejected and the generation start from t.

We show that the probability that next time is accepted in t by veto algorithm, $\tilde{P}(t,z)$, is equivalent to $P(t,z)$. The probability is repented as

$$\tilde{P}(t,z) = \sum_{n=0}^{\infty} \tilde{P}_n(t,z), \tag{B.20}$$

where $\tilde{P}_n(t,z)$ is the probability that an emission is accepted at (t,z) after emissions are rejected n times. Accepted probability at t,z is

$$\exp\left[-\int_0^t \tilde{f}(t')dt'\right] \tilde{f}(t,z)\frac{f(t,z)}{\tilde{f}(t,z)} = \exp\left[-\int_0^t \tilde{f}(t')dt'\right] f(t,z), \tag{B.21}$$

Rejected probability at t, z is

$$\exp\left[-\int_0^t \tilde{f}(t')dt'\right]\tilde{f}(t,z)\left(1-\frac{f(t,z)}{\tilde{f}(t,z)}\right)=\exp\left[-\int_0^t \tilde{f}(t')dt'\right][\tilde{f}(t,z)-f(t,z)], \tag{B.22}$$

So, $\tilde{P}_n(t,z)$ is written as

$$\begin{aligned}\tilde{P}_n(t,z) &= \int_0^t dt_1 \cdots \int_{t_{n-1}}^t dt_n \exp\left[-\int_0^{t_1}\tilde{f}(t')dt'\right]\left\{\int_{\tilde{z}_-(t_1)}^{\tilde{z}_+(t_1)} dz[\tilde{f}(t_1,z)-f(t_1,z)]\right\} \\ &\quad \times\cdots\times \exp\left[-\int_{t_{n-1}}^{t_n}\tilde{f}(t')dt'\right]\left\{\int_{\tilde{z}_-(t_n)}^{\tilde{z}_+(t_n)} dz[\tilde{f}(t_n,z)-f(t_n,z)]\right\} \\ &\quad \times \exp\left[-\int_{t_n}^{t}\tilde{f}(t')dt'\right]f(t,z), \\ &= \exp\left[-\int_0^t \tilde{f}(t')dt'\right]f(t,z)\int_0^t dt_1\cdots\int_{t_{n-1}}^t dt_n\prod_{i=1}^n[\tilde{f}(t_i)-f(t_i)], \qquad \text{(B.23)} \\ &= \tilde{P}_0(t,z)\frac{1}{n!}\left\{\int_0^t dt'[\tilde{f}(t')-f(t')]\right\}^n. \qquad \text{(B.24)}\end{aligned}$$

We get relation which we wished,

$$\begin{aligned}\tilde{P}(t,z) &= \tilde{P}_0(t,z)\int_0^t dt'\exp[\tilde{f}(t')-f(t')], \qquad \text{(B.25)} \\ &= P(t,z). \qquad \text{(B.26)}\end{aligned}$$

C $n!$ factor

We define I as

$$I=\int_0^1 dx_1\int_0^1 dx_2\cdots\int_0^1 dx_n f(x_1,x_2,...,x_n), \tag{C.1}$$

where $f(...,x_i,...,x_j,...) = f(...,x_j,...,x_i,...)$. For example, $f(...,x_i,...,x_j,...) = \prod_i g(x_i)$ satisfy the property. In this case ordering integral is given by

$$\int_0^1 dx_1\int_0^{x_1} dx_2\cdots\int_0^{x_{n-1}} dx_n f(x_1,x_2,...,x_n)=\frac{I}{n!}. \tag{C.2}$$

since such ordering condition $x_{i_1} > x_{i_2} > \cdots > x_{i_n}$ divide integral space into $n!$ regions.

References

[1] G. Aad *et al.* [ATLAS Collaboration], "Observation of a new particle in the search for the Standard Model Higgs boson with the ATLAS detector at the LHC," Phys. Lett. B **716**, 1 (2012) doi:10.1016/j.physletb.2012.08.020 [arXiv:1207.7214 [hep-ex]].

S. Chatrchyan *et al.* [CMS Collaboration], "Observation of a new boson at a mass of 125 GeV with the CMS experiment at the LHC," Phys. Lett. B **716**, 30 (2012) doi:10.1016/j.physletb.2012.08.021 [arXiv:1207.7235 [hep-ex]].

[2] J. C. Collins, D. E. Soper and G. F. Sterman, "Factorization of Hard Processes in QCD," Adv. Ser. Direct. High Energy Phys. **5**, 1 (1989) doi:10.1142/9789814503266_0001 [hep-ph/0409313].

[3] G. Weiglein *et al.* [LHC/LC Study Group Collaboration], "Physics interplay of the LHC and the ILC," Phys. Rept. **426**, 47 (2006) doi:10.1016/j.physrep.2005.12.003 [hep-ph/0410364].

[4] J. M. Butterworth, A. R. Davison, M. Rubin and G. P. Salam, "Jet substructure as a new Higgs search channel at the LHC," Phys. Rev. Lett. **100**, 242001 (2008) [arXiv:0802.2470 [hep-ph]].

[5] A. Abdesselam, E. B. Kuutmann, U. Bitenc, G. Brooijmans, J. Butterworth, P. Bruckman de Renstrom, D. Buarque Franzosi and R. Buckingham *et al.*, "Boosted objects: A Probe of beyond the Standard Model physics," Eur. Phys. J. C **71**, 1661 (2011) [arXiv:1012.5412 [hep-ph]].

[6] A. Altheimer, S. Arora, L. Asquith, G. Brooijmans, J. Butterworth, M. Campanelli, B. Chapleau and A. E. Cholakian *et al.*, "Jet Substructure at the Tevatron and LHC: New results, new tools, new benchmarks," J. Phys. G **39**, 063001 (2012) [arXiv:1201.0008 [hep-ph]].

[7] A. Altheimer, A. Arce, L. Asquith, J. Backus Mayes, E. Bergeaas Kuutmann, J. Berger, D. Bjergaard and L. Bryngemark *et al.*, "Boosted objects and jet substructure at the LHC. Report of BOOST2012, held at IFIC Valencia, 23rd-27th of July 2012," Eur. Phys. J. C **74**, no. 3, 2792 (2014) [arXiv:1311.2708 [hep-ex]].

[8] D. Adams, A. Arce, L. Asquith, M. Backovic, T. Barillari, P. Berta, D. Bertolini and A. Buckley *et al.*, "Towards an Understanding of the Correlations in Jet Substructure," arXiv:1504.00679 [hep-ph].

[9] M. H. Seymour, "Searches for new particles using cone and cluster jet algorithms: A Comparative study," Z. Phys. C **62**, 127 (1994).

[10] J. M. Butterworth, B. E. Cox and J. R. Forshaw, "WW scattering at the CERN LHC," Phys. Rev. D **65**, 096014 (2002) [hep-ph/0201098].

[11] J. Thaler and L. T. Wang, "Strategies to Identify Boosted Tops," JHEP **0807**, 092 (2008) [arXiv:0806.0023 [hep-ph]].

[12] D. E. Kaplan, K. Rehermann, M. D. Schwartz and B. Tweedie, "Top Tagging: A Method for Identifying Boosted Hadronically Decaying Top Quarks," Phys. Rev. Lett. **101**, 142001 (2008) [arXiv:0806.0848 [hep-ph]].

[13] L. G. Almeida, S. J. Lee, G. Perez, G. F. Sterman, I. Sung and J. Virzi, "Substructure of high-p_T Jets at the LHC," Phys. Rev. D **79**, 074017 (2009) [arXiv:0807.0234 [hep-ph]].

[14] T. Plehn, G. P. Salam and M. Spannowsky, "Fat Jets for a Light Higgs," Phys. Rev. Lett. **104**, 111801 (2010) [arXiv:0910.5472 [hep-ph]].

[15] J. Gallicchio and M. D. Schwartz, "Seeing in Color: Jet Superstructure," Phys. Rev. Lett. **105**, 022001 (2010) [arXiv:1001.5027 [hep-ph]].

[16] L. G. Almeida, S. J. Lee, G. Perez, G. Sterman and I. Sung, "Template Overlap Method for Massive Jets," Phys. Rev. D **82**, 054034 (2010) [arXiv:1006.2035 [hep-ph]].

[17] T. Plehn, M. Spannowsky, M. Takeuchi and D. Zerwas, "Stop Reconstruction with Tagged Tops," JHEP **1010**, 078 (2010) [arXiv:1006.2833 [hep-ph]].

[18] J. Thaler and K. Van Tilburg, "Identifying Boosted Objects with N-subjettiness," JHEP **1103**, 015 (2011) [arXiv:1011.2268 [hep-ph]].

[19] D. E. Soper and M. Spannowsky, "Finding physics signals with shower deconstruction," Phys. Rev. D **84**, 074002 (2011) [arXiv:1102.3480 [hep-ph]].

[20] M. Cacciari and G. P. Salam, "Pileup subtraction using jet areas," Phys. Lett. B **659**, 119 (2008) [arXiv:0707.1378 [hep-ph]].

[21] S. D. Ellis, C. K. Vermilion and J. R. Walsh, "Recombination Algorithms and Jet Substructure: Pruning as a Tool for Heavy Particle Searches," Phys. Rev. D **81**, 094023 (2010) [arXiv:0912.0033 [hep-ph]].

[22] D. Krohn, J. Thaler and L. T. Wang, "Jet Trimming," JHEP **1002**, 084 (2010) [arXiv:0912.1342 [hep-ph]].

[23] R. Alon, E. Duchovni, G. Perez, A. P. Pranko and P. K. Sinervo, "A Data-driven method of pile-up correction for the substructure of massive jets," Phys. Rev. D **84**, 114025 (2011) [arXiv:1101.3002 [hep-ph]].

[24] G. Soyez, G. P. Salam, J. Kim, S. Dutta and M. Cacciari, "Pileup subtraction for jet shapes," Phys. Rev. Lett. **110**, no. 16, 162001 (2013) [arXiv:1211.2811 [hep-ph]].

[25] A. J. Larkoski, S. Marzani, G. Soyez and J. Thaler, "Soft Drop," JHEP **1405**, 146 (2014) [arXiv:1402.2657 [hep-ph]].

[26] R. Sato, S. Shirai and K. Tobioka, "Gluino Decay as a Probe of High Scale Supersymmetry Breaking," JHEP **1211**, 041 (2012) doi:10.1007/JHEP11(2012)041 [arXiv:1207.3608 [hep-ph]].

[27] J. Gallicchio and M. D. Schwartz, "Quark and Gluon Tagging at the LHC," Phys. Rev. Lett. **107**, 172001 (2011) [arXiv:1106.3076 [hep-ph]].

[28] J. Gallicchio, J. Huth, M. Kagan, M. D. Schwartz, K. Black and B. Tweedie, "Multivariate discrimination and the Higgs + W/Z search," JHEP **1104** (2011) 069.

[29] J. Gallicchio and M. D. Schwartz, JHEP **1304** (2013) 090.

[30] J. Gallicchio and M. D. Schwartz, "Quark and Gluon Jet Substructure," JHEP **1304**, 090 (2013) [arXiv:1211.7038 [hep-ph]].

[31] D. Krohn, M. D. Schwartz, T. Lin and W. J. Waalewijn, "Jet Charge at the LHC," Phys. Rev. Lett. **110**, no. 21, 212001 (2013) [arXiv:1209.2421 [hep-ph]].

[32] S. Chatrchyan *et al.* [CMS Collaboration], "Search for a Higgs boson in the decay channel H to ZZ(*) to q qbar ℓ^- l+ in pp collisions at $\sqrt{s} = 7$ TeV," JHEP **1204**, 036 (2012) [arXiv:1202.1416 [hep-ex]].

[33] A. J. Larkoski, G. P. Salam and J. Thaler, "Energy Correlation Functions for Jet Substructure," JHEP **1306** (2013) 108.

[34] A. J. Larkoski, J. Thaler and W. J. Waalewijn, "Gaining (Mutual) Information about Quark/Gluon Discrimination," JHEP **1411** (2014) 129.

[35] CMS Collaboration [CMS Collaboration], "Pileup Jet Identification," CMS-PAS-JME-13-005.

[36] G. Aad *et al.* [ATLAS Collaboration], "Light-quark and gluon jet discrimination in pp collisions at $\sqrt{s} = 7$ TeV with the ATLAS detector," Eur. Phys. J. C **74**, no. 8, 3023 (2014) [arXiv:1405.6583 [hep-ex]].

[37] CMS Collaboration, "Performance of quark/gluon discrimination using pp collision data at $\sqrt{s} = 8$ TeV," CMS-PAS-JME-13-002.

[38] T. Sjostrand, S. Mrenna and P. Z. Skands, "PYTHIA 6.4 Physics and Manual," JHEP **0605**, 026 (2006).

[39] T. Sjostrand, S. Mrenna and P. Z. Skands, "A Brief Introduction to PYTHIA 8.1," Comput. Phys. Commun. **178** (2008) 852; T. Sjostrand, S. Ask, J. R. Christiansen, R. Corke, N. Desai, P. Ilten, S. Mrenna and S. Prestel *et al.*, "An Introduction to PYTHIA 8.2," arXiv:1410.3012 [hep-ph].

[40] G. Corcella, I. G. Knowles, G. Marchesini, S. Moretti, K. Odagiri, P. Richardson, M. H. Seymour and B. R. Webber, "HERWIG 6: An Event generator for hadron emission reactions with interfering gluons (including supersymmetric processes)," JHEP **0101**, 010 (2001) [hep-ph/0011363].

[41] M. Bahr, S. Gieseke, M. A. Gigg, D. Grellscheid, K. Hamilton, O. Latunde-Dada, S. Platzer and P. Richardson *et al.*, "Herwig++ Physics and Manual," Eur. Phys. J. C **58** (2008) 639.

[42] T. Gleisberg, S. Hoeche, F. Krauss, M. Schonherr, S. Schumann, F. Siegert and J. Winter, "Event generation with SHERPA 1.1," JHEP **0902**, 007 (2009) [arXiv:0811.4622 [hep-ph]].

[43] G. Aad *et al.* [ATLAS Collaboration], "Jet mass and substructure of inclusive jets in $\sqrt{s} = 7$ TeV pp collisions with the ATLAS experiment," JHEP **1205**, 128 (2012) [arXiv:1203.4606 [hep-ex]].

[44] V. Khachatryan *et al.* [CMS Collaboration], "Search for massive resonances in dijet systems containing jets tagged as W or Z boson decays in pp collisions at $\sqrt{s} = 8$ TeV," JHEP **1408**, 173 (2014) [arXiv:1405.1994 [hep-ex]].

[45] V. N. Gribov and L. N. Lipatov, "Deep inelastic e p scattering in perturbation theory," Sov. J. Nucl. Phys. **15**, 438 (1972) [Yad. Fiz. **15**, 781 (1972)].

[46] G. Altarelli and G. Parisi, "Asymptotic Freedom in Parton Language," Nucl. Phys. B **126**, 298 (1977).

[47] T. Kinoshita, "Mass singularities of Feynman amplitudes," J. Math. Phys. **3**, 650 (1962). doi:10.1063/1.1724268

[48] T. D. Lee and M. Nauenberg, "Degenerate Systems and Mass Singularities," Phys. Rev. **133**, B1549 (1964). doi:10.1103/PhysRev.133.B1549

[49] S. Catani, F. Krauss, R. Kuhn and B. R. Webber, "QCD matrix elements + parton showers," JHEP **0111**, 063 (2001) doi:10.1088/1126-6708/2001/11/063 [hep-ph/0109231].

[50] L. Lonnblad, "Correcting the color dipole cascade model with fixed order matrix elements," JHEP **0205**, 046 (2002) doi:10.1088/1126-6708/2002/05/046 [hep-ph/0112284].

[51] N. Lavesson and L. Lonnblad, "W+jets matrix elements and the dipole cascade," JHEP **0507**, 054 (2005) doi:10.1088/1126-6708/2005/07/054 [hep-ph/0503293].

[52] M. L. Mangano, M. Moretti, F. Piccinini and M. Treccani, "Matching matrix elements and shower evolution for top-quark production in hadronic collisions," JHEP **0701**, 013 (2007) doi:10.1088/1126-6708/2007/01/013 [hep-ph/0611129].

[53] S. Mrenna and P. Richardson, "Matching matrix elements and parton showers with HERWIG and PYTHIA," JHEP **0405**, 040 (2004) doi:10.1088/1126-6708/2004/05/040 [hep-ph/0312274].

[54] S. Frixione and B. R. Webber, "Matching NLO QCD computations and parton shower simulations," JHEP **0206**, 029 (2002) doi:10.1088/1126-6708/2002/06/029 [hep-ph/0204244].

[55] S. Frixione, P. Nason and B. R. Webber, "Matching NLO QCD and parton showers in heavy flavor production," JHEP **0308**, 007 (2003) doi:10.1088/1126-6708/2003/08/007 [hep-ph/0305252].

[56] S. Frixione and B. R. Webber, "The MC and NLO 3.4 Event Generator," arXiv:0812.0770 [hep-ph].

[57] S. Frixione, P. Nason and C. Oleari, "Matching NLO QCD computations with Parton Shower simulations: the POWHEG method," JHEP **0711** (2007) 070 doi:10.1088/1126-6708/2007/11/070 [arXiv:0709.2092 [hep-ph]].

[58] A. H. Mueller, "On the Multiplicity of Hadrons in QCD Jets," Phys. Lett. B **104**, 161 (1981). doi:10.1016/0370-2693(81)90581-5

[59] A. Bassetto, M. Ciafaloni, G. Marchesini and A. H. Mueller, "Jet Multiplicity and Soft Gluon Factorization," Nucl. Phys. B **207**, 189 (1982). doi:10.1016/0550-3213(82)90161-4

[60] Y. I. Azimov, Y. L. Dokshitzer, V. A. Khoze and S. I. Troyan, "Similarity of Parton and Hadron Spectra in QCD Jets," Z. Phys. C **27** (1985) 65. doi:10.1007/BF01642482

[61] Y. I. Azimov, Y. L. Dokshitzer, V. A. Khoze and S. I. Troyan, "Humpbacked QCD Plateau in Hadron Spectra," Z. Phys. C **31**, 213 (1986). doi:10.1007/BF01479529

[62] Y. L. Dokshitzer, V. A. Khoze, S. I. Troian and A. H. Mueller, "QCD Coherence in High-Energy Reactions," Rev. Mod. Phys. **60** (1988) 373. doi:10.1103/RevModPhys.60.373

[63] S. Catani and M. H. Seymour, "The Dipole formalism for the calculation of QCD jet cross-sections at next-to-leading order," Phys. Lett. B **378**, 287 (1996) doi:10.1016/0370-2693(96)00425-X [hep-ph/9602277].

[64] Y. Delenda and K. Khelifa-Kerfa, "Eikonal gluon bremsstrahlung at finite N_c beyond two loops," arXiv:1512.05401 [hep-ph].

[65] B. R. Webber, "Introduction to Event Generators," MCnet School, 2014.

[66] M. Cacciari, G. P. Salam and G. Soyez, "FastJet user manual," Eur. Phys. J. C **72** (2012) 1896; M. Cacciari and G. P. Salam, "Dispelling the N^3 myth for the k_t jet-finder," Phys. Lett. B **641** (2006) 57.

[67] S. Catani, Y. L. Dokshitzer, M. Olsson, G. Turnock and B. R. Webber, "New clustering algorithm for multi-jet cross sections in e^+e^- annihilation," Phys. Lett. B **269** (1991) 432.

[68] S. Catani, Y. L. Dokshitzer, M. H. Seymour and B. R. Webber, "Longitudinally invariant k_t clustering algorithms for hadron hadron collisions," Nucl. Phys. B **406** (1993) 187.

[69] S. D. Ellis and D. E. Soper, "Successive combination jet algorithm for hadron collisions," Phys. Rev. D **48** (1993) 3160.

[70] M. Cacciari, G. P. Salam and G. Soyez, "The anti-k_t jet clustering algorithm," JHEP **0804** (2008) 063.

[71] P. Abreu *et al.* [DELPHI Collaboration], "The Scale dependence of the hadron multiplicity in quark and gluon jets and a precise determination of C(A) / C(F)," Phys. Lett. B **449**, 383 (1999) doi:10.1016/S0370-2693(99)00112-4 [hep-ex/9903073].

[72] S. Chatrchyan *et al.* [CMS Collaboration], "Shape, Transverse Size, and Charged Hadron Multiplicity of Jets in pp Collisions at 7 TeV," JHEP **1206**, 160 (2012) doi:10.1007/JHEP06(2012)160 [arXiv:1204.3170 [hep-ex]].

[73] A. J. Larkoski, D. Neill and J. Thaler, "Jet Shapes with the Broadening Axis," JHEP **1404** (2014) 017.

[74] A. Banfi, G. P. Salam and G. Zanderighi, "Principles of general final-state resummation and automated implementation," JHEP **0503**, 073 (2005) [hep-ph/0407286].

[75] K. Konishi, A. Ukawa and G. Veneziano, "Jet Calculus: A Simple Algorithm for Resolving QCD Jets," Nucl. Phys. B **157** (1979) 45.

[76] Y. L. Dokshitzer, V. A. Khoze, A. H. Mueller and S. I. Troian, "Basics of perturbative QCD," Gif-sur-Yvette, France: Ed. Frontieres (1991) 274 p.

[77] R. K. Ellis, W. J. Stirling and B. R. Webber, "QCD and collider physics," Camb. Monogr. Part. Phys. Nucl. Phys. Cosmol. **8** (1996) 1.

[78] E. Gerwick, S. Schumann, B. Gripaios and B. Webber, "QCD Jet Rates with the Inclusive Generalized k_t Algorithms," JHEP **1304** (2013) 089.

[79] M. Dasgupta and G. P. Salam, "Resummation of nonglobal QCD observables," Phys. Lett. B **512**, 323 (2001) doi:10.1016/S0370-2693(01)00725-0 [hep-ph/0104277].

[80] M. Dasgupta, L. Magnea and G. P. Salam, "Non-perturbative QCD effects in jets at hadron colliders," JHEP **0802** (2008) 055.

[81] G. P. Salam, "Towards Jetography," Eur. Phys. J. C **67** (2010) 637.

[82] J. Pumplin, D. R. Stump, J. Huston, H. L. Lai, P. M. Nadolsky and W. K. Tung, "New generation of parton distributions with uncertainties from global QCD analysis," JHEP **0207** (2002) 012.

[83] A. Sherstnev and R. S. Thorne, "Different PDF approximations useful for LO Monte Carlo generators," arXiv:0807.2132 [hep-ph].

[84] S. Ovyn, X. Rouby and V. Lemaitre, "DELPHES, a framework for fast simulation of a generic collider experiment," arXiv:0903.2225 [hep-ph].

[85] D. Bertolini, T. Chan and J. Thaler, "Jet Observables Without Jet Algorithms," JHEP **1404** (2014) 013.

[86] A. Hocker, J. Stelzer, F. Tegenfeldt, H. Voss, K. Voss, A. Christov, S. Henrot-Versille and M. Jachowski *et al.*, "TMVA - Toolkit for Multivariate Data Analysis," PoS ACAT (2007) 040 [physics/0703039 [PHYSICS]]; P. Speckmayer, A. Hocker, J. Stelzer and H. Voss, "The toolkit for multivariate data analysis, TMVA 4," J. Phys. Conf. Ser. **219** (2010) 032057; `http://tmva.sourceforge.net` .

[87] P. Bolzoni, B. A. Kniehl and A. V. Kotikov, "Gluon and quark jet multiplicities at $N^3LO+NNLL$," Phys. Rev. Lett. **109** (2012) 242002; P. Bolzoni, B. A. Kniehl and A. V. Kotikov, "Average gluon and quark jet multiplicities at higher orders," Nucl. Phys. B **875** (2013) 18, and references therein.

[88] B. Bhattacherjee, S. Mukhopadhyay, M. M. Nojiri, Y. Sakaki and B. R. Webber, "Associated jet and subjet rates in light-quark and gluon jet discrimination," JHEP **1504**, 131 (2015) [arXiv:1501.04794 [hep-ph]].

[89] T. Sjostrand and P. Z. Skands, "Transverse-momentum-ordered showers and interleaved multiple interactions," Eur. Phys. J. C **39** (2005) 129 [hep-ph/0408302].

[90] W. T. Giele, D. A. Kosower and P. Z. Skands, "A simple shower and matching algorithm," Phys. Rev. D **78**, 014026 (2008) [arXiv:0707.3652 [hep-ph]].

[91] W. T. Giele, D. A. Kosower and P. Z. Skands, "Higher-Order Corrections to Timelike Jets," Phys. Rev. D **84** (2011) 054003 [arXiv:1102.2126 [hep-ph]].

[92] S. Gieseke, P. Stephens and B. Webber, "New formalism for QCD parton showers," JHEP **0312**, 045 (2003) [hep-ph/0310083].

[93] B. R. Webber, "QCD Jets and Parton Showers," arXiv:1009.5871 [hep-ph].